พื้นผิวดัดแปรด้วยพอลิเมอร์สำหรับการประยุกต์ใช้งานทางชีวภาพ

นางสาวพรเพ็ญ แซ่อึ้ง

วิทยานิพนธ์นี้เป็นส่วนหนึ่งของการศึกษาตามหลักสูตรปริญญาวิทยาศาสตรดุษฎีบัณฑิต
สาขาวิชาวิทยาศาสตร์มหโมเลกุล
คณะวิทยาศาสตร์ จุฬาลงกรณ์มหาวิทยาลัย
ปีการศึกษา 2558

POLYMER-MODIFIED SURFACES FOR BIOMEDICAL APPLICATION

Miss Pornpen Sae-ung

A Dissertation Submitted in Partial Fulfillment of the Requirements
for the Degree of Doctor of Philosophy Program in Macromolecular Science
Faculty of Science
Chulalongkorn University
Academic Year 2015

Thesis Title	POLYMER-MODIFIED SURFACES FOR BIOMEDICAL APPLICATION
By	Miss Pornpen Sae-ung
Field of Study	Macromolecular Science
Thesis Advisor	Associate Professor Voravee Hoven, Ph.D.
Thesis Co-Advisor	Gamolwan Tumcharern, Ph.D.

Accepted by the Faculty of Science, Chulalongkorn University in Partial Fulfillment of the Requirements for the Doctoral Degree

.....Dean of the Faculty of Science
(Associate Professor Polkit Sangvanich, Ph.D.)

THESIS COMMITTEE

.....Chairman
(Professor Orawon Chailapakul, Ph.D.)

.....Thesis Advisor
(Associate Professor Voravee Hoven, Ph.D.)

.....Thesis Co-Advisor
(Gamolwan Tumcharern, Ph.D.)

.....Examiner
(Professor Tirayut Vilaivan, Ph.D.)

.....Examiner
(Assistant Professor Nuanphun Chantarasiri, Ph.D.)

.....External Examiner
(Cheeraporn Ananthanawat, Ph.D.)

พรเพ็ญ แซ่อึ้ง : พื้นผิวดัดแปรด้วยพอลิเมอร์สำหรับการประยุกต์ใช้งานทางชีวภาพ (POLYMER-MODIFIED SURFACES FOR BIOMEDICAL APPLICATION) อ.ที่ปรึกษาวิทยานิพนธ์หลัก: รศ. ดร.วรวีร์ โฮเว่น, อ.ที่ปรึกษาวิทยานิพนธ์ร่วม: ดร.กมลวรรณ ธรรมเจริญ, 94 หน้า.

ในวิทยานิพนธ์นี้สนใจพัฒนาพื้นผิวดัดแปรด้วยพอลิเมอร์ 3 ชนิดสำหรับการประยุกต์ใช้งานทางชีวการแพทย์ งานวิจัยในส่วนแรกเกี่ยวข้องกับเตรียมอนุภาคนาโนทองคำที่ติดโบไวน์ซีรั่มอัลบูมินเพื่อประยุกต์ใช้เป็นไบโอเซนเซอร์โดยใช้ไคโตซานที่ติดโบไวน์ซีรั่มอัลบูมินเป็นทั้งตัวรีดิวซ์และสารทำให้เสถียร เพื่อหลีกเลี่ยงการสูญเสียสภาพธรรมชาติของโบไวน์ซีรั่มอัลบูมิน งานวิจัยนี้สังเคราะห์อนุภาคนาโนทองคำโดยอาศัยวิธีทางเคมีด้วยเสียงซึ่งจัดเป็นวิธีที่ไม่เป็นพิษและไม่ทำลายสารตัวอย่าง ซึ่งจำเป็นต้องใช้ทวีน 80 เป็นสารทำให้เสถียรและตัวรีดิวซ์ร่วม อนุภาคนาโนทองคำที่ทำให้เสถียรด้วยไคโตซานที่ติดโบไวน์ซีรั่มอัลบูมินรวมกลุ่มในสภาวะที่มีแอนติโบไวน์ซีรั่มอัลบูมินเนื่องจากอันตรกิริยาที่จำเพาะเจาะจงของแอนติเจนและแอนติบอดี งานวิจัยในส่วนที่สองเป็นการพัฒนาอนุภาคแท่งระดับนาโนเมตรของทองคำที่ถูกทำให้เสถียรด้วยมัลติฟังก์ชันโคพอลิเมอร์สำหรับการนำส่งเพปไทด์นิวคลีอิกแอซิด (พีเอ็นเอ) เมทาคริลิกแอซิด (เอ็มเอ) และ 2-เมทาคริโลอิลออกซีเอทิลฟอสโฟริลโคลีน (เอ็มพีซี) ในโคพอลิเมอร์เป็นหมู่ฟังก์ชันสำหรับการตรึงพีเอ็นเอและเพิ่มความเข้ากันได้ทางชีวภาพของอนุภาคตามลำดับ อนุภาคแท่งระดับนาโนเมตรของทองคำที่มีความเสถียรสูงและไม่เป็นพิษสามารถเตรียมโดยการใช้โคพอลิเมอร์ที่ปรับปรุงด้วยไทออลและติดพีเอ็นเอเป็นสารทำให้เสถียร เนื่องจากพีเอ็นเอถูกต่อกับโคพอลิเมอร์ด้วยตัวเชื่อมที่เป็นเตตระเพปไทด์ (ไกลซีน-ฟีนิลอะลานีน-ลูซีน-ไกลซีน) การปลดปล่อยจึงสามารถถูกเหนี่ยวนำให้เกิดขึ้นได้ในภาวะที่มีเอนไซม์คาเทปซินบี แสดงความเป็นไปได้ในการประยุกต์ใช้งานด้านแอนติเซนส์ของตัวนำส่งที่ตรียมจากอนุภาคแท่งระดับนาโนเมตรของทองคำที่ถูกพัฒนาขึ้น จากการที่เอ็มพีซีที่มีสมบัติต้านการยึดเกาะที่ดี งานวิจัยในส่วนสุดท้ายจึงสนในเตรียมพื้นผิวแพทเทิร์นที่มีสมบัติต้านการยึดเกาะและต้านแบคทีเรียเพื่อป้องกันการเกิดไบโอฟิล์มจากเอ็มพีซี แพทเทิร์นที่ประกอบด้วยโคพอลิเมอร์ของไดไฮโดรไลโปอิกแอซิด (ดีเฮชแอลเอ) และเอ็มพีซี และซิลเวอร์ฟิล์มแสดงทั้งการต้านการยึดเกาะของแบคทีเรียบริเวณส่วนเอ็มพีซีและการฆ่าแบคทีเรียบนเส้นซิลเวอร์แสดงถึงการแสดงผลรวมกันของทั้งการต้านการยึดเกาะและต้านแบคทีเรียบนพื้นผิวแพทเทิร์นนี้

สาขาวิชา วิทยาศาสตร์มหโมเลกุล ลายมือชื่อนิสิต .....

ปีการศึกษา 2558 ลายมือชื่อ อ.ที่ปรึกษาหลัก .....

ลายมือชื่อ อ.ที่ปรึกษาร่วม .....

5373814223 : MAJOR MACROMOLECULAR SCIENCE
KEYWORDS: GOLD NANOPARTICLES / GOLD NANORODS / ANTIBACTERIA

PORNPEN SAE-UNG: POLYMER-MODIFIED SURFACES FOR BIOMEDICAL APPLICATION. ADVISOR: ASSOC. PROF. VORAVEE HOVEN, Ph.D., CO-ADVISOR: GAMOLWAN TUMCHARERN, Ph.D., 94 pp.

In this thesis, three different polymer-modified surfaces have been developed for biomedical applications. In the first part, BSA-functionalized gold nanoparticles (BSA-CS-AuNPs) were prepared for biosensing application by using bovine serum albumin-modified chitosan (BSA-CS) as both reducing and stabilizing agents. To avoid BSA denaturation, a green and non-destructive approach based on sonochemical method was employed for AuNPs synthesis with the need of Tween 80 as steric stabilizing agent and co-reducing agent. The BSA-CS-AuNPs underwent aggregation in the presence of anti-BSA via antigen-antibody specific interactions. In the second part, multifunctional copolymer-stabilized gold nanorods (AuNRs) have been developed for peptide nucleic acid (PNA) delivery. Methacrylic acid (MA) and 2-methacryloyloxyethyl phosphorylcholine (MPC) in the copolymer were used for PNA binding and providing biocompatibility on AuNRs, respectively. The highly stable and nontoxic PNA-immobilized AuNRs were successfully prepared by using thiol-modified and PNA-conjugated copolymer (PNA-Cys-PMAMPC) as stabilizer. As PNA was conjugated with the copolymer by tetrapeptide linker (-Gly-Phe-Leu-Gly-), its release can be induced in the presence of cathepcin B indicating the potential antisense applications of the developed AuNRs-based carriers. In the last part, MPC which is also known to exhibit excellent antifouling property was utilized to prepare dual functional patterned surface having both antifouling and antimicrobial properties for preventing biofilm formation. Pattern of copolymer containing dihydrolipoic acid (DHLA) and MPC backfilled with Ag film showed both bacteria adhesion resistance on MPC area and bacterial killing on Ag lines implying the combined antifouling and antibacterial effects on this patterned surface.

Field of Study: Macromolecular Science Student's Signature .....

Academic Year: 2015 Advisor's Signature .....

Co-Advisor's Signature .....

ACKNOWLEDGEMENTS

First of all, I would like to express my sincere and deep gratitude to my advisor, Associate Professor Dr. Voravee P. Hoven and my co-advisors, Dr. Gamolwan Tumcharern and Professor Dr. Todd Emrick for their valuable guidance, encouragement, and support. Working with them has been the best course of my study. I learned many things either research or guideline for living from them. I would also like to thank all my committee members, Professor Dr. Orawan Chailapakul, Professor Dr. Tirayut Vilaivan, Associate Professor Dr. Nuanphun Chantarasiri and Dr. Cheeraporn Ananthanawat for their very useful comments and suggestions and time to review the thesis.

I gratefully acknowledge Chulalongkorn University Dutsadiphiphat Scholarship for academic scholarship provided by Chulalongkorn University.

I am thankful to the friendly staffs at both Chulalongkorn University and University of Massachusetts Amherst, and all my friends, especially VH and VT group members as well as Emrick group members for their laugh, friendliness, helpful discussions and comments, cheerful attitude and encouragements during my thesis work.

I also wish to especially thank my family members for their love, kindness and support throughout my PhD study.

Finally, I strongly believed that I can complete my PhD degree because of all your support and I really appreciated it.

CONTENTS

Page

Page

Page

LIST OF FIGURES

Figure **Page**

LIST OF SCHEMES

LIST OF TABLES

Table **Page**

LIST OF ABBREVIATION

ACVA	: 4,4′-Azobis(4-cyanovaleric acid)
AuNPs	: Gold nanoparticles
AuNRs	: Gold nanorods
BSA	: Bovine serum albumin
CPD	: 4-Cyano-4-(thiobenzoylthio)pentanoic acid
CS	: Chitosan
CTAB	: Cetyltrimethylammonium bromide
DHLA	: Dihydrolipoic acid
DMPA	: 2,2-Dimethoxy-2-phenylacetophenone
EDC	: N-(3-(dimethylamino)propyl)-N′-ethylcarbodiimide hydrochloride
MA	: Methacrylic acid
MPC	: 2-Methacryloyloxyethyl phosphorylcholine
NHS	: N-hydroxysuccinimide
PNA	: Peptide nucleic acid
RAFT	: Reversible addition-fragmentation chain transfer

CHAPTER I
INTRODUCTION

Surface modification by polymer has become increasingly attractive and versatile route for the development of materials for biomedical application because the desired and multifunctional properties can simultaneously be incorporated by selecting the right choice of monomer. By employing controlled polymerization process, the polymer chain length, functionality as well as composition can also be well manipulated. As compared with the conventional 2D self-assembled monolayer-based system, 3D characteristic of the polymer matrix provides greater functional group density per surface area for covalently anchoring designated biomolecules for specific biomedical applications. Taking advantage of tunable functionality of polymer, this thesis aims to prepare, characterize and determine the potential of three polymer-functionalized surfaces for biomedical applications.

For the first project, chitosan as biopolymer was used for the synthesis of gold nanoparticles (AuNPs). Chitosan is obtained by partial deacetylation of chitin. It has been reported that an abundant amino groups available in chitosan structure can act as both reducing and stabilizing agent in the synthesis of AuNPs. We are interested to further explore the use of amino groups not only as reducing moieties in AuNPs synthesis but also as possible active sites for biomolecule conjugation so that biomolecule-attached AuNPs can be prepared directly using the biomolecule-conjugated chitosan in a single step without the requirement for ligand exchange. Herein this research, BSA was selected as a model biomolecule to be attached to chitosan. To avoid BSA denaturation, the AuNPs synthesis was performed via sonochemical method in the presence of BSA-conjugated chitosan (BSA-CS). Potential application of the developed AuNPs stabilized by BSA-CS (BSA-CS-AuNPs) as antigen-antibody-based sensing platform was tested against anti-BSA.

The second project aims to develop carriers for peptide nucleic acid (PNA) from nanorods (AuNRs) to be used for antisense application. The inherent toxicity of cetyltrimethylammonium bromide (CTAB) used as template and stabilizer to control

particle shape of AuNRs limits the bio-related applications. To be able to use AuNRs as biocompatible antisense carrier, this research introduces a synthetic copolymer, poly(methacrylic acid)-*ran*-(2-methacryloyloxyethyl phosphorylcholine) (PMAMPC), as dual-functional stabilizer to replace the CTAB which can be done via ligand exchange. The 2-methacryloyloxyethyl phosphorylcholine (MPC) would function as biomimetic hydrophilic group providing biocompatibility and colloidal stability to the AuNRs whereas the carboxyl groups in methacrylic acid (MA) could be used as reactive sites for covalently conjugating with PNA. Cytotoxicity of the developed AuNRs was tested against HepG2 cells. By conjugating the PNA to PMAMPC via tetrapeptide, Gly-Phe-Leu-Gly, it is anticipated that release of PNA can be selectively induced by cathepsin B, an enzyme abundantly available in cancerous cells.

Poly(2-methacryloyloxyethyl phosphorylcholine) (PMPC) is well recognized for its excellent biofouling resistance. The goal of the third project is to develop a simple, universal and non-silane-based method for patterned PMPC coating from a copolymer consisting of MPC and the methacrylate of dihydrolipoic acid (DHLA), poly(MPC-DHLA). Thiol groups in DHLA serve as crosslinkable units via thiol-ene click reaction so that antifouling PMPC film can be stably attached on the surface. After backfilling patterned PMPC generated by photolithography with silver film, a model of antibacterial agent, we aims that the dual functional patterned surface with antifouling and antibacterial characteristics would be obtained.

CHAPTER II
GREEN SYNTHESIS AND POTENTIAL BIOSENSING APPLICATION OF GOLD NANOPARTICLES STABILIZED BY BIOMOLECULE-MODIFIED CHITOSAN

2.1 Introduction

Preparation of gold nanoparticles (AuNPs) has been extensively studied due to their unique physical and chemical properties for potential applications in catalysis, biology and electrochemistry [1-3]. Several methods, such as the use of chemical reductants [4, 5], sonochemical [6, 7] and photochemical activation [8-11], can be employed for the synthesis of AuNPs. Among them, the chemical reduction approach is the most common route for the preparation of AuNPs and involves the treatment of gold salts with a chemical reducing agent, such as citric acid, borohydride or other organic compounds, to form zerovalent AuNPs. Because AuNPs usually tend to aggregate in the medium, stabilizing agents, such as thiol compounds [12, 13], surfactants [14, 15] and polymers [16-18], are therefore necessary in the synthesis of AuNPs. It has been reported that polymers are effective stabilizing agents for AuNPs because they are capable of providing both electrostatic and steric stabilizations. In particular, polymers containing amino groups can act as both reducing and stabilizing agents due to the fact that gold salts can be reduced by the amino groups in the polymer's structure [19-21]. Therefore, the reduction and stabilization processes can be accomplished in a single step in the presence of an amino-containing polymer.

Chitosan is a polysaccharide obtained by partial deacetylation of chitin, a natural substance found abundantly in the exoskeletons of insects, the shells of crustaceans and fungal cell walls. The number of amino groups in the structure of chitosan is determined by the degree of deacetylation which can range from more than 50% up to 100% [22]. The large numbers of the amino groups in the chitosan structure are capable of acting as both a reducing and stabilizing agent in the synthesis of AuNPs without the requirement for an additional reducing agent[23-32]. Moreover, AuNPs stabilized by chitosan can also be synthesized by ultraviolet

radiation [33], direct heating in a microwave oven [34, 35], laser-assisted method [36] or by a sonication method [37].

Immunoassays based on the aggregation of AuNPs rely on specific interactions between the immobilized antibody on the surface of the AuNPs and the target antigen in the solution [38-40], although *vice versa* is possible for sensing the level of antigen-specific antibodies. AuNPs tend to aggregate because the dielectric constant in the vicinity of the surface is altered resulting in a change in the optical property of the AuNPs [41]. Not only can the shifted signal reflect the degree of AuNPs aggregation, it can also be used as quantitative measure of the tested antigen. The two main strategies used for conjugating biomolecules to the AuNPs are physisorption and chemisorption [42]. Although physisorption is simple, the process often suffers from chemical instability and uncontrolled orientation of antibody's active sites. In contrast, chemisorption requires more complicated procedures, the complexity is nevertheless worth the sacrifice considering that it can provide a better stability and site-directed immobilization of the antibody. Readily available reactive functional groups in the stabilizing agent that can be chemically bound to the desired antibody should make the synthetic process of AuNPs to be used for immunoassay much simpler and more convenient. There have been reports on the use of some biomolecules, such as cysteine, leucine, asparagine and bovine serum albumin (BSA), as both a reducing and stabilizing agent or only as a stabilizing agent for the synthesis of biomolecule-conjugated AuNPs [43-51]. Nevertheless, it should be emphasized that this approach is only applicable for the biomolecules having functional groups with reducing power.

Although there are a number of literature reports describing the synthesis of AuNPs using chitosan as the stabilizing and reducing agent, the preparation of AuNPs using chitosan conjugated with biomolecules and their biosensing applications, to the best of our knowledge, have not yet been addressed. Herein, this research evaluated the ability to use the readily available amino groups in chitosan as not only reducing moieties but also as active sites for immobilizing biomolecules. It is anticipated that this proposed strategy should be applicable to a broader range of biomolecules, and is not only limited to those with reducing power. Using bovine serum albumin (BSA)

as an antigen model, the AuNPs were synthesized using BSA-attached chitosan (BSA-CS) as both the reducing and stabilizing agent and then tested for their biosensing applications with a specific anti-BSA antibody.

2.2 Materials and methods

2.2.1 Materials

CS flakes of three different viscosity averaged molecular weights (M_V) (M_V = 15 kDa (low molecular weight; LCS), 80 kDa (medium molecular weight; MCS) and 200 kDa (high molecular weight; HCS)), each with a degree of deacetylation of 90%, were obtained from Seafresh Chitosan (Lab) Co., Ltd. (Thailand). Glacial acetic acid was purchased from Merck (Germany). Polyclonal anti-BSA antibodies developed in rabbit, and anti-immunoglobulin G (anti-IgG) antibodies produced in goat, BSA, dialysis bag (cut-off molecular weight of 12,400 g/mol), phosphate buffered saline, pH 7.4 (PBS) and succinic anhydride (SA) were bought from Sigma (USA). *N*-(3-dimethylaminopropyl)-*N'*-ethyl-carbodiimide hydrochloride (EDC) and *N*-hydroxysuccinimide (NHS) were obtained from Fluka (Switzerland). Polysorbate 80 (Tween 80) and hydrogen tetrachloroaurate trihydrate ($HAuCl_4.3H_2O$) were obtained from Aldrich (USA). Centrifugal filter tubes with a molecular weight cut-off membrane of 100,000 g/mol were bought from Millipore (USA). All the above chemicals were analytical grade and used as received without further purification. All solutions were made using ultrapure distilled water that was obtained after purification using a Millipore Milli-Q system (USA) that involves reverse osmosis, ion exchange and filtration (18.2 MΩ cm resistance). Moreover, all glasswares used for the synthesis of AuNPs were cleaned with freshly prepared aqua regia solution (HCl: HNO_3 at a (v/v) ratio of 3:1) and rinsed thoroughly with distilled water prior to use.

2.2.2 Preparation of AuNPs stabilized by chitosan (CS-AuNPs)

The stock solution of the chitosan having designated MW (LCS, MCS or HCS) was prepared by dissolving a certain amount of chitosan in 1.0 % (v/v) aqueous acetic acid. CS-AuNPs were first synthesized by direct heating method to obtain an optimized condition. The synthetic method can be summarized as follows: the

chitosan solution (0.1% (w/v), varied MW and volume) and 2.943 mM aqueous solution of $HAuCl_4$ (varied volume) in 18 mL of Milli-Q water were separately heated with stirring at 60 °C in an oil bath for 5 min. Tween 80 (varied concentration), a non-ionic surfactant, was added into the aqueous solution of $HAuCl_4$, and five minutes later the chitosan solution was added into the mixture and heated to 85 °C under vigorous stirring until a red solution was obtained. The synthesized AuNPs were kept at 4 °C. Then, sonochemical method was repeatedly studied based on the optimized condition obtained from conventional thermal treatment to be used in the synthesis of BSA-CS-AuNPs. The preparation of CS-AuNPs via sonochemical method was similar to heating method, except that the sonochemical method was used instead of the direct heating method to avoid BSA denaturation. These particles were synthesized as follows: the aqueous solution of $HAuCl_4$ (2.943 mM, varied volume) in 18 mL of Milli-Q water was mixed with Tween 80 (optimized concentration from heating method) and stirred for 5 minutes at ambient temperature. Then, the CS solution (optimized MW, 0.1% (w/v), varied volume) was added into the mixture. After stirring for 10 minutes, the mixture was placed in a sonication bath (model Transsonic 460/H, Elma, Germany) for 40 minutes. Finally, a red solution of CS-AuNPs was obtained and kept at 4 °C.

2.2.3 Preparation of AuNPs stabilized by BSA-attached chitosan (BSA-CS-AuNPs)

BSA-attached chitosan (BSA-CS) was employed as both the reducing and stabilizing agent in the synthesis of BSA-CS-AuNPs using the optimum conditions previously identified for the synthesis of CS-AuNPs. The procedure for the attachment of BSA to chitosan consists of the three following steps (**Error! Reference ource not found.**). It should be emphasized that the MCS having medium M_v of 80 kDa was used for the modification. Chitosan was first modified with SA to produce reactive sites, carboxyl groups, on the chitosan backbone that could be activated with EDC and NHS. The SA-modified chitosan (SA-CS) was synthesized according to a method modified from that of Don and Chen [52]. The reaction was carried out in formic acid to avoid the hydrolysis of SA in aqueous solution. MCS (0.750 g) was dissolved in 30.0 g of formic acid and then 4.06 g (10 mole equivalents) of SA was

added. The solution was stirred for 24 h at ambient temperature and then dialyzed against deionized water in a dialysis bag at ambient temperature for 5 days and lyophilized to obtain the final product. Attachment of BSA to the carboxyl groups on chitosan was performed according to the following stepwise procedure: SA-CS (0.01 g) was dissolved in Milli-Q water (10 mL), EDC (3 mole equivalents) and NHS (3 mole equivalents) were then added to the SA-CS solution and the mixture was stirred at ambient temperature for 15 min. Then, BSA (1.0 mg/mL) was added to the mixture and continuously stirred at ambient temperature for 2 h to attach the BSA to the SA-CS. To remove excess EDC, NHS and BSA, the mixture was placed into the centrifugal filter tube containing a 100,000 g/mol cut-off filter and centrifugally washed with Milli-Q water at 5,000 rpm for 20 min (refrigerated centrifuge model 7780, Kubota Corporation, Japan) until excess reagents were entirely removed, as monitored by measuring the conductance of the supernatant after each washing cycle by a conductometer (model Orion 3 star Conductivity Benchtop, Thermo Electron Corporation, USA). The Milli-Q water was then added to the membrane centrifuge tube before sonication for 15 min. The final product (BSA-CS) was obtained after lyophilyzing the solution removed from the tube. The AuNPs stabilized by BSA-CS (BSA-CS-AuNPs) were prepared by using the same method with CS-AuNPs synthesis via sonochemical method, except that BSA-CS was used instead of CS.

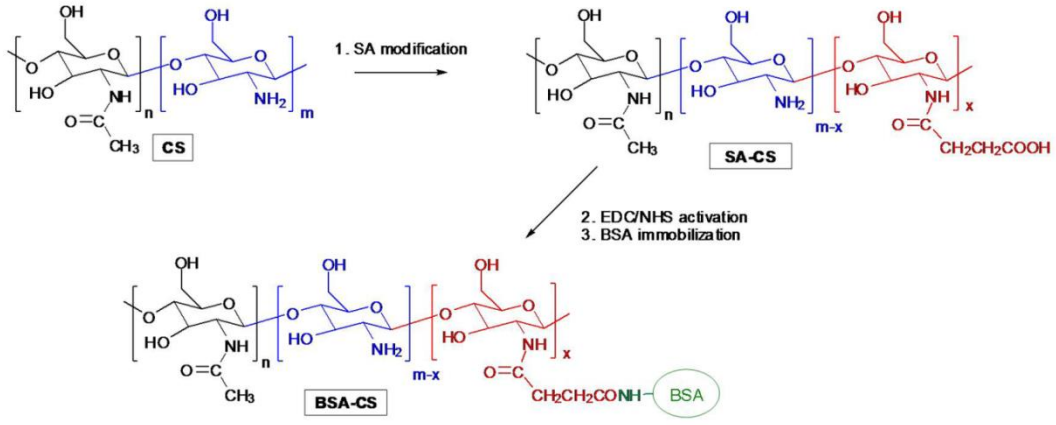

Scheme 2.1 A synthetic route for the preparation of BSA-CS.

2.2.4 Detection of anti-BSA by BSA-CS-AuNPs

The solution of BSA-CS-AuNPs was centrifuged at 18,000 rpm for 30 min and re-suspended in PBS to obtain a concentration of 35.86 nM. Afterwards, the solution of anti-BSA in PBS (100 µg/mL, varied volume) was added to 50 µL of the BSA-CS-AuNPs solution and the mixture was kept at ambient temperature for 2 days. Control experiments were performed by using the same concentration of anti-IgG antibody as that of anti-BSA in PBS, or PBS only.

2.2.5 Characterizations

The hydrodynamic size and zeta-potential (ζ) of hydrated particles were determined by photon correlation spectroscopy (PCS), based upon dynamic light scattering (DLS), using a Nanosizer Nano-ZS (Malvern Instruments, UK). The solutions of AuNPs (1 mL) were sonicated for 3 min before measurement, which was performed at 25 $^{\circ}$C using a scattering angle of 173°. All data are displayed as the mean ± standard deviation (SD) and are derived from at least three independent experiments. The data were calculated using the Helmholtz-Smoluchowski equation. The morphology and actual size of anhydrous particles were analyzed by transmission electron microscopy (TEM) on a JEOL JEM-2010 transmission electron microscope (Japan) operating at 200 keV. The TEM samples were prepared by dropping approximately 10 µL of AuNPs solution onto the carbon-coated copper grid and drying in a dessicator before analysis. The average diameters are reported from measurements of 100 random particles for each sample using Semafore software. The presence of the polymer around the AuNPs was confirmed by a Seiko SPA 400 atomic force microscope (SII Nanotechnology Inc., Japan). The samples were prepared by dropping the AuNPs solution on a freshly cleaved mica plate and dried in a dessicator for 4 h prior to analysis. Measurements were performed in air at ambient temperature using tapping mode and silicon tips with a resonance frequency of 115-190 kHz.

2.3 Results and discussion

2.3.1 Preparation and characterization of CS-AuNPs

Firstly, AuNPs were synthesized by heat treatment and using chitosan as both the reducing and stabilizing agent to obtain the optimum condition for the preparation of AuNPs stabilized by BSA-CS. The effect of the chitosan: $HAuCl_4$ (w/w) ratio (in terms of varying the (v/v) ratio of fixed molarity solutions) on the mean size of the synthesized CS-AuNPs was evaluated by PCS (**Figure 2.1f**). The mean particle size of the CS-AuNPs depended upon the chitosan:$HAuCl_4$ (v/v) ratio. Because the electrostatic forces between the amino groups on chitosan and $AuCl_4^-$ in solution are a driving force for the formation and stabilization of the AuNPs, the effect of the chitosan:$HAuCl_4$ (v/v) ratio on the mean particle size could be described based on the number of adsorbing chitosan molecules on the surface of AuNPs. When the chitosan:$HAuCl_4$ (v/v) ratio was low (5:5), there were only a few chitosan molecules coated on the particles, resulting in the AuNP aggregation during the synthesis and so the formation of large AuNPs. For a high chitosan:$HAuCl_4$ (v/v) ratio (9:1), the large AuNPs might be formed due to the coating of an excess amount of chitosan on the outside layer. To verify the effect of the MCS:$HAuCl_4$ (v/v) ratio on the mean size of CS-AuNPs, as analyzed by PCS, it was compared to that characterized by TEM. The data from TEM analysis also indicated that a relatively larger size of AuNPs was formed at a low MCS: $HAuCl_4$ (v/v) ratio (5:5) implying that there was aggregation of AuNPs during the synthesis. For the high MCS: $HAuCl_4$ (v/v) ratio (9:1), the mean size obtained from TEM analysis was, however, inconsistent with that obtained from the PCS analysis. There was no significant size variation between the AuNPs synthesized using the MCS:$HAuCl_4$ (v/v) ratios of 9:1, 8:2, 7:3 and 6:4. Since the measurement is based on the dynamic light scattering of particles, PCS is capable of measuring the hydrodynamic size of the AuNPs which combines both the gold core and the polymeric shell of the surrounding chitosan. So the excess chitosan coating on the outer layer of the CS-AuNPs in the case of the high MCS: $HAuCl_4$ (v/v) ratio can easily be realized. Unlike PCS, the high voltage based TEM analysis performed here can only visualize the gold core of the CS-AuNPs, as this exhibits a greater electron

density than the coating chitosan layer. The chitosan shell can be visualized only after appropriate staining and using a relatively lower accelerating voltage in the TEM than the 200 keV that was used in this research. This also explained why the mean sizes of the CS-AuNPs obtained from the PCS analysis were always significantly larger than that visualized by TEM. For the morphology and actual size of the CS-AuNPs analyzed by TEM displayed in **Figure 2.1a-e**, the particles were clearly spherical in shape, and the mean ($\pm$ SD) sizes were in a range of 13.3-30.0 nm. It should be noted that the CS-AuNPs had relatively broad size distribution (SD $\sim$ 3-8 nm) as compared with the AuNPs synthesized by the conventional method using trisodium citrate as reducing and stabilizing agent. This may be explained as a result of unavoidably broad molecular weight distribution of naturally obtained chitosan. In this particular study, a chitosan:$HAuCl_4$ (v/v) ratio of 7:3 was found to be the optimal value that can produce the smallest AuNPs with a narrow size distribution (expressed in terms of the polydispersity index (PDI) shown in **Appendix A, Figure A-1** which was lower than 0.7) and high stability (expressed in terms of the ζ-potential shown in **Figure A-1 in appendix A** which was higher than +20 mV).

Moreover, the effect of the chitosan molecular weight on the mean size of the prepared CS-AuNPs was also studied and agreed with that previously reported [23], in that the mean size of AuNPs was not significantly affected by the chitosan molecular weight (**Figure A-1, Appendix A**). This is because the increasing entanglement of polymeric chains as a function of the molecular weight did not affect the reducing power of amino groups as well as the ability to stabilize the synthesized AuNPs, given that the same amount of active amino groups were present in the same weight of chitosan regardless of its different molecular weight. Nevertheless, the range of chitosan molecular weight used in this research is rather narrow (15, 80 and 200 kDa) and so may not be broad enough to detect any such influences. When a chitosan:$HAuCl_4$ (v/v) ratio of 7:3 was used for the synthesis, the ζ-potential of the AuNPs stabilized by the MCS (30.2 $\pm$ 5.0 mV) was slightly higher than that of the AuNPs stabilized by the LCS (24.9 $\pm$ 3.1 mV), suggesting that more stable AuNPs were

formed in the former case. Also, the HCS (200 kDa) exhibited quite poor solubility. For these reasons, MCS was then selected for further use in the synthesis of AuNPs.

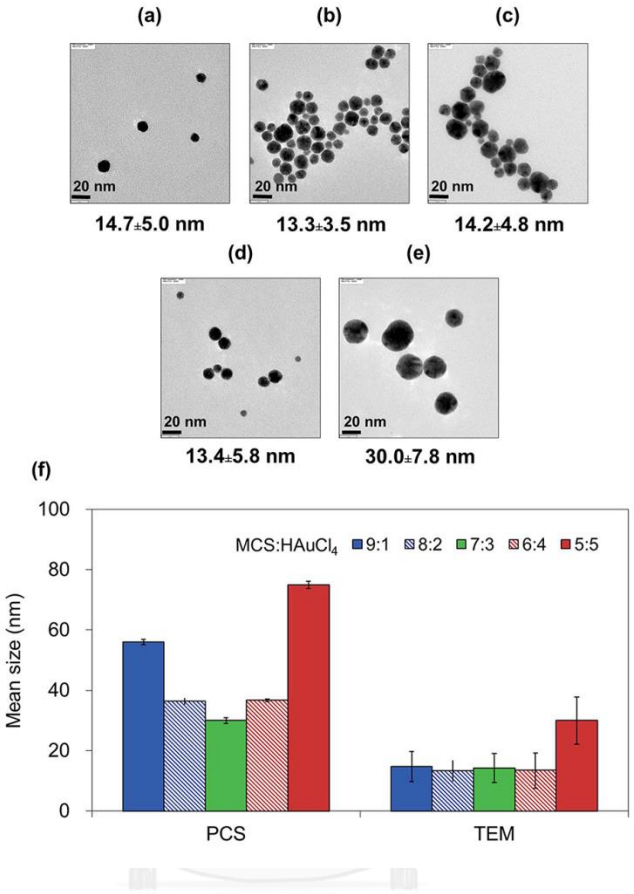

Figure 2.1 Representative TEM images of CS-AuNPs prepared by using CS:$HAuCl_4$ (v/v) ratio of (a) 9:1, (b) 8:2, (c) 7:3, (d) 6:4, (e) 5:5 and (f) mean (±SD) size of the CS-AuNPs as analyzed by PCS and TEM.

In general, there are two types of repulsive forces that facilitate the AuNPs stabilization, electrostatic and steric repulsion. Here, CS-AuNPs cannot be re-dispersed in neutral (or alkaline) aqueous solution after the purification step due to the lack of permanent charge in the chitosan molecules at a pH above their pKa (~6.5) which should provide electrostatic stabilization. To be able to re-disperse the CS-AuNPs, Tween 80 was then added to the reaction solution to introduce steric stabilization to the particles. **Table 2.1** presents the effect of varying the Tween 80 concentration on the mean size, PDI and ζ-potential of the synthesized CS-AuNPs, where the lowest Tween 80 concentration that yielded re-dispersable small size

AuNPs was found to be 1% (v/v). Compared with the CS-AuNPs synthesized in the absence of Tween 80, the ζ-potentials of CS-AuNPs made in the presence of 0.25, 0.50, and 1.0% (v/v) of Tween 80 dramatically decreased. This is somewhat expected because the AuNPs were shielded by the Tween 80. Upon raising the Tween 80 concentration to 2.0% (v/v), the ζ-potential of redispersed particles increased over three-fold to 10.1 mV. This may be due to the extensive formation of micelles at the concentration of a lot higher than the critical micelle concentration (CMC) of Tween 80 (0.012 mM). It should be noted that the lowest concentration used in this study (0.25% (v/v)), equivalent to 2.0 mM, significantly exceeded the CMC value. Therefore, upon using chitosan as both the reducing and stabilizing agent in the synthesis of AuNPs, the optimal condition that yielded CS-AuNPs with a small size, high ζ-potential and a narrow size distribution was the chitosan:$HAuCl_4$ (v/v) ratio of 7:3 with medium molecular weight of chitosan (80 kDa) and 1.0% (v/v) of Tween 80. This condition was further studied in the next step.

Table 2.1 Mean (±SD) size, PDI and ζ-potential of the MCS-AuNPs using a MCS:$HAuCl_4$ (v/v) ratio of 7:3 and varied Tween 80 concentrations, as analyzed by PCS (independent experiment = 3).

[Tween80] (%(v/v))	Size (nm)		PDI		ζ-potential (mV)	
	As synthesized	After re-dispersion	As synthesized	After re-dispersion	As synthesized	After re-dispersion
-	30.0±1.0	N/A[a]	0.349±0.02	N/A[a]	30.2±5.0	N/A[a]
0.25	62.6±1.5	68.6±3.0	0.460±0.01	0.386±0.02	12.5±0.4	3.4±0.2
0.50	64.3±9.6	72.3±4.0	0.386±0.05	0.407±0.01	13.4±1.5	3.0±0.1
1.00	25.5±2.3	45.6±3.3	0.460±0.02	0.394±0.03	15.5±1.9	3.5±0.6
2.00	24.8±1.1	39.3±4.4	0.462±0.03	0.276±0.02	10.0±0.8	10.1±0.7

[a]The data is not available because AuNPs aggregated during the purification step.

According to the results obtained from the UV-vis spectroscopic analysis (**Figure A-2, Appendix A**), the spectrum of as-synthesized CS-AuNPs exhibited an absorption band at 525 nm, a typical plasmon resonance band for AuNPs. Moreover,

the absorption band after storage for over 4 months was only slightly shifted from the as-synthesized one, suggesting a high degree of stability of the synthesized AuNPs. To confirm the presence of the chitosan around the AuNPs, and to identify the possible interaction between the CS and AuNPs, the FTIR spectrum of the CS-AuNPs was recorded (**Figure A-3, Appendix A**). CS-AuNPs spectrum showed the characteristic IR features of CS around 1626 cm^{-1}, which can be assigned to the C=O stretching of the secondary amide of acetamide group in chitosan. Furthermore, the disappearance of the N-H bending vibration of the primary amine at 1596 cm^{-1} implied that amino groups may locate close to the AuNPs, causing an impediment in the IR vibration.

In order to prepare AuNPs for biosensing applications, BSA was selected as a model antigen. Because BSA can be denatured at temperatures above 72 ºC [53], the synthesis of AuNPs by using heat treatment in the previous part is not appropriate for the synthesis of BSA-CS-AuNPs. , Therefore, sonochemical treatment was chosen as an alternative way to avoid possible thermal denaturation of BSA. The method has been known to provide thermal energy through implosive collapse of acoustic cavitation bubbles and used for reduction of Au^{3+} to $Au^{(0)}$ [6, 7, 37]. Although extremely high temperature and pressure are locally generated, it is believed that the cooling rate should be so rapid that the overall temperature of the system is not high enough to denature the structure of protein. In fact, the temperature of the sonicated aqueous solution was monitored throughout the experiment and found to be $< 40^{\circ}C$, well below the denaturation temperature (T_d) of BSA ($T_d \approx 72^{\circ}C$).

To find the optimal condition for the synthesis of AuNPs via sonication, the experiment was studied based on the preliminary results from heating method. The impact of the chitosan: $HAuCl_4$ (v/v) ratio on the mean size of the synthesized CS-AuNPs was repeatedly studied by using sonochemical method with medium molecular weight of chitosan (80 kDa) and 1.00% (v/v) of Tween 80. The results from PCS showed the same trend as compared with the thermal treatment that was chitosan:$HAuCl_4$ (v/v) ratio of 7:3 providing the smallest size CS-AuNPs (**Figure 2.2a**). In addition, from the TEM images (**Figure 2.2b**), it was also found that the CS-AuNPs

prepared by sonication and using chitosan:$HAuCl_4$ (v/v) ratio of 7:3 were still spherical in shape, and the mean size was in a range of 9.1±2.3 nm which was similar to AuNPs prepared by heating suggesting that sonochemical synthesis could be used for the synthesis of AuNPs with the same optimum condition previously identified for the synthesis based on thermal treatment.

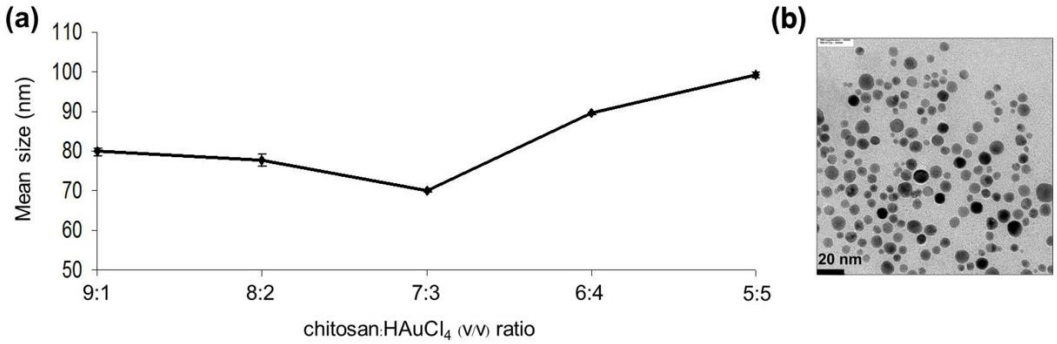

Figure 2.2 (a) Mean (±SD) size of the CS-AuNPs synthesized by sonication using MCS (80 kDa), 1.0% (v/v) of Tween 80 and five different CS:$HAuCl_4$ (v/v) ratios**,** as analyzed by PCS and (b) TEM image of the CS-AuNPs synthesized by sonication using MCS, CS:$HAuCl_4$ (v/v) ratio of 7:3 and 1.0% (v/v) Tween 80.

Moreover, the effect of Tween 80 adding on AuNPs formation in sonochemical method was also investigated. The formation of AuNPs (expressed by the occurrence of UV-vis absorption band of AuNPs at 523 nm) in the presence of chitosan and Tween 80 was compared with AuNPs formed in the presence of only chitosan or Tween 80 (control experiments). From the results, it was found that the stable AuNPs could be only produced when chitosan and Tween 80 were added together (**Figure 2.3**). To explain this outcome, the kinetic of AuNPs formation in the presence of only chitosan in sonochemical method was determined and compared with the conventional thermal method (**Figure A-4, Appendix A**). By using heating method, AuNPs were obtained after 20 min of reaction time while disappearance of intensity of characteristic absorption band of AuNPs was obtained in sonochemical method after 90 min of reaction time implying that the rate of AuNPs formation in sonochemical method was slow and much slower than the heating method. Also, using sonication together with chitosan which acts as the mild reducing agent

somehow retards the rate of AuNPs formation. To increase this rate, the addition of Tween 80 which can act as a co-reducing agent is still necessary because AuNPs would only be formed when chitosan and Tween 80 were added together as shown in **Figure 2.3**. These results were consistent with what has been previously described by Hormozi-Nezhad and co-workers about the dual function of Tween 80 which simultaneously acts as both co-reducing and stabilizing agent [54].

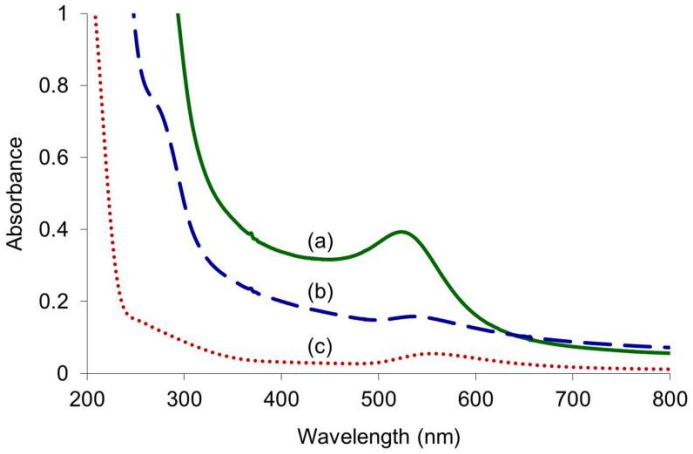

Figure 2.3 UV-vis absorption spectra of CS-AuNPs synthesized by (a) adding chitosan and Tween80 (green solid line), (b) adding only Tween 80 (blue dashed line) and (c) only adding chitosan (red dotted line).

2.3.2 Preparation and characterization of BSA-CS-AuNPs

In order to prepare AuNPs for biosensing applications, BSA was selected as a model antigen. The pathway for the attachment of BSA to chitosan (in this case, MCS) consists of three steps, as shown in **Error! Reference source not found.**. In the irst step, chitosan was modified by SA to introduce carboxyl groups onto the chitosan molecule via amidation of the chitosan amino groups and SA. FTIR analysis was used to confirm the success of the SA modification (**Figure A-5, Appendix A**). As compared with the virgin chitosan, the FTIR spectrum of SA-CS shows an increment of the C=O stretching and N-H bending of the secondary amide at 1665 cm^{-1} and 1578 cm^{-1}, respectively, and a decrement of the N-H bending of the primary amine at 1596 cm^{-1}. The attachment of BSA onto the chitosan was also confirmed by the appearance of the absorption band at around 275 nm in the UV-vis spectra, due to

the tryptophan and tyrosine phenyl groups (**Figure 2.4**) [55]. This signal in the BSA-CS spectrum is also seen at the same position in pure BSA and can be easily distinguished from those of the SA-CS. The carboxyl groups in SA-CS were bound with BSA through EDC/NHS activation and the resulting BSA-CS was then used for the preparation of AuNPs using the optimum condition previously identified for the synthesis of CS-AuNPs.

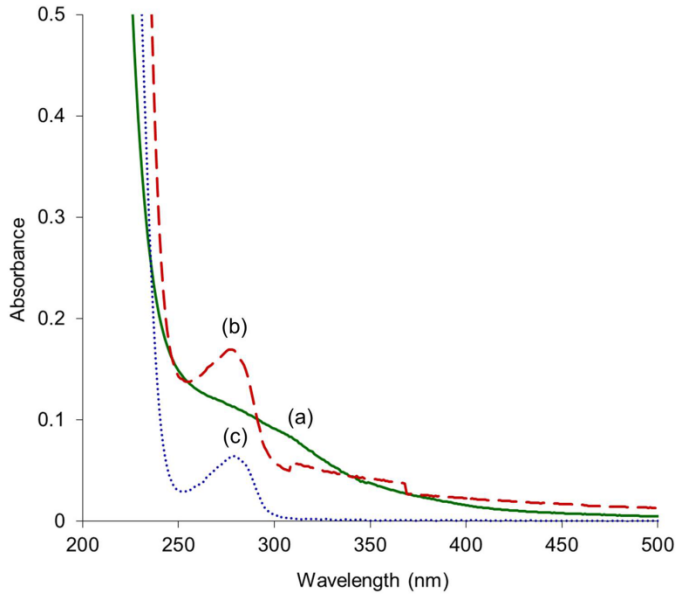

Figure 2.4 UV-vis absorption spectra of (a) SA-CS (green solid line), (b) BSA-CS (red dashed line) and (c) BSA (blue dotted line).

The sonication approach yielded BSA-CS-AuNPs with a mean particle size, PDI and ζ-potential of 286 nm, 0.436 and +19.9 mV, respectively, according to the PCS analysis. In addition to the commonly observed spherical morphology, the BSA-CS-AuNPs also appeared in the form of triangles, as can be seen in **Figure 2.5(a)**. In fact, it has been reported before that BSA can function as a structure directing agent to produce AuNPs with a triangular morphology under mild conditions [48]. For the spherical morphology, the core size of the BSA-CS-AuNPs was 8.2 ± 2.8 nm (n = 100). This dimension of the core, as analyzed by TEM, was apparently similar to that of the CS-AuNPs synthesized by the same method (9.1 ± 2.3 nm), but the hydrodynamic size, as determined by PCS, between BSA-CS-AuNPs (286 nm) and CS-AuNPs (56.6

nm) was enormously different (over five-fold) indicating that the BSA-CS-AuNPs had a very thick shell layer. This is quite reasonable considering that the chitosan was immobilized by the relatively larger molecules of BSA (MW = 66.5 kDa). The presence of the polymeric BSA-CS shell around the AuNPs can also be confirmed by AFM analysis, based on the fact that the organic layer of the BSA-CS is less dense and softer than the inorganic core of the AuNPs. **Figure 2.5(b)** clearly demonstrates the presence of BSA-CS surrounding the AuNPs. As can be seen from the 3D image on the right hand side, the core gold appears as protrusions with a greater height than the softer polymeric shell. It should be noted that the relative dimension of the core gold and polymeric shell may not correspond with the actual size, as measured by TEM and the hydrodynamic size analyzed by PCS. This may be explained by two reasons: (1) AFM analysis was performed under semi-dried conditions and (2) there was force applied during the measurement. According to the UV-vis analysis (**Figure A-6, Appendix A**), a typical plasmon resonance band of the as-synthesized BSA-CS-AuNPs at 531 nm slightly shifted to 537 nm upon storage for one month at 4°C, suggesting that the BSA-CS-AuNPs were quite stable.

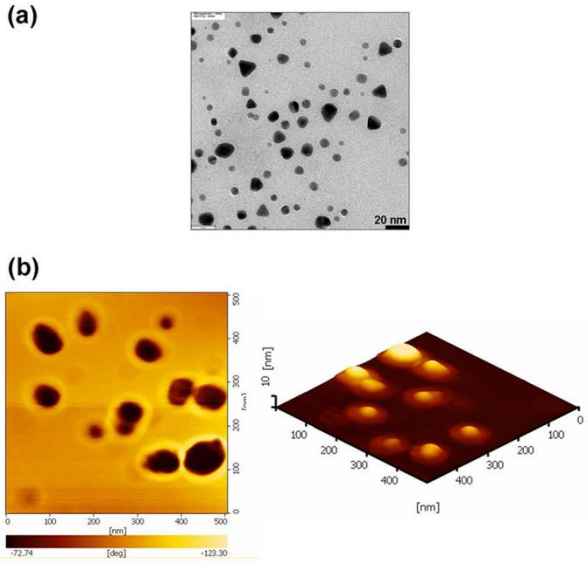

Figure 2.5 Representative (a) TEM and (b) AFM images of BSA-CS-AuNPs prepared by sonication using a BSA-CS:$HAuCl_4$ (v/v) ratio of 7:3 and 1.00% (v/v) Tween 80.

2.3.3 Detection of anti-BSA by BSA-CS-AuNPs

In this section, anti-BSA was used as the target molecule to be detected by the BSA-CS-AuNPs. In principal, two BSA molecules would typically bind one anti-BSA molecule. The specific interactions between BSA attached on the BSA-CS-AuNPs and anti-BSA should then lead to a change in chemical around the particles and eventually aggregation of the anti-BSA/BSA-CS-AuNP complex. **Figure 2.6(a)** shows the appearance of the BSA-CS-AuNPs solution after the addition of anti-BSA at various concentrations. The blank is BSA-CS-AuNPs in PBS solution without any anti-BSA. The minimum concentration of anti-BSA that could sufficiently induce aggregation of the BSA-CS-AuNPs as to be observed by naked eye was found to be 20 μg/mL (125 nM). This limit of detection is in close proximity to that (100 nM) previously reported based on AuNPs functionalized with BSA and determined by DLS [56]. This is impressive then, given that our detection was carried out without the requirement for instrumentation. In addition, we also found that the precipitates showed a red color instead of a violet color. It may be because the anti-BSA can induce the aggregation of the BSA-CS-AuNPs, but the vicinity between the AuNPs is not adequate to change the plasmon absorption band due to the fact that the synthesized AuNPs have a very thick shell layer. Therefore, the optical property of the AuNPs did not change.

To confirm that the aggregation was induced by specific interactions between BSA and anti-BSA, the BSA-CS-AuNPs were also treated with anti-IgG, a non-specific target molecule, at the same concentration as the anti-BSA (30 μg/mL). **Figure 2.6(b)** illustrates the appearance of the BSA-CS-AuNPs solutions two days after the addition of anti-BSA or anti-IgG antibodies (both in PBS), or just PBS (control). There was no evidence of aggregation of the BSA-CS-AuNPs upon an addition of the anti-IgG or the PBS control, implying that the binding of anti-BSA to the BSA-CS-AuNPs was the result of a specific antigen-antibody interactions. These results strongly indicate the potential of the synthesized AuNPs stabilized by biomolecule-modified chitosan for use in a chromogenic biosensor based on the aggregation of AuNPs.

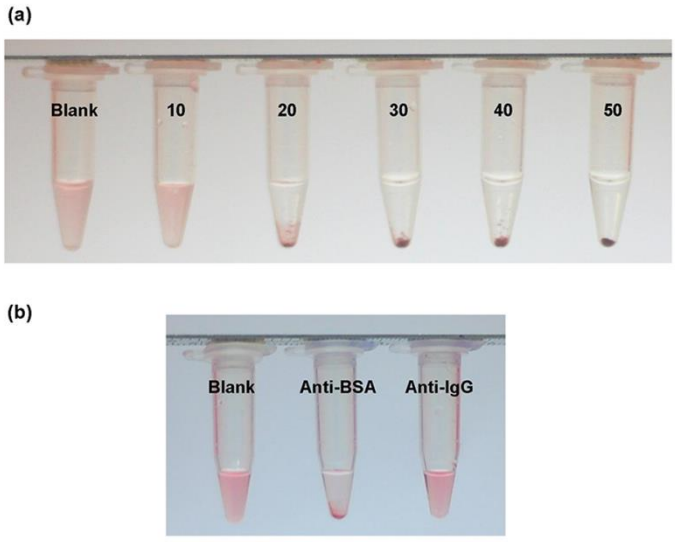

Figure 2.6 Appearance of BSA-CS-AuNPs solution after the addition of (a) anti-BSA at various (indicated) concentrations (μg/mL) and (b) PBS (blank), anti-BSA or anti-IgG (30 μg/mL).

2.4 Conclusions

In this paper, a green and non-destructive approach by using chitosan together with sonochemical method was chosen to prepare bio-functionalized AuNPs. Because chitosan could be used as both the reducing and stabilizing agent as well as provides amino groups as active sites for immobilizing biomolecules so that bio-functionalized AuNPs can be simultaneously done in a single step. The addition of Tween 80 which can act as both steric stabilizer and co-reducing agent was found to be necessary to provide reasonable rate of AuNPs formation. The AuNPs formed were mostly spherical with a diameter of 8.2 nm, although with some triangles, and can maintain their stability in aqueous solution for more than one month. The minimum concentration of anti-BSA that could induce the aggregation of BSA-CS-AuNPs that can be visualized by naked eye was 20 μg/mL (125 nM). BSA-CS-AuNPs were also tested with anti-IgG to confirm the specific interaction-induced aggregation. This research strongly indicates the potential of biomolecule-attached chitosan as

both a reducing and stabilizing agent for the green synthesis of AuNPs to be developed as a biosensor based on other antigen-antibody pair.

CHAPTER III

MULTIFUNCTIONAL POLYMER-STABILIZED GOLD NANORODS AS CARRIERS FOR PEPTIDE NUCLEIC ACID DELIVERY

3.1 Introduction

Currently, gene therapy is one of the effective ways for antigene and antisense applications. Oligonucleotides, such as deoxyribonucleic acid (DNA) [57, 58], small interfering RNA (siRNA) [59, 60] and peptide nucleic acid (PNA) [61, 62] can be used to silence gene expression. However, a major drawback that limits the gene silencing application is its low transfection efficiency into cell due to rapid degradation by nucleases, poor intracellular uptake, and inefficient endosomal escape. To overcome this limitation, delivery carriers, such as cell-penetrating peptide, dendrimer and metal nanoparticles are required and have been developed to achieve the efficient intracellular delivery [60, 63-65]. Among them, gold nanorods (AuNRs) are promising nanocarrier because they are nontoxic, biocompatible and easy to be surface-functionalized with therapeutics via reactive groups of stabilizing agent or thiol-gold interactions [59, 66-68]. Recently, it has also been reported that the elongated spherical particles can be taken up into cells more efficiently than spherical and hexagonal prism-shaped particles [69].

AuNRs can be synthesized via seed-mediated growth method in which cetyltrimethylammonium bromide (CTAB) is used as template to control particle shape. Inherent toxicity of CTAB coated on the AuNRs limits the bio-related applications of the CTAB-stabilized AuNRs. One effective approach to reduce the toxicity of the as-prepared AuNRs is to coat biocompatible (co)polymers on the AuNRs surface [57, 67, 68, 70, 71]. In addition to the enhanced stability and biocompatibility provided by the coated (co)polymer, multiple functions may be introduced to the AuNRs through appropriate selection of monomers to be incorporated in the (co)polymeric stabilizer. In particular, monomers containing reactive groups should be capable of covalently conjugating with oligonucleotides (i.e. neutral PNA) that cannot bind with the carrier through electrostatic interactions

or immobilizing molecules that can specifically react with targeted cells and thus minimizing possible side effects on non-targeted cells [72, 73]. Poly(ethylene glycol) (PEG) is one of the most common hydrophilic, water-soluble and biocompatible polymer employed for developing gene delivery system. Although the stability and biocompatibility of AuNRS can be improved by PEG coating, multiple reactive functional groups for covalent conjugation are limited because PEG has only one (or even none if methoxy PEG is used) functional group at its chain end. Zwitterionic polymers, especially poly(2-methacryloyloxyethyl phosphorylcholine) (PMPC) synthesized as biomimetics of phospholipids structure in cell membrane possess excellent biocompatibility [58, 74]. The presence of PMPC once employed as stabilizer for nanoparticles not only decreases toxicity, but also improves colloidal stability under physiological environment arising from high hydrophilicity of phosphorylcholine (PC) group [70, 75]. As compared with PEG, zwitterionic PMPC has previously shown superior characteristics in stabilizing gold nanoparticles [76] as well as suppressing toxicity of the AuNRs [70]. More interestingly, it has also been reported that PMPC-stabilized AuNRs possessed higher capability to be internalized by cancer cells than PEG-stabilized AuNRs [77]. This is a consequence of fast speed of cancer cells proliferation leading to the requirement for fast supplement of cholines from outside to make new cell membranes [78].

Peptide nucleic acid (PNA) is a DNA analog having negatively charged sugar-phosphate backbone of DNA totally replaced by an uncharged peptide-like backbone, originally developed by Nielsen and coworkers in 1991 [79, 80]. The diminished electrostatic repulsion between PNA and DNA backbones leads to a number of superior hybridization characteristics such as higher thermal stability, stronger affinity with less dependence on salt concentration, greater sequence specificity, and higher capability of strand invasion to double-stranded DNA [81]. The high specificity of PNA makes it an excellent molecule for DNA hybridization. Here in this research, we are particularly interested in the PNA system recently introduced by Vilaivan and co-workers, known as acpcPNA. Its conformationally rigid pyrrolidinyl PNA derived from D-prolyl-2-aminocyclopentane-carboxylic acid (acpc) backbones allows for the formation of PNA•DNA duplex with even higher affinity and specificity

than the original Nielsen's aegPNA. The acpcPNA has been widely used as a probe to detect DNA base sequence employing various techniques including MALDI-TOF mass spectrometry [82], quartz crystal microbalance (QCM) [83], surface plasmon resonance (SPR) [84-86], fluorescence spectroscopy [87], electrochemistry [88] and enzyme-based colorimetric assay [89]. The first antisense application of this acpcPNA system was recently reported by Arayachukiat *et al.* Employing oxidized carbon nanoparticles as carriers, a 12-base-long acpcPNA complementary to the antisense strand of the NF-KB binding site in the promoter region of the IL6 gene was delivered in the macrophage cell line, RAW 264.7 The accumulation of the acpcPNAs in the nucleus led to the decreasing of IL6 mRNA and IL-6 protein levels upon stimulation [90].

Taking advantages of AuNRs being carriers that can effectively be uptaken by cells being and tunable surface properties as a function polymer used as stabilizer, as well as potential antisense application of acpcPNA, this work aims to develop delivery system for acpcPNA based on AuNRs stabilized with multifunctional biocompatible polymer to the best of our knowledge, has never been reported before. In light of our recent success of using poly(methacrylic acid)-*ran*-(2-methacryloyloxyethyl phosphorylcholine) or PMAMPC as polymeric precursor layer for probe immobilization that exhibited excellent biocompatibility and antifouing properties for specific protein detection in dilute blood plasma using SPR technique [91], the same copolymeric system will be introduced as dual-functional stabilizer for AuNRs. The carboxyl groups from methacrylic acid (MA) units would act as active sites for PNA covalent binding whereas the 2-methacryloyloxyethyl phosphorylcholine (MPC) units would function as biomimetic hydrophilic entities that should provide biocompatibility and colloidal stability to AuNRs. PNA bearing 15 base pairs of which sequence is complementary to green fluorescence protein (GFP) gene is conjugated with the copolymer with tetrapeptide (-Gly-Phe-Leu-Gly-) linker. The degradation of this linker should be induced by Cathepsin B which is enriched in lysosome Intracellular uptaking and GFP silencing of the developed carriers by cathepsin B-overexpressing human liver cancer cell, HepG2, will be evaluated.

3.2 Materials and methods

3.2.1 Materials

Hydrogen tetrachloroaurate ($HAuCl_4 \bullet 3H_2O$), methacrylic acid (MA) (contains 250 ppm MEHQ as inhibitor, 99%), 4,4′-azobis(4-cyanovaleric acid) (ACVA), 4-cyano-4-(thiobenzoylthio)pentanoic acid (CPD), hydrazine monohydrate, cetyltrimethylammonium bromide (CTAB, 97%), L-ascorbic acid, cathepsin B, ethylenediaminetetraacetic acid disodium salt dehydrate (EDTA disodium salt), phosphate buffered saline pH 7.4 (PBS) and dialysis membrane (3.5 kDa MWCO) were purchased from Sigma-Aldrich (USA). 2-Methacryloyloxyethyl phosphorylcholine (MPC) was bought from NOF Corp. (Japan). Cysteamine hydrochloride, *N*-hydroxysuccinimide (NHS) and *N*-(3-(dimethylamino)propyl)-*N*′-ethylcarbodiimide hydrochloride (EDC) were obtained from Fluka (USA). Sodium borohydride ($NaBH_4$) and silver nitrate ($AgNO_3$) were purchased from Merck (Germany). Glutathione (GSH) was obtained from American Peptide company. 3-(4,5-Dimethylthiazol-2-yl)-5-(3-carboxymethoxyphenyl)-2-(4-sulfophenyl)-2H-tetrazolium (MTS) assay reagent composed of the electron coupling agent phenazine ethosulfate (PES) was obtained from Promega (USA). RPMI-1640 medium, penicillin-streptomycin (pen-step), sodium pyruvate and HEPES were bought from HyClone™ GE Healthcare (USA). Fetal bovine serum (FBS) was purchased from GIBCO™ Thermo Fisher Scientific (USA). MA was purified by vacuum distillation. All other materials were used as received without further purification. All solutions were made using ultrapure distilled water purified by using a Millipore Milli-Q system (USA) (18.2 MΩ cm resistance). Moreover, all glassware used for the synthesis of AuNRs were cleaned with freshly prepared aqua regia solution (HCl: HNO_3 at a (v/v) ratio of 3:1) and rinsed thoroughly with distilled water prior to use.

3.2.2 Characterizations

Synthesis and modification of PMAMPC were characterized by ^1H nuclear magnetic resonance (NMR) spectroscopy recorded on a Varian, model Mercury-400 NMR spectrometer (USA) operating at 400 MHz using D_2O as a solvent and fourier transform infrared (FT-IR) spectroscopy recorded on a FT-IR spectrometer (Nicolet,

USA), model Impact 6700 in a frequency range of 400–4000 cm^{-1} with 32 scans at resolution 4 cm^{-1}. Optical property of the synthesized AuNRs was measured by an Agilent 8453 UV-Vis spectrometer. Morphology and size of the synthesized AuNRs were visualized by transmission electron microscopy (TEM) on a JEOL Model JEM-2100 electron microscope operating at an acceleration voltage of 100 kV. For sample preparation, approximately 10 µL of AuNRs solution was dropped on the carbon-coated copper grid and dried in a desiccator overnight before measurement. Semafore software was used for measuring particle sizes and the average data was obtained from measurements of 50 random particles for each sample. The hydrodynamic diameter and zeta-potential (ζ) of AuNRs were determined by using a dynamic light scattering (DLS) instrument (Zetasizer Nano ZS, Malvern Instrument Ltd., UK) at 25ºC with a scattering angle of 173°. Immobilization and liberation of fluorescein-labeled PNA were studied by monitoring fluorescence signal recorded by a Cary Eclipse fluorescence spectrophotometer (Agilent Technologies, Inc., USA) in a scanning wavelength range of 504–800 nm.

3.2.3 Synthesis of gold nanorods (AuNRs)

AuNRs were synthesized via seed-mediated growth method according to previous report [57] with slight modifications. Firstly, Au seeds were formed at 27°C by mixing $HAuCl_4$ (1.6 mM, 1.12 mL) and CTAB (0.2 M, 2.50 mL) and then adding freshly prepared and cooled $NaBH_4$ aqueous solution (10.0 mM, 0.50 mL). After vigorous stirring for 2 min, the brownish solution was kept at 27°C for another 1 h to complete seed growth step. Then, AuNRs were grown from gold seeds by using CTAB as template as follows: growth solution was first prepared by mixing CTAB (0.2 M, 2.50 mL), $HAuCl_4$ (15.0 mM, 0.25 mL), freshly prepared $AgNO_3$ (4.0 mM, 0.14 mL) and Milli-Q water 2.0 mL. To this growth solution, freshly prepared ascorbic acid (78.8 mM, 62.0 µL) was added and the mixture was gently mixed and turned from yellow to colorless solution. Finally, 50.0 µL of gold seed solution was added and this solution was gently mixed for 1 min and kept constant at 27°C for 1 day. The deep red solution of AuNRs was finally obtained and kept at 4 °C.

3.2.4 Synthesis of thiol-terminated PMAMPC (PMAMPC-SH)

The overall stepwise procedure for polymerization and modification of the synthesized polymer is shown in **Scheme 3.1**.

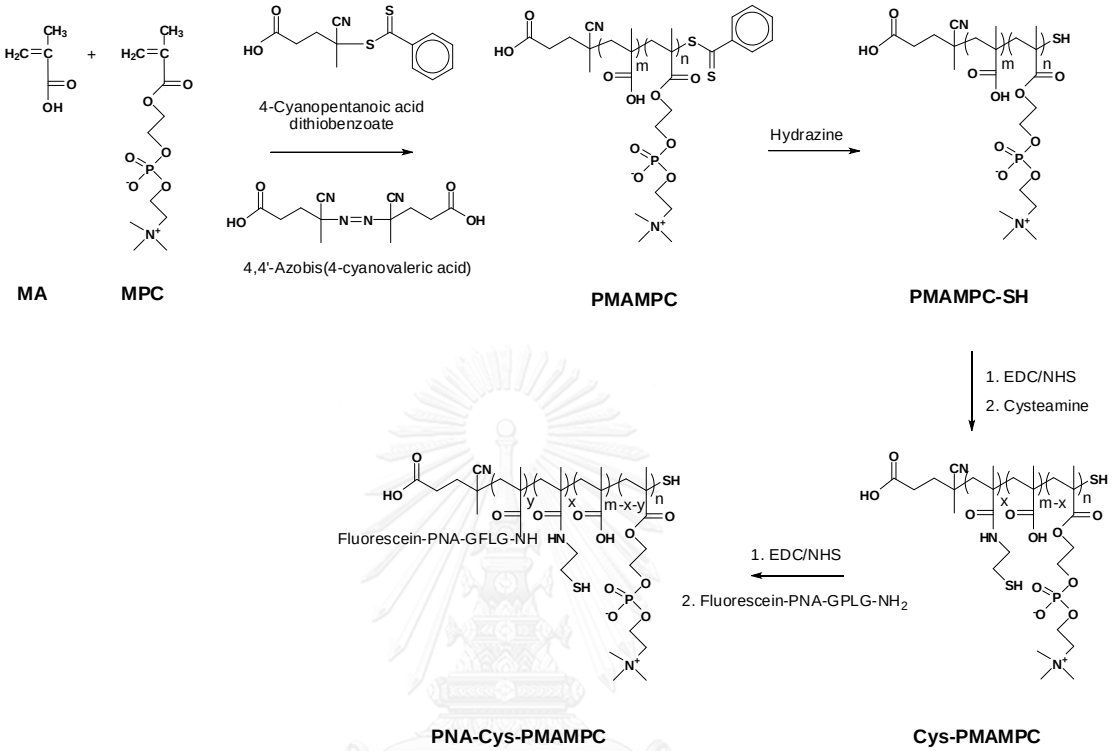

Scheme 3.1 Stepwise procedure for polymerization and modification of the synthesized polymer.

Reversible addition-fragmentation chain transfer (RAFT) polymerization is a conventional radical polymerization in the presence of a reversible chain transfer reagent (CTA). The CTA or RAFT agent such as dithioesters, thiocarbamates, and dithiocarbonates (xanthates), are used to trap the majority of the active propagating species into the dormant thiocarbonyl compound in the polymerization via a reversible chain-transfer process. This limits the possibility of termination steps by radical combination and disproportionation resulting in continuous propagating of polymer chain as well as well controlled polymerization. The desired molecular weight with low polydispersity can be obtained by controlling the concentration of initiator and CTA. PMAMPC with varying degree of polymerization (DP) and MA:MPC comonomer ratio were prepared by RAFT polymerization according to a method

modified from that of Akkahat *et al.* [91] MPC (442.9 mg, 1.50 mmol) and MA (190.6 µL, 2.25 mmol) were dissolved in 2.0 mL of mixed solvent (1:1 v/v, EtOH: 10 mM PBS). Then, the mixture was transferred to another vial containing ACVA (2.62 mg, 9.35 µmol) and CPD (10.46 mg, 37.4 µmol). The reaction mixture was degassed by purging with nitrogen gas for 30 min and then stirred in oil bath at 70 °C for 6 h. After polymerization, the polymer solution was opened to air to quench the reaction, purified by dialysis (MWCO 3,500 Da) against DI water for 3 days and lyophilized by a freeze dryer (model Freezeone 77520 Benchtop, Labconco, USA) to obtain a cotton-like orange powder. Because MPC is hygroscopic, PMAMPC was stored at -20°C until use. The condition mentioned above was used to prepare PMAMPC having targeted DP of 100 and 60:40 MA:MPC comonomer ratio. To prepare the polymer with different DP and comonomer ratios, the amount of all reagents was varied as shown in **Table 3.1**. To convert dithiobenzoate group at polymer chain end to thiol group for grafting onto AuNRs surface, an aqueous solution of PMAMPC (5.0 mM) was treated with hydrazine (30 mol equivalents of PMAMPC) at room temperature for 6 h or until the polymer solution became colorless. The final cotton-like white powder was obtained after purification by dialysis against deionized water for 3 days and lyophilization.

3.2.5 Modification of PMAMPC-SH with cysteamine (Cys-PMAMPC)

Some carboxyl groups in PMAMPC-SH were further modified with cysteamine to increase thiol groups and thus improve polymer grafting efficiency onto AuNRs surface. Cysteamine was attached to carboxyl groups in PMAMPC-SH via amidation by using EDC/NHS as coupling agents as follows: the aqueous solution of PMAMPC (5 % w/v, 4.0 mL, 0.55 mmol of MA units) was first activated by stirring with EDC (0.20 M) and NHS (0.05 M) at ambient temperature for 30 min. After activation step, cysteamine (0.1 mol equivalent of MA unit) was added and the mixture was stirred for 1 day. To obtain the final product, the modified polymer solution was dialyzed against deionized water for 3 day, lyophilized and kept at -20°C.

3.2.6 Immobilization of PNA on Cys-PMAMPC (PNA-Cys-PMAMPC)

The acpcPNA, *N*-Fluorescein-ATGAACTTCAGGGTC-Gly-Phe-Leu-Gly-LysNH_2-*C* composed of 15 mer sequences corresponding to green fluorescence protein (GFP) gene with tetrapeptide linker (-Gly-Phe-Leu-Gly-) being an enzymatic degradable linker was synthesized by solid phase peptide synthesis according to procedures described in literature [92]. Moreover, to be able to monitor PNA conjugation by fluorescence spectrometer, fluorescein was also attached at the N-termini of acpcPNA while still on the solid support by incubating the resin with NHS-fluorescein 2.0 mg in 20 µL of anhydrous DMF containing 2.0 µL of *N*-ethyldiisopropylamine (DIEA) in the dark for 3 days. After cleavage from the solid support, the crude PNA was purified by reversed-phase HPLC with UV detection at 260 nm equipped with Varian Polaris C18 analytical HPLC column (3 mm particle size 4.6×50 mm) using a gradient of 0.1% TFA in MeOH and 0.1% TFA in Milli Q water as eluent. The purified PNA was obtained after lyophilization and characterized by MALDI-TOF mass spectrometry (Microflex MALDI-TOF mass spectrometer, Bruker Daltonics).

After that, PNA was immobilized to Cys-PMAMPC via amide bond formation by reaction between amino groups in lysine at the C-termini of PNA and the remaining carboxyl groups in Cys-PMAMPC. The carboxyl groups in aqueous Cys-PMAMPC solution (10.0% w/v, 200 µL) were first activated with EDC (0.20 M) and NHS (0.05 M) at ambient temperature for 30 min. The PNA was then added (10.0 µM) and the reaction was stirred in the dark for 1 day. After purification by dialysis (MWCO 12,400 Da) against deionized water for 3 day, the solution was lyophilized to obtain the final product.

3.2.7 Preparation of AuNRs stabilized by Cys-PMAMPC (Cys-PMAMPC-AuNRs) and PNA-Cys-PMAMPC (PNA-Cys-PMAMPC-AuNRs)

Before surface modification**,** the synthesized CTAB-coated AuNRs were washed twice by centrifugation (Mikro 120, Hettich Lab Technology, USA) at 14,000 rpm for 20 min and resuspended in Milli-Q water to remove excess CTAB. Then, CTAB bilayer on AuNRs surface was replaced by the modified polymers via the stronger Au-S interaction using the following protocol according to the previous work [70] with

some modifications. In brief, to the sonicated polymer solution (3 mg in 1.0 mL of 10 mM PBS, pH 7.4), AuNRs solution (180 µg/mL, 500 µL) was added dropwise. The mixture was sonicated for 30 min at RT and incubated overnight. The obtained polymer-stabilized AuNRs were finally washed with Milli-Q water by two centrifugation cycles to remove unbound ligand and kept at 4°C. For PNA-Cys-PMAMPC-AuNRs preparation, it should be noted that the reaction was performed in the dark to prevent light exposure.

3.2.8 *In vitro* release of PNA from PNA-Cys-PMAMPC-AuNRs

Because of PNA sequence bearing cathepsin B cleavable tetrapeptide linker (-Gly-Phe-Leu-Gly-) and labeling with fluorescein, the selective PNA release can be fluorescently monitored. The PNA sequence was released from AuNRs surface by incubating the PNA-Cys-PMAMPC-AuNRs solution together with cathepsin B (1 u/mL) in freshly prepared phosphate buffer (0.1 M, 1.0 mL) containing 0.05 M NaCl, 1.0 mM EDTA disodium salt and 5.0 mM reduced glutathione (GSH) at 37°C for 1 day [93]. After PNA releasing, the AuNRs were precipitated and washed by three centrifugation cycles and the supernatant containing released PNA was collected. The amount of released PNA was determined by measuring the fluorescence emission of fluorescein in the total supernatant and then calculated from calibration curve of fluorescein at 525 nm. The percentage of PNA releasing was calculated from the relative ratio between the amount of released PNA and sum of released PNA and the remaining PNA on AuNRs surface as shown in the equation 2.1. The PNA remained on the AuNRs surface was obtained after AuNRs digestion in 0.05 M of KCN for 1 h.

$$\%\ PNA\ release = \frac{the\ amount\ of\ released\ PNA}{the\ amount\ of\ released\ PNA + the\ amount\ of\ remaining\ PNA\ on\ AuNRs} \times 100 \quad \text{equation 2.1}$$

3.2.9 Cytotoxicity test

HepG2 as liver hepatocellular cells were cultured in RPMI-1640 medium containing 10% of fetal bovine serum, 1 % of penicillin-streptomycin, 1 % of sodium pyruvate and 1% of HEPES at 37 °C under 5% CO_2 for 2 days. Cells were passaged and then cultured again in the same condition for another 2 days and passage 2 of

cell was used for experiment. To evaluate toxicity and biocompatibility, Cys-PMAMPC, PNA-Cys-PMAMPC, CTAB-AuNRs, Cys-PMAMPC-AuNRs and PNA-Cys-PMAMPC-AuNRs were comparatively studied by MTS cell viability assay. A 100 µL of cell suspension in RPMI medium (5,000 cells.well) was first plated onto 96-well plates and cultured for 24 h and then replaced with 100 µL of RPMI medium containing variable samples concentrations and maintained at 37 °C under 5% CO_2 condition for 24 h. Then, 10 µL of MTS solution was added. After incubating for another 4 h, the absorbance at 492 nm of the cell suspension in 96-well plates was determined by a microplate reader (Biochrom® Anthos 2010, UK) and data were analyzed using ADAP 2.0 Basic software. The absorbance of treated cell suspensions were subtracted with their blanks and compared to the untreated cell (assumed 100% cell viability) to achieve % cell viability.

3.3 Results and discussion

3.3.1 Polymerization and characterization of PMAMPC

Random copolymers of PMAMPC were prepared via RAFT polymerization using ACVA as radical initiator and CPD as chain transfer agent (CTA) as shown in **Scheme 3.1**. The method was capable of controlling molecular weight and comonomer composition. It can also provide thiol groups at polymer chain end that can act as anchoring group for grafting onto AuNRs surface. Degree of polymerization (DP) and copolymer compositions were varied by varying the ratio of [monomers]/[CTA] and mole fraction of monomers in the feed, respectively, while the ratio of [CTA]/[initiator] of 4 was fixed. **Figure 3.1** illustrates ^{1}H NMR spectra of the synthesized copolymer before and after reduction. All characteristic signals were consistent with our published paper [91] as follows: the signals of methyl protons (H_b and H_b'), methylene protons (H_a and $H_{a'}$), H_c, H_d, H_e and aromatic protons of dithiobenzoate group at polymer chain end (H_f) appear at 0.4-1.2, 1.6-2.2, 3.8-4.3, 3.4-3.6, 2.8-3.2 and 7.4-8.2 ppm, respectively. % Conversion was calculated from the relative ratio between the peak integration of methylene protons in polymer backbone at 1.6-2.2 ppm and sum of integral intensities of methylene protons in

polymer backbone and vinyl protons in the remaining monomer which appear at 5.5 ppm and 6.0 ppm as shown in equation B-1 in appendix B. The % conversions of all copolymers reached higher than 70% in 6 h of polymerization time. In addition, molecular weight (M_n) and the actual comonomer composition in copolymer could be also calculated from ^{1}H NMR spectra using the equation B-2 to B-6 in Appendix B. **Table 3.1** shows that the obtained DP and comonomer ratio in the copolymer were close to targeted DP and comonomer ratio in feed indicating well-controlled characteristic of RAFT polymerization.

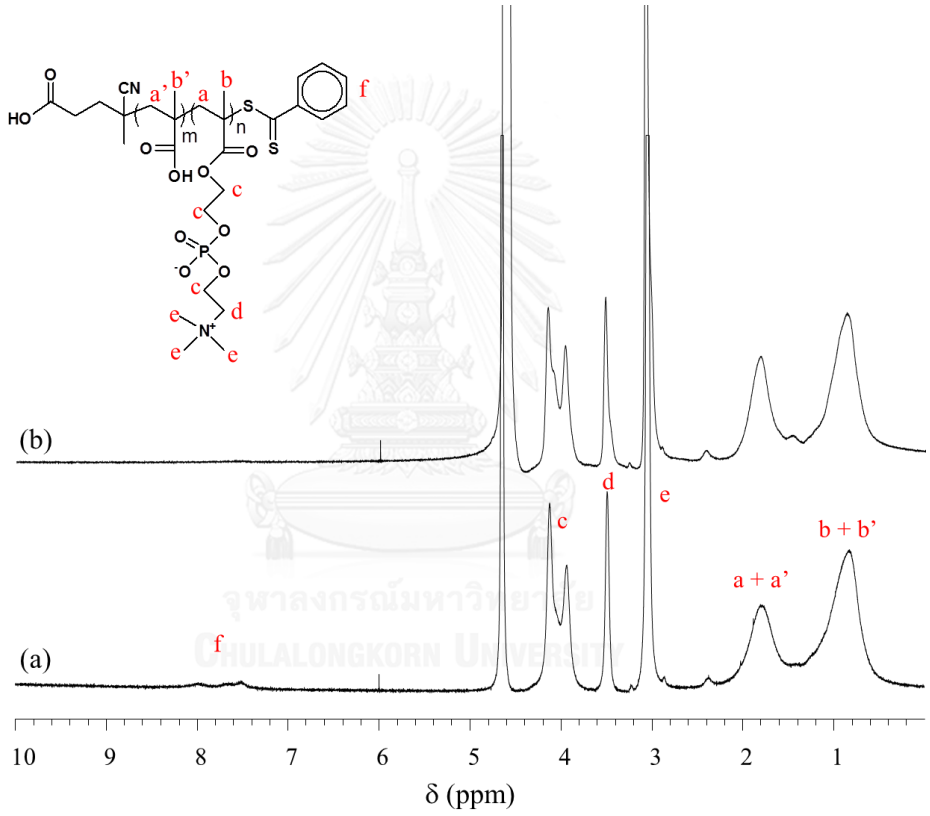

Figure 3.1 ^{1}H NMR spectra of (a) PMAMPC and (b) PMAMPC-SH.

Table 3.1 Molecular weight and comonomer composition of PMAMPC determined by ^{1}H NMR.

In feed			MA/MPC/CPD/ACVA (mmol)	In copolymer		
DP	M_n (Da)	MA:MPC composition		DP	M_n (Da)	MA:MPC composition
30	4744	70:30	1.31/0.56/0.0624/0.0156	40	6818	63:37
30	5999	50:50	0.94/0.94/0.0624/0.0156	33	6157	56:44
30	7255	30:70	0.56/1.31/0.0624/0.0156	37	9656	20:80
100	13070	80:20	2.99/0.75/0.0374/0.0094	106	15389	73:27
100	17254	60:40	2.25/1.50/0.0374/0.0094	92	17051	54:46
100	21438	40:60	1.50/2.25/0.0374/0.0094	90	22335	24:76

Upon treating the synthesized PMAMPC with hydrazine, cleavage of the terminal dithiobenzoate group at the PMAMPC chain end was verified by ^{1}H NMR spectra (**Figure 3.1**) and UV–vis spectroscopy (**Figure 3.2**). The signal of aromatic protons of dithiobenzoate group and the absorption band corresponding to the dithiobenzoate group around 300 nm disappear after hydrazine treatment confirming that the terminal dithiobenzoate groups were converted to thiol groups. The success of polymer reduction, as well as thiol group formation could also be verified again by the appearance of polymer which changed from pink to white material as a result of dithiobenzoate group removal (**inset of Figure 3.2**).

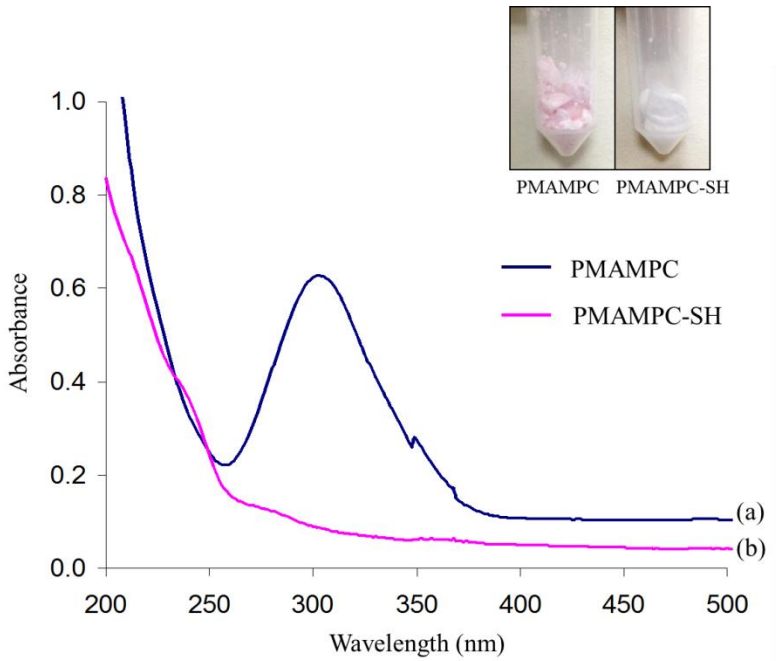

Figure 3.2 UV-vis spectra of (a) PMAMPC and (b) PMAMPC-SH.

3.3.2 Preparation and characterization of Cys-PMAMPC-AuNRs

AuNRs were synthesized by a seed-mediated growth method using CTAB as template. UV-vis spectrum of the as-synthesized CTAB-AuNRs shows the transverse and longitudinal plasmon bands at 500–600 and 700–800 nm, respectively (**Figure 3.3**). The morphology and size were also visualized by TEM (**Figure 3.4**). Obviously, well-defined AuNRs with a narrow size distribution of 24.6 ± 3.2 nm in length and 8.5 ± 1.4 nm in width (aspect ratio of 2.9) were obtained. Then, thiol-terminated PMAMPC was directly grafted onto AuNRs surface through sulfur–gold interaction. It is well known that the aggregation of the particles arising from surrounding dielectric constant change might occur after surface modification which can lead to lower stability of the particles. Therefore, to obtain highly stable polymer-stabilized AuNRs, the effects of molecular weight and comonomer composition of PMAMPC were studied and the results are presented in **Figure 3.3**. It was found that only absorption spectra of AuNRs grafted with PMAMPC having DP of 100 and MA:MPC of 30:70 and 50:50 were not broadened and red-shifted suggesting insignificant particles aggregation. This outcome suggested that the copolymer with DP of 30 is not large

enough to provide steric stabilization to the AuNRs. Also, the hydrophilic MPC composition in the copolymer has to exceed 50% in order for the AuNRs to be well dispersed in aqueous solution without aggregation. These findings were also consistent with TEM images showing that well-dispersed AuNRs were only obtained from the two conditions mentioned above (**Figure 3.4**). Because some carboxyl groups of MA units have to be further functionalized with cysteamine and PNA, PMAMPC-AuNRs of DP = 100 with higher MA unit (MA:MPC of = 50:50) (having size of 26.5 ± 3.8 nm in length, 8.2 ± 1.2 nm in width and aspect ratio of 3.2) were then selected for further study.

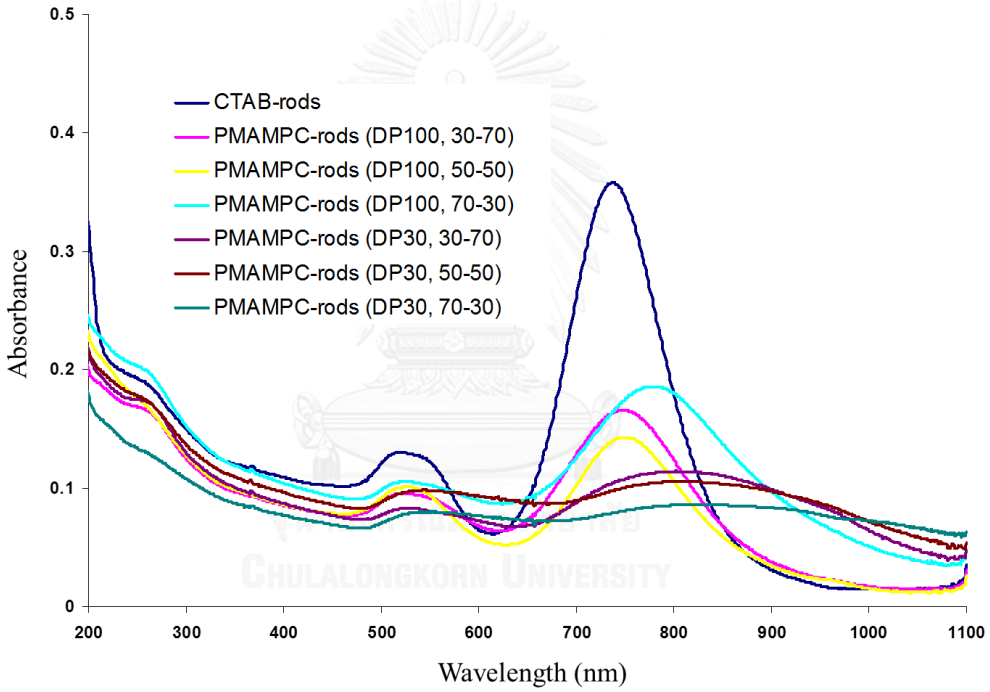

Figure 3.3 UV-vis spectra of PMAMPC-stabilized AuNRs prepared from PMAMPC having varied DP and comonomer composition in comparison with CTAB-AuNRs.

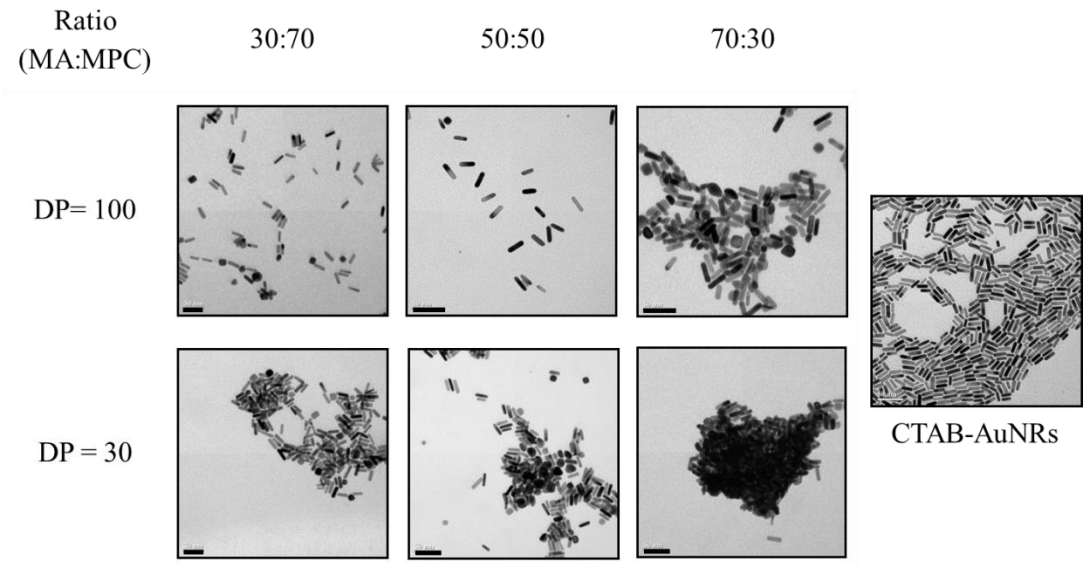

Figure 3.4 TEM images of PMAMPC-stabilized AuNRs prepared from PMAMPC having varied DP and comonomer composition in comparison with CTAB-AuNRs (scale bar: 50 nm).

Previously, compact grafting via the formation of loops-and-trains conformation of polymer ligand has provided metal nanoparticles with excellent colloidal stability [94, 95]. Multidentate polymers which can be prepared by modifying anchoring site such as thiol and amine functional groups onto structure's polymer ligand have been mainly used for this purpose. Based on this concept, herein, some carboxyl groups in MA units were converted to thiol groups by modifying with cysteamine (0.10 mol equivalent) to achieve highly stable AuNRs for using in complex biorelevant media. The success of thiol modification could be confirmed by FTIR spectroscopy as shown in **Figure 3.5**. Before modification, FTIR spectrum reveals characteristic absorption bands of both MPC and MA units at 1706 cm^{-1}, 1162 cm^{-1}, 1222 cm^{-1}, 1056 cm^{-1} and 962 cm^{-1} corresponding to C=O stretching of carboxyl and ester groups, C-O stretching of carboxyl group, C-O stretching of ester group, P-O stretching and -$N^{+}(CH_3)_3$ stretching, respectively. As compared with PMAMPC, the appearance of N-H bending at 1544 cm^{-1} together with shoulder of the C=O stretching peak at 1650 cm^{-1} of amide group in the cysteamine-modified PMAMPC could be used as evidences to confirm the success of amidation. In addition, % immobilization of cysteamine could

be calculated from FTIR spectrum by comparing an area of new N-H bending peak at 1544 cm^{-1} with an area of C=O stretching of carboxylic, ester and amide groups at 1600-1800 cm^{-1} representing the total units. Based on this calculation, the obtained % cysteamine immobilization was found to be 3.8%. This value was close to the initial cysteamine in feed (5.0%). Notably, 0.1 mol equivalent of MA units was equal to 0.05 mol equivalent of total units when 50:50 MA:MPC comonomer ratio was used.

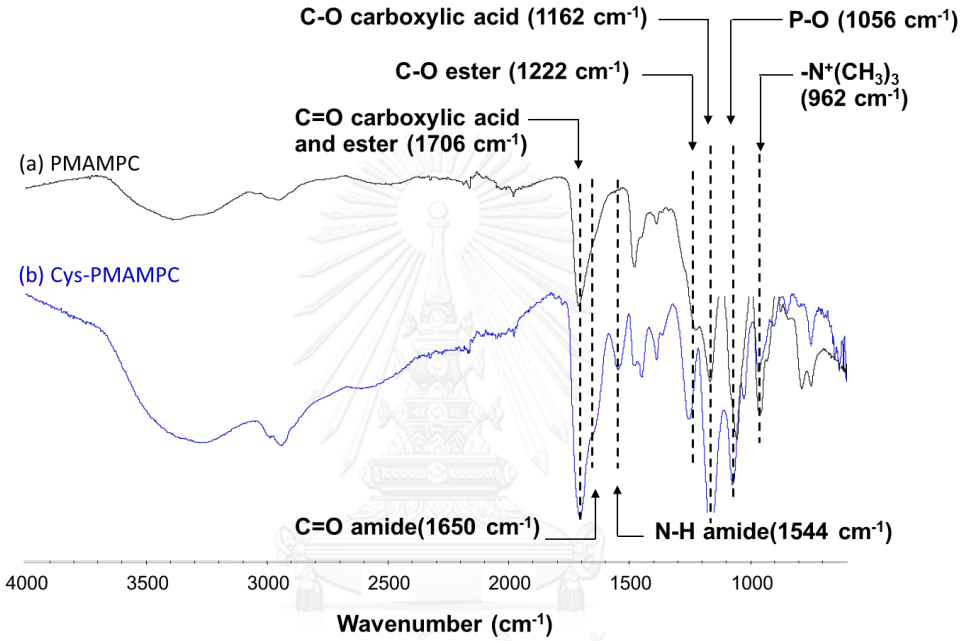

Figure 3.5 FTIR spectra of (a) PMAMPC and (b) Cys-PMAMPC.

In contrast to AuNRs stabilized by PMAMPC without cysteamine modification, Cys-PMAMPC-stabilized AuNRs showed superior stability considering from good dispersion of particles without any aggregations in 10 mM PBS as well as in RPMI media, as a complex medium used for cell culture, when visualizing by naked eye (**Figure 3.6 (a) and (b)**). This observation was also consistent with the previous published work which showed that about 3.6 thiol groups in a single ligand molecule is nearly optimal for stabilization of quantum dots in water [94].

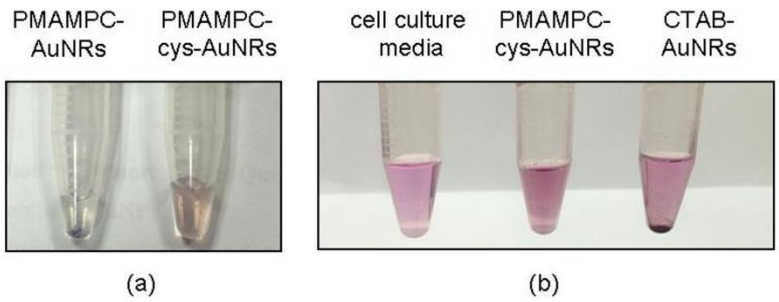

Figure 3.6 Digital images of polymer-stabilized AuNRs dispersed in (a) 10 mM PBS and (b) RPMI-1640 medium.

3.3.3 Preparation and characterization of PNA-Cys-PMAMPC-AuNRs

The synthesis of acpcPNA could be verified by mass spectrometry. As shown in **Figure 3.7**, the observed m/z of 5,961.93 being very close to the calculated m/z (5960.79) confirms that acpcPNA with desired sequence was successfully prepared.

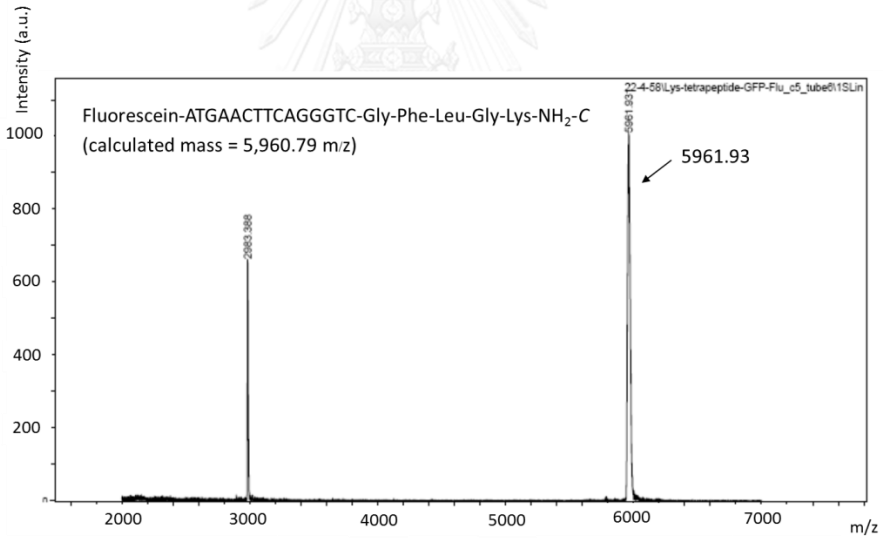

Figure 3.7 Mass spectrum of acpcPNA corresponding to GFP gene.

PNA-modified PMAMPC was first synthesized and then grafted onto CTAB-AuNRs. The sequential modification of PMAMPC with cysteamine and PNA was evaluated by FTIR analysis (**Figure 3.8**). The appearance and increment of N-H bending of secondary amide at 1544 cm^{-1} after cysteamine and PNA immobilization, respectively, as well as the increment of % of the area of N-H bending peak as

compared with that of C=O stretching due to carboxylic, ester and amide groups from 3.8 to 9.1% after PNA immobilization implied the success of both chemical modification steps.

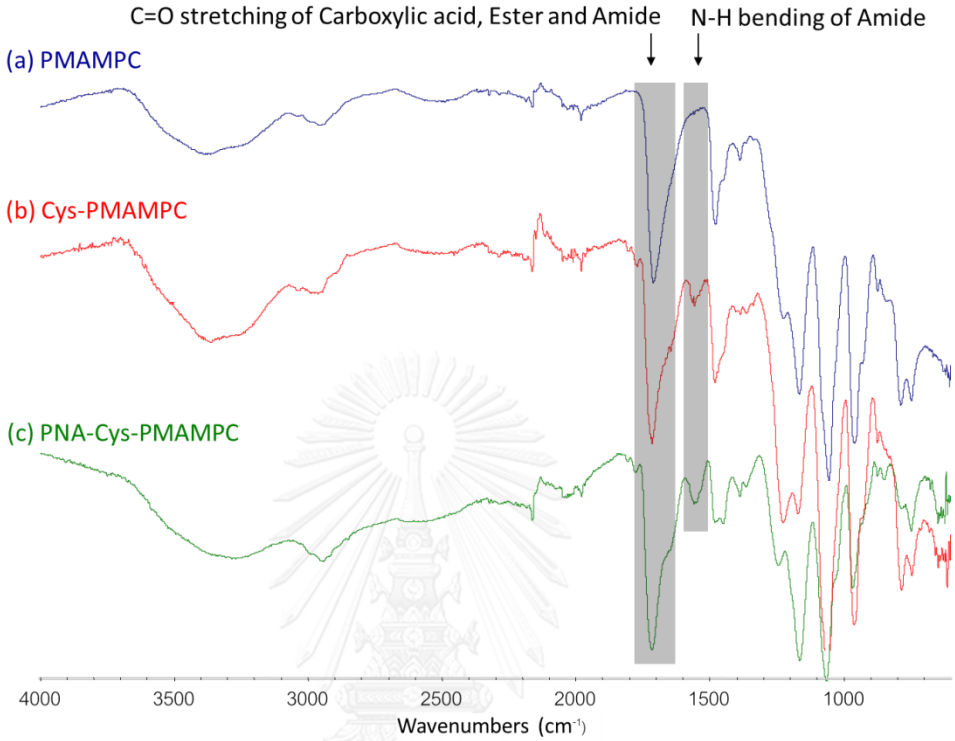

Figure 3.8 FTIR spectra of (a) PMAMPC, (b) Cys-PMAMPC and (c) PNA-Cys-PMAMPC.

The morphology and size of AuNRs stabilized by the modified PMAMPC were characterized by TEM (**Figure 3.9**). As compared with the as-synthesized CTAB-AuNRs, well-dispersed AuNRs with similar aspect ratio were obtained after polymer grafting. Furthermore, to confirm the presence of polymeric shell around AuNRs, hydrodynamic size and ζ-potential were also measured by DLS (**Table 3.2**). In contrast to the as-prepared CTAB-AuNRs, charges on AuNRs after grafting with Cys-PMAMPC and PNA-Cys-PMAMPC appeared in a negative range, as well as the hydrodynamic radius was significantly increased. These observations were reasonable to assume the surrounding of the modified PMAMPC on AuNRs that could act as effective stabilizing layer providing highly stable functionalized AuNRs.

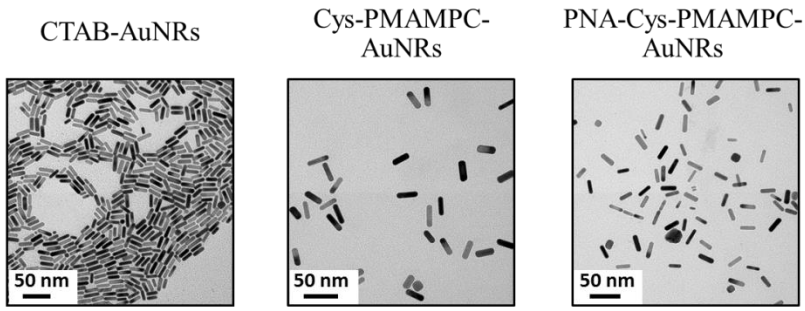

	CTAB-AuNRs	Cys-PMAMPC-AuNRs	PNA-Cys-PMAMPC-AuNRs
Length (nm)	24.6 ± 3.2	27.9 ± 2.8	26.0 ± 3.0
Width (nm)	8.5 ± 1.4	8.7 ± 1.1	8.3 ± 1.3
Aspect ratio	2.9	3.2	3.1

Figure 3.9 TEM images of AuNRs stabilized by (a) CTAB, (b) Cys-PMAMPC and (c) PNA-Cys-PMAMPC.

Table 3.2 Size and ζ-potential values of as prepared CTAB-AuNRs and AuNRs stabilized by the modified PMAMPC as determined by DLS.

	CTAB-AuNRs	Cys-PMAMPC-AuNRs	PNA-Cys-PMAMPC-AuNRs
Size (nm)	19.9 ± 0.8	154.6 ± 4.4	178.1 ± 27.0
ζ-potential (mV)	38.2 ± 2.0	-16.1 ± 0.8	-20.9 ± 1.4

The presence of PNA on AuNRs and the amount of immobilized PNA could be evaluated by fluorescence spectroscopy by monitoring the fluorescein emission at PNA chain end. As shown in **Figure 3.10**, there was no emission signal arising from PNA-immobilized AuNRs because of the overlapping between transverse absorption of AuNRs at 500-600 nm and fluorescence emission of fluorescein at 525 nm resulting in fluorescence quenching of fluorescein by AuNRs. Interestingly, after AuNRs digestion by KCN, the fluorescence of fluorescein was obviously turned on confirming the presence of PNA on the AuNRs surface. Based on the calibration curve of fluorescein at 525 nm (**Figure 3.11**), the amount of immobilized PNA was found to be 1.39×10^{14} probe/cm^2. This value is two times higher than that (6.6×10^{13} probe/cm^2) obtained via DNA immobilization on poly(ethylene glycol methacrylate)-

stabilized magnetic nanoparticles by click chemistry previously reported [73] demonstrating that this method is quite effective for oligonucleotide immobilization.

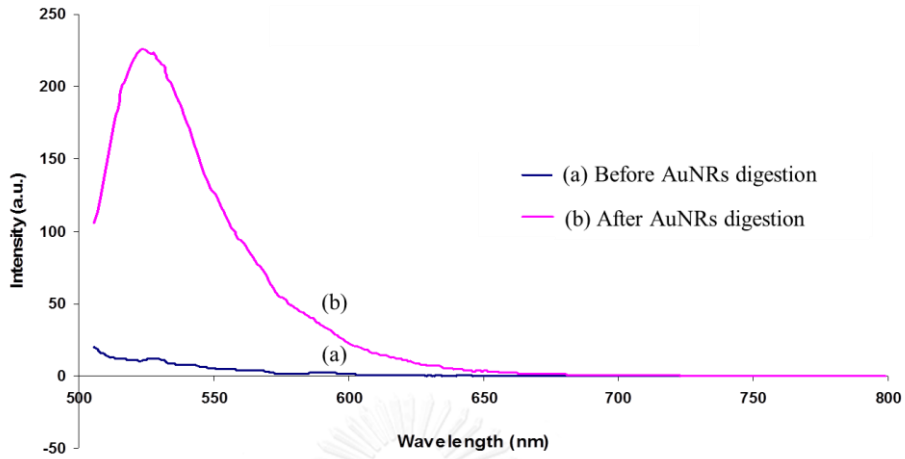

Figure 3.10 Fluorescence spectra of PNA-Cys-PMAMPC-AuNRs (a) before and (b) after AuNRs digestion with KCN.

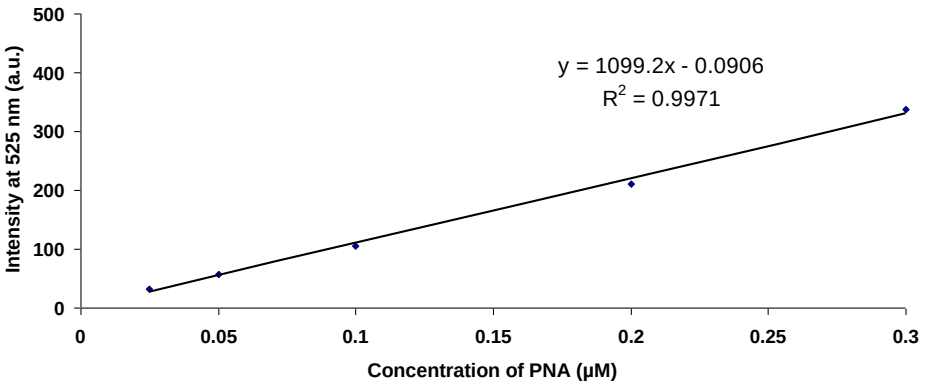

Figure 3.11 Calibration curve of PNA plotted by using fluorescence signal of fluorescein at 525 nm.

As mentioned above, PNA sequence was connected to PMAMPC through the cathepsin B degradable tetrapeptide linker (-Gly-Phe-Leu-Gly-) to provide selective release. *In vitro* enzymatic release was first investigated to obtain the optimal condition. **Figure 3.12** displays the fluorescence signal of the released PNA in supernatant as well as the signal from the remaining PNA on AuNRs obtained after AuNRs digestion. Based on the calibration curve in **Figure 3.11**, % PNA releasing was

found to be 22.9 % with releasing time of 1 day. This quite slow releasing agreed with the previous work [96]. In that particular research, cell penetrating peptide Tat was used as a carrier for the doxorubicin (DOX) release. DOX was conjugated with the peptide via the tetrapeptide linker. The release rate was found to decrease with the increasing number of DOX per peptide. Thus, the peptide conjugated with four DOX displayed the slowest release rate (40% in 8 h) implying that the retarded release may primarily be caused by the steric hindrance that limited the cathepsin B accessibility to the tetrapeptide linker.

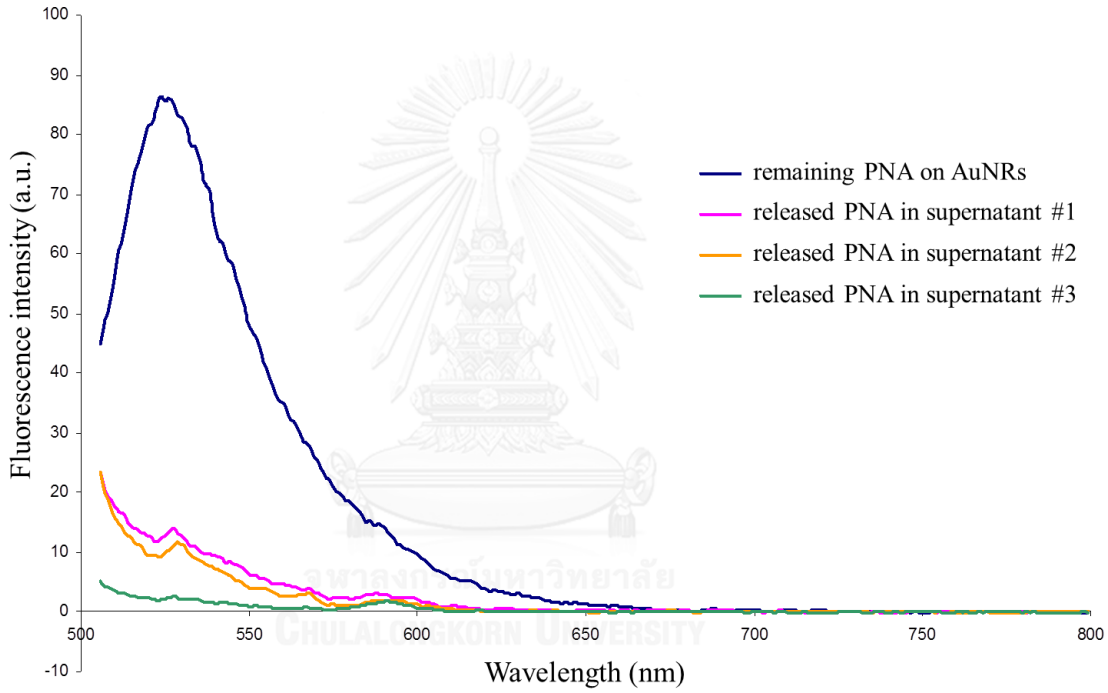

Figure 3.12 Fluorescence spectra of released PNA in washing supernatants (3 times) and remaining PNA on AuNRs.

3.3.4 Cytocompatibility test

Inherent toxicity of CTAB coated on the AuNRs limits the use of these particles for bio-related applications. To investigate whether the toxicity of CTAB-coated AuNRs would be reduced after replacing CTAB with the modified PMAMPC ligand, % cell viability of HepG2 cell after incubation with Cys-PMAMPC-AuNRs and PNA-Cys-PMAMPC-AuNRs was evaluated and compared with the CTAB-AuNRs as negative

control and Cys-PMAMPC and PNA-Cys-PMAMPC without AuNRs as positive control. **Figure 3.13** illustrates that all samples, except CTAB-AuNRs, were non-toxic for the concentration up to 50 μg/mL suggesting that the toxicity of AuNRs could be improved after polymer grafting. On the other hand, the CTAB-AuNRs clearly exhibited toxicity when the concentration was raised above ~25 μg/mL. In agreement with the former report, similar concentration of AuNRs coated with poly(acrylic acid) that provided non-toxicity on SW 1222 cell line have been observed [71].

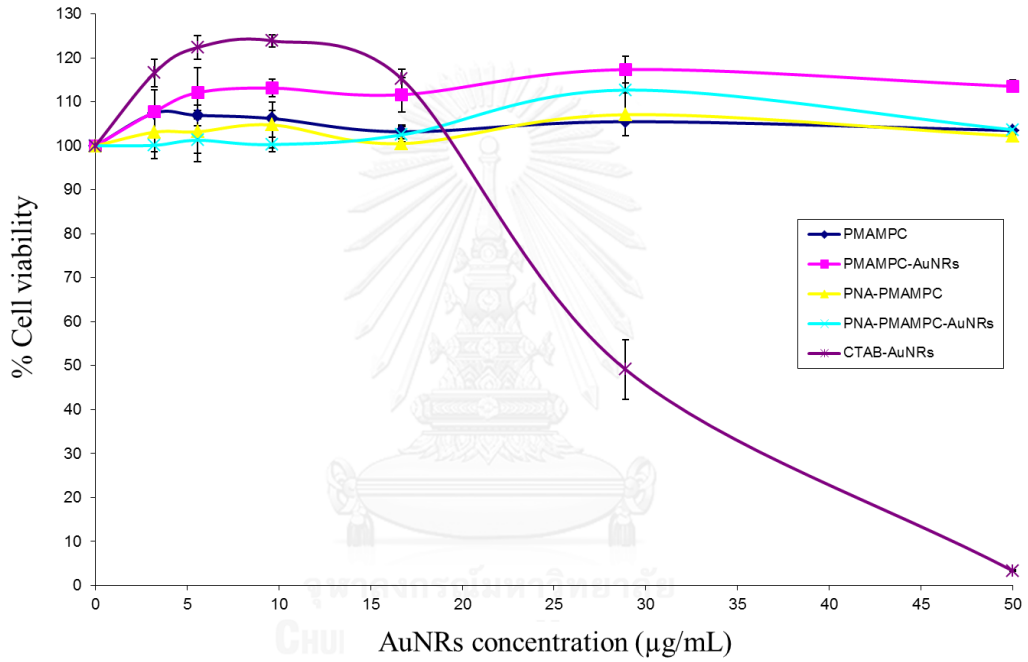

Figure 3.13 Cell viability of HepG2 cells after incubation with AuNRs stabilized by the modified PMAMPC as determined by MTS assay.

3.4 Conclusions

In summary, multifunctional copolymer-stabilized gold nanorods have been developed as nanocarrier for PNA delivery system. By using PMAMPC as polymeric stabilizer, carboxyl groups from MA units could be used as active sites for PNA conjugation whereas MPC units provided biocompatibility and colloidal stability for

AuNRs. The modification of thiol groups to prepare multidentate PMAMPC copolymer ligand was found to be necessary to achieve AuNRs with superior stability in 10 mM PBS as well as in complex cell culture media which is therefore suitable for bio-applications. The PNA-immobilized AuNRs were also successfully prepared by using PNA-Cys-PMAMPC as stabilizer. The AuNRs formed were highly stable with PNA grafting density of 1.39×10^{14} probe/cm^2. Based on *in vitro* selective release that can be induced via degradation of tetrapeptide linker in the presence of cathepsin B in, 22.9 % PNA releasing was obtained. In contrast to the as-prepared CTAB-AuNRs, the toxicity of AuNRs after polymer grafting on HepG2 cell could be suppressed demonstrating the potential application of the developed AuNRs for bio-related application. For the future work, the PNA releasing and gene silencing in HepG2 cells will be evaluated to determine the possibility to use the developed carriers for antisense applications.

CHAPTER IV
ANTIFOULING AND ANTIBACTERIAL PATTERNED SURFACES PREPARED FROM SILVER-BACKFILLED ZWITTERIONIC COPOLYMER FILMS

4.1 Introduction

Adhesion and subsequent proliferation of bacteria or biofilm formation on any surfaces can lead to bacterial infections occurring in medical devices, such as surgical equipments, catheters, implants, contact lenses, and artificial organs which may result in the loss of function of the devices, as well as infection of the patient. Moreover, microorganisms in biofilms have also been found to be up to 1000 times more antibiotic resistance than non-biofilm microorganisms [97, 98]. To overcome these problems, the prevention of bacteria adhesion in an early stage is necessary. In general, there are two approaches for preparing anti-biofilm surface. One is to prevent an initial adhesion of bacteria by coating with anti-adhesive molecules, for example, poly(ethylene glycol)(PEG)-based copolymer [99], polyzwitterion [100], pH-responsive polymer [101], as well as small molecule [102] that can inhibit the growth of biofilm through disruption of bacterial cell-cell communication, known as "quorum sensing". The other is coating of bactericidal agents, such as quaternary ammonium-containing polymer [98, 103] and different forms of silver such as, ion [104], nanoparticles [105] and film [106] which are well recognized to work through both release-killing and contact-killing mechanisms. It has been recently reported that more effective biofilm resistance can be attained by combining the two approaches. With its well-recognized antifouling activity, PEG was combined with quaternary ammonium group [107] or silver nanoparticles (AgNPs) [108, 109] to achieve dual functional surfaces. Sileika *et al.* [108] imparted antifouling and antimicrobial properties to polycarbonate substrates. By using polydopamine dip-coating method, antifouling PEG and *in situ* generated AgNPs nucleated from a silver salt solution were grafted on polydopamine primer film-coated substrates. These novel surfaces showed dual antifouling and antimicrobial performance against both gram-positive and gram-negative bacterial strains. Although PEG has been widely

used for antifouling propose, its autooxidative degradation due to the presence of ether groups and terminal hydroxyl groups resulting in aldehyde and carboxylic acid production limits its use in some applications [110]. Zwitterionic polymers, especially poly(2-methacryloyloxyethyl phosphorylcholine) (PMPC) synthesized as biomimetics of phospholipids structure in cell membrane possess excellent biocompatibility and biofouling resistance [74]. Antifouling characteristic of PMPC relies on hydration layer formed by strong H-bonding between zwitterionic phosphorylcholine and water that leads to the prevention of non-specific adhesion [111]. Because of its lower cytotoxicity as compared with PEG [70], PMPC has emerged as alternative to PEG. Its application for generating dual antifouling and antimicrobial surface has been recently described by Wang *et al.* [112] Bio-inspired terpolymer containing dopamine methacrylamide (DMA) was synthesized as anchoring group for substrate adhesion whereas 2-(dimethylamino)-ethyl methacrylate (DMAEMA) and MPC have been incorporated as bactericidal cations for contact killing and antifouling resistance. The resulting terpolymer, P(DMA-*co*-MPC-*co*-DMAEMA) were coated onto the substrate surface by a simple one-step self-assembly method. The surface-coated terpolymer was able to kill both gram-positive and gram-negative bacteria and effectively released the adhered bacteria from the surface. Fuchs *et al.*[113], on the other hand, reported surface coated with poly(hydroxyethyl methacrylate-*co*-2-methacryloyloxyethyl phosphorylcholine) (p(HEMA-*co*-MPC)) film embedded with non-leaching AgNPs. This bio-inspired hybrid film provided antifouling activity, as well as antibacterial activity (99.9%) after incubation. Based on the agar diffusion tests where inhibition zone could not be seen, it was reasonable to conclude that most of the Ag was conserved in film thus providing a material with long-term antibacterial efficacy against *E. coli.* via contact active mechanism.

Taking the advantage of PMPC being capable of providing biocompatibility and biofouling resistance together with the concept to impart dual antifouling and antibacterial functions on the surface, it would be highly beneficial if this hybrid film can be prepared in a pattern format. This type of design, to the best of our knowledge, has never been reported. The ability to proportionally tune the

antifouling and antibacterial area on the surface would allow for the correlation of both characteristics and the biofilm resistance to be established.

Surface-patterned PMPC generally relies on covalent grafting via silane chemistry which is quite complicated to perform, only limited to inorganic substrates such as glass, silicon wafer [114-117] and not applicable for soft organic materials required for some medical devices. For example, catheters and contact lenses are generally made from poly(dimethylsiloxane) (PDMS). To overcome such obstacles, there are a few literatures describing the simple universal coating method without grafting process that can be implemented on any surfaces. Enomoto *et al.* [118] prepared random copolymer, p(MMA/DMAB) composed of methyl methacrylate (MMA) and 2,2-dimethoxy-1,2-di(4-methacryloyloxy)phenylethane-1-one (DMAB) by free radical polymerization and then spin-coated on quartz glass. DMAB unit can simultaneously act as a crosslinkable monomer and photoradical initiator to graft PMPC onto p(MMA/DMAB) film-modified surface via photo-cleavage of the DMAB. By using a photomask to obtain selective UV-irradiated sites, PMPC pattern on (MMA/DMAB) film could be successfully generated. Kuroda *et al.* [119] synthesized diblock copolymers, $PMPC_{120}$-*b*-$P(TSM/CEA_x)_y$) containing PMPC block and random copolymer block of 3-(tris(trimethylsiloxy)silyl)propyl methacrylate (TSM) and 2-cinnamoylethyl acrylate (CEA) via reversible addition–fragmentation chain transfer (RAFT) polymerization. A thin film of this diblock copolymer was formed on PDMS substrate by using physical adsorption of TSM units and photo-crosslinking of CEA units. By applying a photomask, only the area that was irradiated with UV was selectively crosslinked to improve the coating stability and thus PMPC pattern on PDMS was obtained.

In this study, we have developed a simple coating method for preparing crosslinked and patterned PMPC on silicon wafer surface by using a copolymer consisting of MPC and the methacrylate of dihydrolipoic acid (DHLA), poly(MPC-DHLA). This copolymer was synthesized and previously employed for surface functionalization of gold nanorods via gold-sulfur interaction. Thiol groups in DHLA serve as crosslinkable units via thiol-ene click reaction in the presence of alkene molecule to obtain stable polymer film on the surface. Antifouling PMPC patterns

are then generated by using photolithography method with negative lift-off photoresist of which stepwise procedure is schematically described in **Scheme 4.1**. To prepare dual functional patterned surface with both antifouling and antibacterial characteristics, silver film is chosen as bactericidal platform to be backfilled on PMPC pattern by metal evaporation method. Responses of *E.coli*, to the patterned PMPC/Ag are then evaluated

4.2 Materials and Methods

4.2.1 Materials

2-Hydroxyethyl methacrylate (HEMA), 4-(dimethylamino)pyridine (DMAP), (±)-α-lipoic acid (LA), 2-methacryloyloxyethyl phosphorylcholine (MPC), 4,4′-azobis(4-cyanovaleric acid) (ACVA), 4-cyano-4-(thiobenzoylthio)pentanoic acid (CPD), sodium borohydride, 2,2-dimethoxy-2-phenylacetophenone (DMPA) and 1,3,5-triallyl-1,3,5-triazine-2,4,6(1*H*,3*H*,5*H*)-trione were purchased from Sigma-Aldrich. 2,2,2-Trifluoroethanol (TFE) (99+%) was obtained from Alfa Aesar. Spectra/Por®7 dialysis membrane (3.5 kDa MWCO, pretreated RC tubing) was bought from VWR Scientific. *N*-(3-(dimethylamino)propyl)-*N′*-ethylcarbodiimide hydrochloride (EDC) was purchased from TCI Chemical. Negative lift-off photoresist, NR9-1000PY, and resist developer, RD6, were obtained from Futurrex, Inc. Quartz photomask (4 inch) was bought from Benchmark Technologies, Inc. Silver (purity: 99.99%) and titanium (purity: 99.995%) pallets were purchased from Kurt J. Lesker company. MPC was purified by stirring in anhydrous diethyl ether and then filtrating to remove inhibitor and stored at 4 °C. All other materials were used as received without additional purification.

4.2.2 Characterizations

^{1}H nuclear magnetic resonance (NMR) spectra were recorded on a Bruker 500 spectrometer operating at 300 MHz. Molecular weights of the synthesized poly(MPC-DHLA) were analyzed by GPC in TFE with 20 mM sodium trifluoroacetate at 40 °C using an Agilent 1200 system equipped with an isocratic pump operated at 1 mL/min, a degasser, an autosampler, a Polymer Standards Service (PSS) PFG guard column (8x50 mm), 3 PSS PFG analytical linear M columns (8x300 mm, particle size 7

μm), and a refractive index detector. PMMA standards (1.5-250 kDa) were used for generating a calibration curve. Thickness of polymer film was measured by using a Gaertner LSE stokes ellipsometer (632.8 nm He Ne Laser at a fixed incidence angle of 70°). Gartner Ellipsometry Program (GEMP) was used as software. The refractive index (n) of organic layer on silicon wafer was assumed to be 1.5 while n of silica layer on Si wafers was 1.46. Optical and fluorescence images of the prepared surfaces were captured by Olympus BX51 Fluorescence Microscope. The morphology of patterned surface was imaged by tapping-mode atomic force microscope (AFM) on a Digital Instrument Dimension 3100 atomic force microscope under ambient conditions using silicon cantilevers. Scanning Probe Image Processor (SPIP) was used as software. Surface modification was confirmed by X-ray photoelectron spectroscopy (XPS) using a Physical Electronics Quantum 2000 Microprobe instrument with a monochromatic Al 50-W X-ray source under ultrahigh vacuum. The take-off angle and spot area were fixed at 45° and 10 μm, respectively. Scanning electron microscopy (SEM) images were taken by FEI Magellan operating at 10 keV without additional sputter coating.

4.2.3 Polymerization of poly(MPC-DHLA)

A monomer based on HEMA conjugated with lipoic acid (HEMA-LA) was synthesized according to our previous report [70] with slight modifications. Briefly, lipoic acid (8.00 g, 38.8 mmol) was dissolved in 100 mL of anhydrous dichloromethane in a dry round-bottom flask. To this stirring solution, EDC (11.20 g, 58.2 mmol) and HEMA (4.69 mL, 38.8 mmol) were added. DMAP (0.47 g, 3.88 mmol) was then added as solid. The reaction mixture was stirred under nitrogen atmosphere at room temperature for 24 h. After the reaction was complete, the mixture was washed with 100 mL of 1 M HCl (3 times), 100 mL of saturated $NaHCO_3$ (4 times), and 100 mL of saturated NaCl (3 times), respectively. The organic layer was dried with $MgSO_4$, filtered, and concentrated by rotary evaporation to obtain HEMA-LA monomer as yellow oil (7.7 g, 62.4% yield). The final product was stored at -80ºC. ^{1}H NMR (300 MHz, $CDCl_3$): δ/ppm = 6.10 (s, 1H), 5.60 (s, 1H), 4.30 (s, 4H), 3.55 (m, 1 H), 3.15 (m, 2H), 2.45 (m, 1H), 2.30 (t, 2H), 1.90 (s, 3H), 1.85 (m, 1H), 1.70 (m, 4H), 1.45 (m, 2H).

Then, a copolymer MPC and HEMA-LA (poly(MPC-LA)) having a degree of polymerization (DP) of approximately 100 with varied comonomer composition (10-30%) were prepared by RAFT polymerization according to our previous report [70, 120] with some modifications as follows: CPD (8.4 mg, 0.03 mmol) and ACVA (2.8 mg, 0.01 mmol) were added as solid to MPC monomer (620 mg, 2.1 mmol) in 20 mL vial. TFE (2 mL) was added afterwards. The mixture was placed in ice bath, and then HEMA-LA monomer (286.2 mg, 0.9 mmol) was slowly added. The reaction mixture was degassed by using dry nitrogen gas for 30 min then stirred at 70 °C for 6 h. The polymerization was quenched by rapidly cooling the solution in liquid nitrogen and opening to air. To remove the remaining monomer and the excess reagents, the polymer was precipitated in diethyl ether. Then, as-synthesized poly(MPC-LA) was reduced to obtain poly(MPC-DHLA) as follows: poly(MPC-LA) was re-dissolved again in 15 mL of degassed water and stirred in an ice bath. Sodium borohydride (4 mole equivalent with respect to HEMA-LA) was added as solid under nitrogen atmosphere, and the reaction mixture was stirred in an ice bath for 2 h. The pH was adjusted to ~3 by using 1.0 M HCl. Finally, polymer was purified by dialysis (MWCO 3,500 Da membrane) at 4°C against methanol for 1 day and RO water for another 2 days and lyophilized to obtain a cotton-like white powder. The condition mentioned above was used to prepare poly(MPC-DHLA) with 30% DHLA composition. To prepare poly(MPC-DHLA) with 10, 15, and 20% DHLA composition, MPC = 2.70, 2.55, and 2.40 mmol and HEMA-LA = 0.30, 0.45, and 0.60 mmol were used instead, respectively.

4.2.4 Preparation of poly(MPC-DHLA) patterned surfaces

Poly(MPC-DHLA) patterns were prepared in 2 steps. A poly(MPC-DHLA) film was first coated on Si wafer by spin coating, and then line pattern was generated by photolithography. To obtain a stable polymer film, poly(MPC-DHLA) was crosslinked via thiol-ene click reaction based on radical mechanism by reacting between thiol groups in DHLA and 1,3,5-triallyl-1,3,5-triazine-2,4,6(1*H*,3*H*,5*H*)-trione and using 2,2-dimethoxy-2-phenyl-acetophenone as radical initiator. For polymer film coating, Si wafer surfaces (1.2×1.2 cm^2) were first cleaned by sequential sonication in acetone, isopropanol, soap water, RO water, acetone, and isopropanol for 15 min followed by

oxygen plasma treatment for 20 min. The cleaned Si wafer were spin-coated with poly(MPC-DHLA) solution (5 mg/mL in ethanol) containing 1,3,5-triallyl-1,3,5-triazine-2,4,6(1*H*,3*H*,5*H*)-trione (10 mole equivalent with –SH group) and 2,2-dimethoxy-2-phenyl-acetophenone (1 mole equivalent with –SH group) at 3,000 rpm for 90 sec. Then, the poly(MPC-DHLA)-coated surface was crosslinked via thiol-ene click reaction by irradiating with UV light (CL-100 ultraviolet cross-linker at 365 nm and power of 100 mJ/cm^2) for 4 h, rinsed sequentially with methanol, acetone, toluene, acetone, and isopropanol, and dried under nitrogen gas (**Scheme 4.1, step I**).

For surface patterning by photolithography, the overall process modified from our previous work [121] as illustrated in **Scheme 4.1**. To obtain good adhesion between polymer film and photoresist layer, negative lift-off photoresist NR9-1000PY which is able to form stable crosslinked structure when irradiating with UV was used and spin-coated on top of the poly(MPC-DHLA)-coated surface at 3,000 rpm for 30 sec (**Scheme 4.1, step II**). After baking at 150°C for 1 min, a photomask was applied on the photoresist-coated surface followed by UV exposure with vacuum contact mode (Suss MicroTec MA6 Mask Aligner, 12 mW/cm^2) at 365 nm for 15 sec. The irradiated pattern was post-baked at 100°C for 1 min, treated with RD6 developer for 10 sec, rinsed with deionized water for 2 min, and dried with nitrogen gas (**Scheme 4.1, step III**). To destroy some area of polymer film and finally obtain poly(MPC-DHLA) pattern, the unmasked area was etched with oxygen plasma (STS Vision 320 Reactive Ion Etch (RIE) system) at 40 W for 6 min (**Scheme 4.1, step IV**), and the remaining photoresist was washed with acetone and isopropanol and dried with nitrogen gas (**Scheme 4.1, step V**).

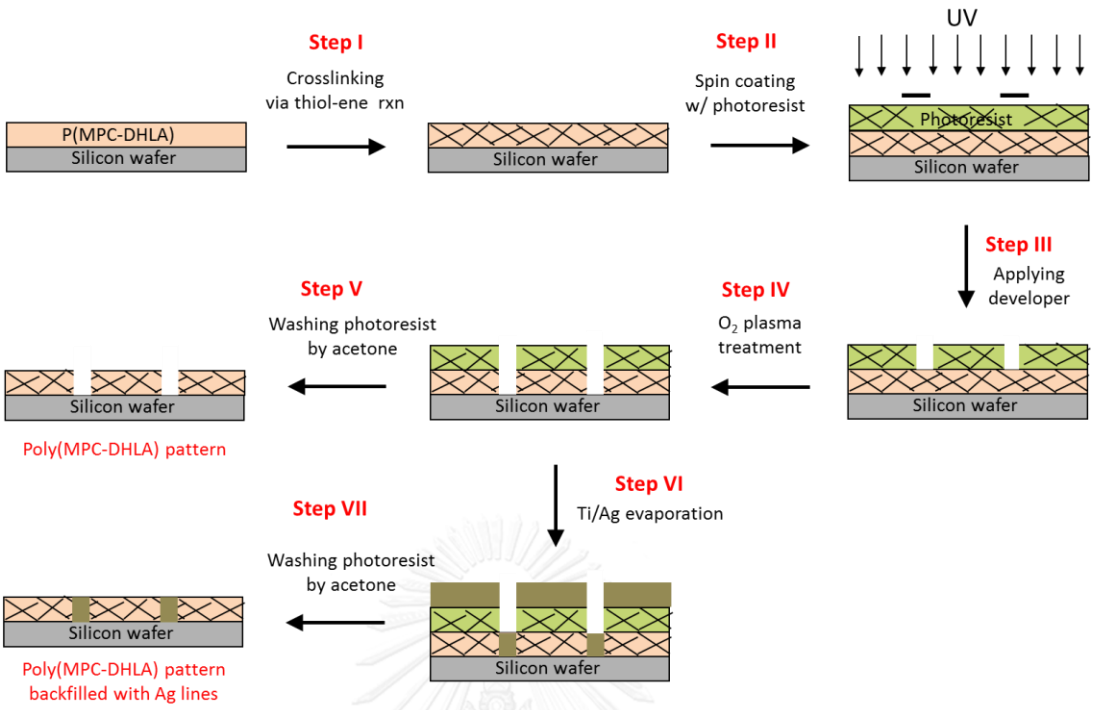

Scheme 4.1 Stepwise method for preparing poly(MPC-DHLA) patterned surface followed by backfilling with Ag film to generate poly(MPC-DHLA)/Ag pattern with dual antifouling and antibacterial functions.

4.2.5 Preparation of poly(MPC-DHLA) pattern backfilled with Ag film

To inherit the poly(MPC-DHLA) pattern with antibacterial activity, the poly(MPC-DHLA) pattern prepared from previous section of which the poly(MPC-DHLA) area was still covered with photoresist, was then backfilled with Ag film by using metal evaporation method (CHA SE-600 electron beam evaporator, Ag evaporation rate = 0.5 Å/s, and final thickness of Ag film = 10 nm) (**Scheme 4.1, step VI**). To assure that Ag lines stably adhered on the substrate, Ti was used as adhesive layer and first deposited on the surface before Ag deposition (Ti evaporation rate = 0.3 Å/s and final thickness of Ti film = 3 nm). Because negative lift-off photoresist was used in this work, the photoresist layer formed undercut shape after immersing in developer . This feature allows for simple removal of the remaining photoresist by rinsing with acetone and propanol and drying with N_2 gas which finally yielded the well-defined poly(MPC-DHLA) with Ag lines patterned surfaces

4.2.6 Antifouling Assay

Bacterial adhesion was evaluated using a modified adhesion protocol [122] using Escherichia coli K12 MG1655 (E. coli, DSMZ, Leibniz-Institut, Germany). Patterned surfaces were placed at the base of 6-well plates (Fisher Scientific) to which 5 mL of M9 media with 100 µg/mL ampicillin inoculated to a working concentration of 1 x 10^8 cells/mL. Following 24 h growth at 37 °C, the surfaces were washed 3× in phosphate buffered saline then plated and imaged immediately for fluorescence using a Zeiss Axio Imager. Imaging was performed under 20× and 50× magnification 10-15 times per sample. Manual cell counting was performed in ImageJ to distinguish location of bacterial adhesion across the patterned substrate.

4.2.7 Antibacterial Assay

Patterned MPC-DHLA surfaces backfilled with silver were evaluated in a modified surface-based Live/Dead assay. Samples were incubated for 2 h in M9 media containing E. coli at a working concentration of 1 x 10^8 cells/mL. Following growth, samples were stained with propidum iodide for 15 minutes, washed with PBS, and imaged using a Zeiss Axio Imager. The amount of live, GFP containing, and dead bacteria was quantified using ImageJ cell counter. The percentage of E. coli reduction is obtained as % reduction = dead cells/ (live + dead cells) *100.

4.3 Results and discussion

4.3.1 Polymerization and characterization of poly(MPC-DHLA) copolymers

HEMA-LA monomer was first synthesized according to our previous reports by carbodiimide coupling of HEMA monomer and lipoic acid [70, 120]. ^{1}H NMR (**Figure C-1 in Appendix C**) could be used to confirm the formation of HEMA-LA. This monomer was obtained as yellow oil with 62.4% yield. It should be emphasized that the monomer has to be stored as a solution in CH_2Cl_2 at −80°C to prevent disulfide exchange and gel formation.

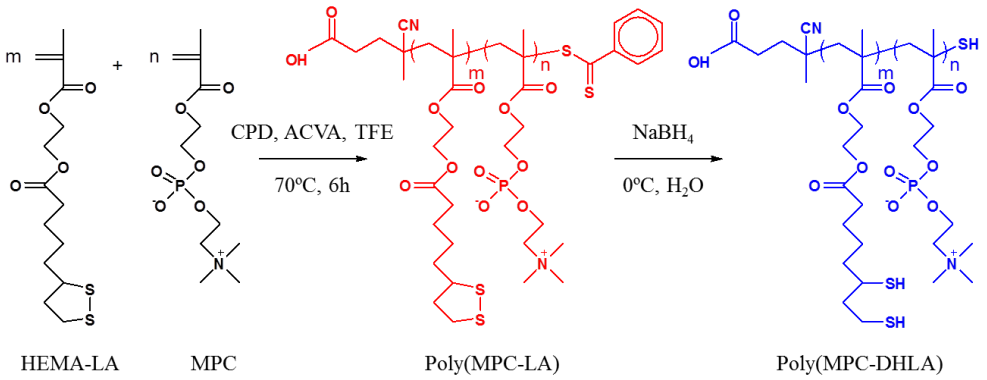

Scheme 4.2 Preparation of poly(MPC-DHLA) by RAFT copolymerization.

Random copolymers of poly(MPC-LA) were prepared via RAFT polymerization in TFE using ACVA and CPD as radical initiator and chain transfer agent (CTA), respectively as shown in **Scheme 4.2**. The ratio of [CTA]/[initiator] of 3 was fixed. For the targeted DP of 100, poly(MPC-LA) with varied copolymer composition was obtained as cotton-like orange solid with % yield in a range of 47 -89%. **Figure 4.1a-c** represents the ^{1}H NMR spectra of the synthesized poly(MPC-LA). All characteristic signals were consistent with those reported in the literature [70]. From **Figure 4.1a**, % conversion was calculated from the relative ratio between the peak integration of methyl protons from polymer backbone at 0.7–1.2 ppm and sum of integral intensities of protons from polymer backbone at 0.7–1.2 ppm and vinyl protons from the remaining monomer which appear at 5.65 ppm and 6.15 ppm. The % conversions of all copolymers were found to be in a range of 63 to 84 % upon using 6 h of polymerization time. In addition, ^{1}H NMR was also used to evaluate the actual copolymer composition by comparing relative ratio between the peak integration of protons from HEMA-LA unit ($H_{j'+e'}$, 2.3–2.6 ppm) and protons from polymer backbone. From the obtained data shown in **Table 4.1**, it was found that % HEMA-LA in the copolymer was close to the comonomer ratio in the feed indicating well-controlled characteristic of RAFT polymerization. Unimodal molecular weight distribution as revealed by GPC analysis (**Figure 4.1d-f**) together with PDI values (shown in **Table 4.1**) being close to 1.0 evidently confirmed that polymerization could be well controlled.

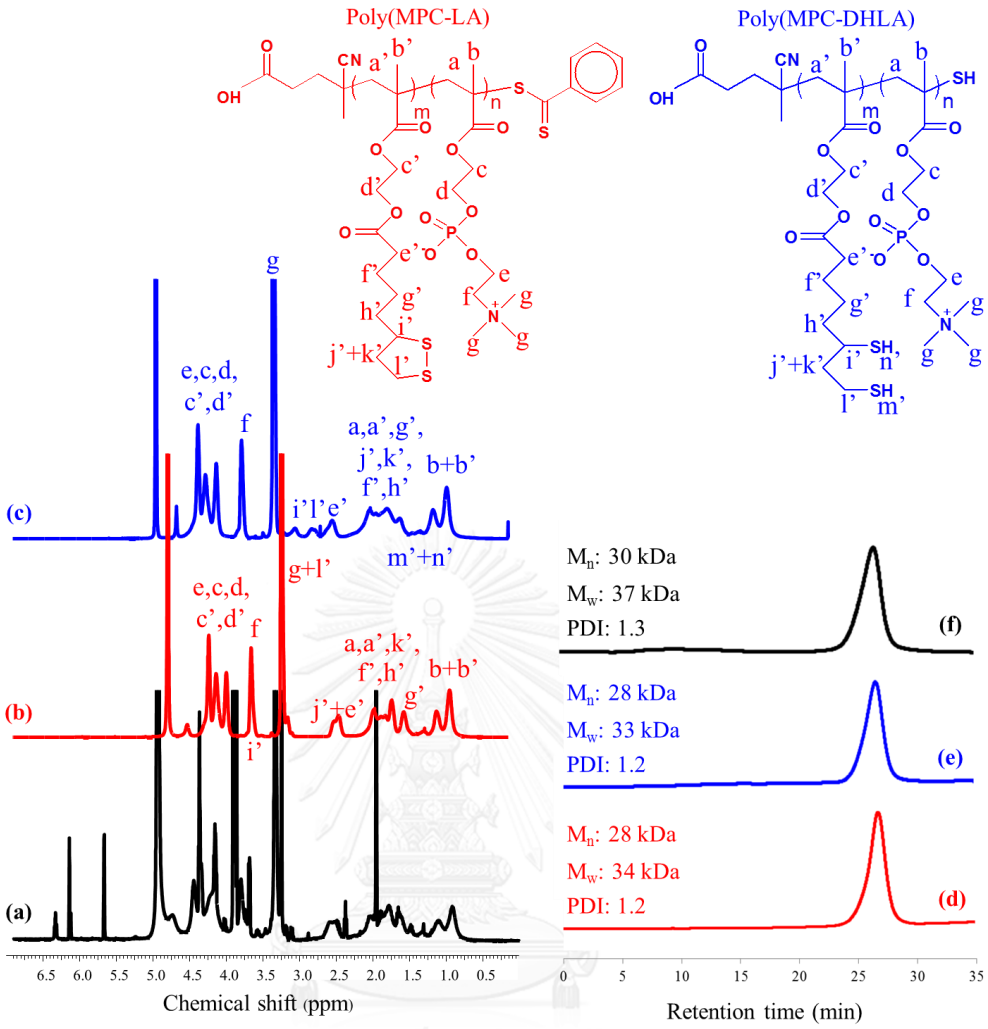

Figure 4.1 ^{1}H NMR spectra of (a) crude poly(MPC-LA), (b) purified poly(MPC-LA), and (c) purified poly(MPC-DHLA) and GPC traces of (d) purified poly(MPC-LA), (e) purified poly(MPC-DHLA), and (f) purified poly(MPC-DHLA) after storage for 1.5 months.

Table 4.1 Molecular weight, PDI, % conversion and % composition of HEMA-LA and DHLA in poly(MPC-LA) and poly(MPC-DHLA), respectively.

% HEMA-LA in feed	Before reduction				After reduction		
	% conversion[a]	M_n (kDa)[b]	PDI[b]	% HEMA-LA composition[a]	M_n (kDa)[b]	PDI [b]	% DHLA composition[a]
10.0	84.0	31.6	1.1	15.6	33.1	1.1	15.0
15.0	83.6	36.9	1.1	17.3	37.4	1.1	18.0
20.0	63.0	30.1	1.1	26.7	31.6	1.2	28.0
30.0	66.0	28.0	1.2	39.0	28.0	1.2	42.0

[a] Determined by ^{1}H NMR in MeOD [b] Evaluated by GPC

The synthesized poly(MPC-LA) was further reduced with sodium borohydride to convert the disulfides to dithiols and cleave the aromatic chain-end giving poly(MPC-DHLA) copolymer which is cotton-like white solid, as product. After reduction, DHLA signals of H_i, and H_l, at 2.8 ppm and 2.65 ppm, respectively, were observed (**Figure 1c**) indicating the ring opening of five-membered ring containing disulfide bond. The fact that DHLA compositions in poly(MPC-LA) are very close to the HEMA-LA compositions in the poly(MPC-DHLA) together with the almost unaltered molecular weight upon reduction, and unimodal GPC trace with low PDI implied that HEMA-LA was completely converted to DHLA and side reactions, such as gelation via disulfide formation or hydrolysis were absent. In addition, the unchanged molecular weight and PDI of the synthesized poly(MPC-DHLA) after storage in cold room under N_2 gas for 1.5 months indicated the high stability of this copolymer without gelation more than one month.

4.3.2 Preparation and characterization of poly(MPC-DHLA) patterned surfaces

To prepare crosslinked polymer film onto Si wafer surface via thiol-ene click reaction, the synthesized poly(MPC-DHLA) with varied % DHLA composition were spin-coated with 1,3,5-triallyl-1,3,5-triazine-2,4,6(1*H*,3*H*,5*H*)-trione as tri-ene compound, and 2,2-dimethoxy-2-phenyl-acetophenone (DMPA) as radical initiator. The stability of the prepared polymer film was first evaluated by comparing the polymer film thickness measured by ellipsometry before and after immersing in 10 mM PBS (pH 7.4) for 2 days [123]. From the results shown in **Table 4.2**, it was found

that at least 28% DHLA which acts as crosslinkable entities in the copolymer was necessary to provide reasonably stable polymer film on the surface given that approximately 6.57% decrease in thickness was detectable after stability testing. Moreover, the stability testing of the copolymer film (28% DHLA) containing tri-ene and DMPA without UV irradiation was also conducted and used as the control experiment. In this case, the thickness of the polymer film after stability testing was dramatically decreased to 2.7±0.03 nm indicating that highly stable polymer film was obtained as a result of crosslinking via thiol-ene click reaction only after UV irradiation. Although the copolymer with 42%DHLA gave the most stable film with minimal thickness loss upon stability test, it was not chosen for further study mainly because its lower MPC composition as compared with that of the copolymer with 28%DHLA may sacrifice the hydrophilicity and subsequent anti-fouling activity once used for pattern generation. To have an appropriate balance between stability and antifouling property, poly(MPC-DHLA) with 18% and 28% DHLA were therefore selected for making antifouling pattern in the next step.

Table 4.2 Thickness of crosslinked poly(MPC-DHLA) film on Si wafer surface measured by ellipsometry before and after stability testing.

% DHLA in poly(MPC-DHLA)	Thickness (nm)		% Decreasing of polymer thickness
	Before stability testing	After stability testing	
15.0	8.9±0.2	3.7±0.3	58.4
18.0	21.7±0.6	13.5±1.5	37.8
28.0	19.8±0.7	18.5±0.8	6.57
42.0	22.1±0.1	21.5±0.2	2.71

As shown in **Figure 4.2a**, very well-defined pattern of poly(MPC-DHLA) film could be made and obviously seen by optical microscope. To enhance the pattern visibility, the patterned poly(MPC-DHLA) was also stained with rhodamine 6G that can specifically be absorbed by MPC [124]. From **Figure 4.2b**, the emission of rhodamine 6G could only be detected on the poly(MPC-DHLA) area whereas negative photoresist as a controlled substrate could not be stained with rhodamine 6G as

displayed in **Figure 4.2c**. These results strongly verified that the photoresist coating was completely removed after photolithography and poly(MPC-DHLA) with well-defined pattern can be obtained.

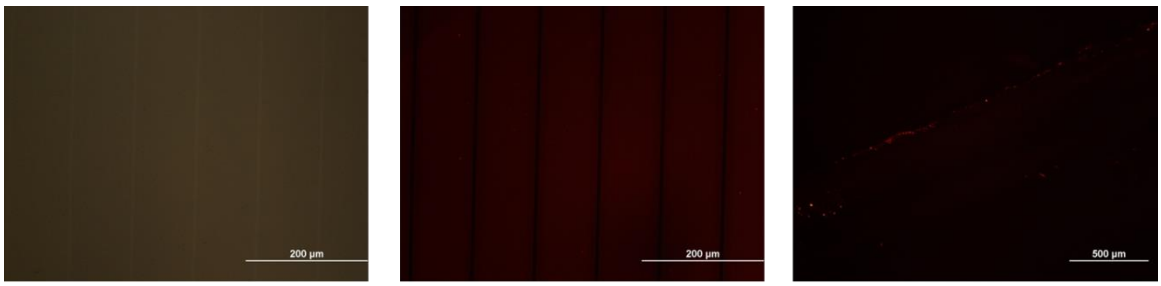

Figure 4.2 (a) Optical image of poly(MPC-DHLA) (28%DHLA) pattern, (b) fluorescence image of (b) poly(MPC-DHLA) (28%DHLA) pattern and (c) negative photoresist-coated Si wafer surface after rdodamine 6G staining.

AFM analysis (**Figure 4.3**) confirmed the patterned morphology of the poly(MPC-DHLA) film with estimated thickness of the copolymer area of 17.3 nm which is in good agreement with the value determined by ellipsometry (19.8 nm) for the copolymer with 28%DHLA. The line gap of 10.0 µm truly matches the dimension of the photomask used for pattern generation by photolithography. The sharp boundary between the copolymeric film and the line gap reflected the effectiveness of O_2 plasma treatment in removing unmasked, crosslinked poly(MPC-DHLA) film in **Step IV, Scheme 4.1**.

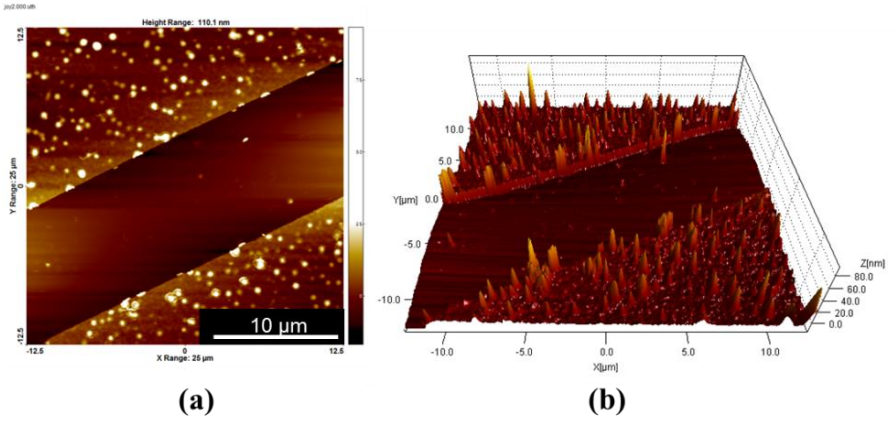

Figure 4.3 (a) 2D and (b) 3D AFM images of poly(MPC-DHLA) (28%DHLA) pattern.

4.3.3 Preparation and characterization of poly(MPC-DHLA) pattern backfilled with Ag

Ag film backfilling in the line gaps was performed while the pattern was still masked with photoresist in order to prevent Ag deposition on the copolymer area as shown in **step VI, Scheme 4.1**. From the optical images presented in **Figure4.4a**, it was found that most Ag lines were lifted off after stability testing for 1 day by immersing in M9 medium, a medium used for *E.coli*. culturing, implying low adhesion between Ag lines and Si wafer surface. To enhance adhesion between Ag and Si wafer surface as well as to increase the stability of Ag lines, titanium (Ti) was used as adhesive layer and first deposited on the surface prior to Ag deposition [125, 126]. In contrast, all Ag lines deposited on Ti adhesive layer could be clearly seen on the surface after stability testing indicating that Ag lines were stably attached (**Figure 4.4b)**.

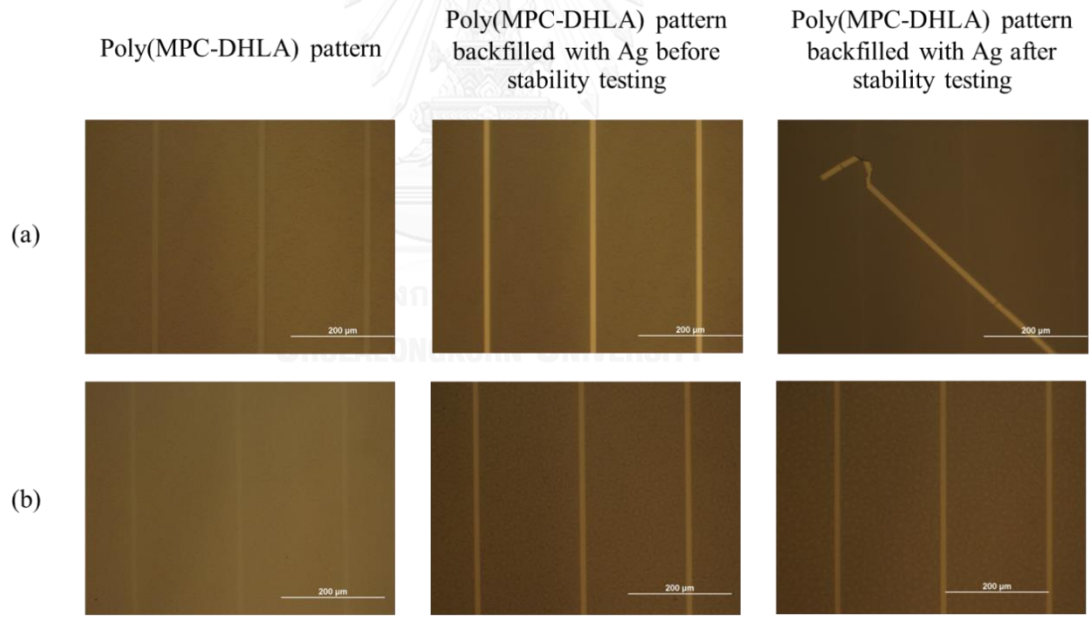

Figure 4.4 Optical images of patterned surfaces (a) without and (b) with Ti as adhesive layer.

The patterned characteristic was also verified by SEM analysis, (see inset in **Figure 4.5**). As evaluated by EDX, a signal due to Ag at around 3 keV [127] only appears in the profile scan of Ag line area. The absence of such signal in the

poly(MPC-DHLA) area suggested that there was no cross contamination between pattern and lines and the coated photomask can completely prevent Ag deposition on the copolymer area.

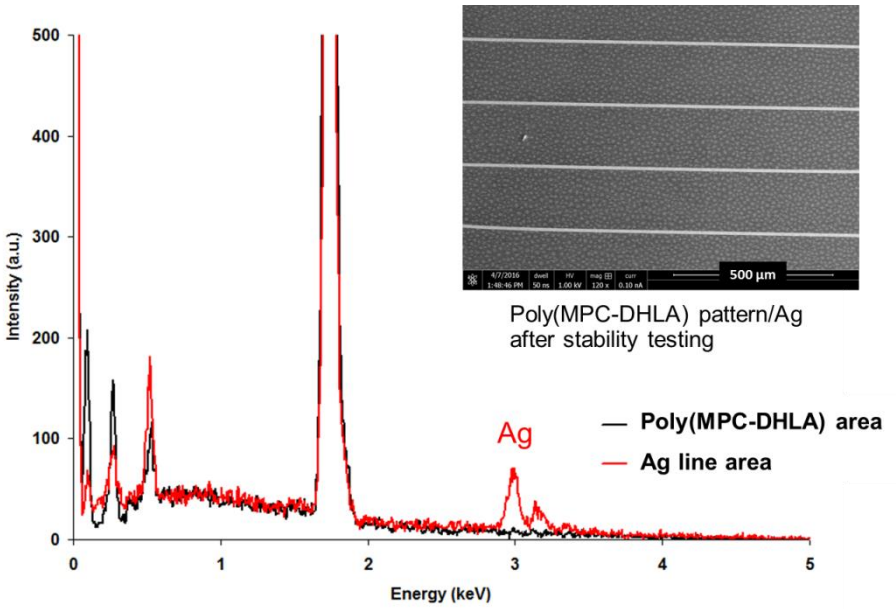

Figure 4.5 EDX spectra measured at 2 different positions, poly(MPC-DHLA) and Ag line areas. The inset: SEM image of poly(MPC-DHLA) pattern backfilled with Ag lines after stability testing.

The successful Ag backfilling was also confirmed by the existence of Ag3d peaks at 374 and 368 eV in XPS spectrum of Ag line (**Figure 4.6**). XPS atomic compositions on the line area illustrated in **Table 4.3** indicates the %Ag decrease after stability testing implying that there was some Ag^+ release from the Ag lines. In addition, as measured on the copolymer area (**Table 4.4**), the XPS atomic compositions (corresponding spectra are shown in **Figure C-2 in Appendix C**) coincide well with the theoretical ratio calculated from the copolymer repeat unit. This can be used as supporting evidence for poly(MPC-DHLA) pattern formation.

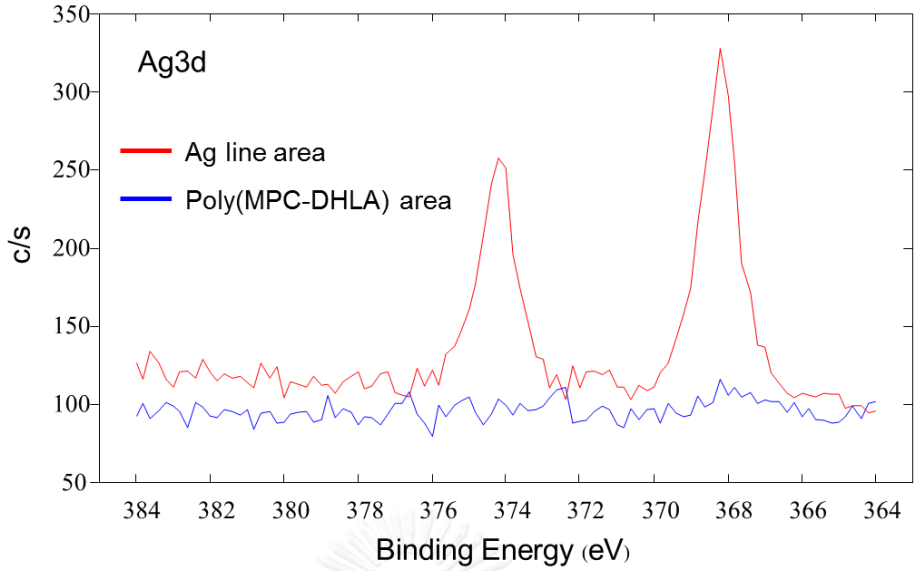

Figure 4.6 XPS spectra of Ag3d measured at 2 different positions, poly(MPC-DHLA) and Ag line areas.

Table 4.3 Percentage of atomic compositions measured by XPS on metal line area.

	Atomic Percentage (%)	
	Ag3d	Ti2p
Before stability testing	96.9	3.1
After stability testing	29.3	70.7

Table 4.4 Percentage of atomic compositions measured by XPS on poly(MPC-DHLA) area.

Elements	Atomic Percentage (%)	
	Calculated	XPS
C1s	64.1	65.3
O1s	27.0	26.6
N1s	5.8	5.2
P2p	3.1	2.9

4.3.4 Antifouling and antibacterial properties of poly(MPC-DHLA) pattern backfilled with Ag lines

Antifouling activity was first evaluated on poly(MPC-DHLA) pattern having 18% and 28% DHLA without Ag lines. **Figure 4.7a-b** show fluorescence images of bare Si wafer as a control surface and poly(MPC-DHLA) pattern with 28%DHLA, respectively, after incubating with *E.coli.* expressing green fluorescent protein (GFP) for 2 h. Interestingly, bacteria were only stuck on the line gap (silicon stripe) between poly(MPC-DHLA) area suggesting that the antifouling property arisen from the poly(MPC-DHLA). **Figure 4.7c** illustrates quantitative result showing total number of bacteria on the poly(MPC-DHLA) pattern having 18% and 28% DHLA. Apparently, the number of total adhered bacteria on both patterns was significantly lower than that on the bare silicon wafer control. In addition, as compared between the poly(MPC-DHLA) with 18% and that with 28% DHLA, the former with higher %MPC composition showed slightly better antifouling property than the latter implying the impact of PMPC content. The number of bacteria on the area of poly(MPC-DHLA) pattern and the line gap (silicon stripe) quite comparable. Thus, it was reasonable to assume that the number of attached bacteria per area on the copolymer area is much less than that on the silicon stripe given that the width of copolymer pattern (200 μm) is 20 times greater than the silicon stripe (10 μm). Poly(MPC-DHLA) pattern with 28% DHLA was therefore used for further investigation to obtain highly stable patterned film on the surface with reasonably good antifouling characteristic.

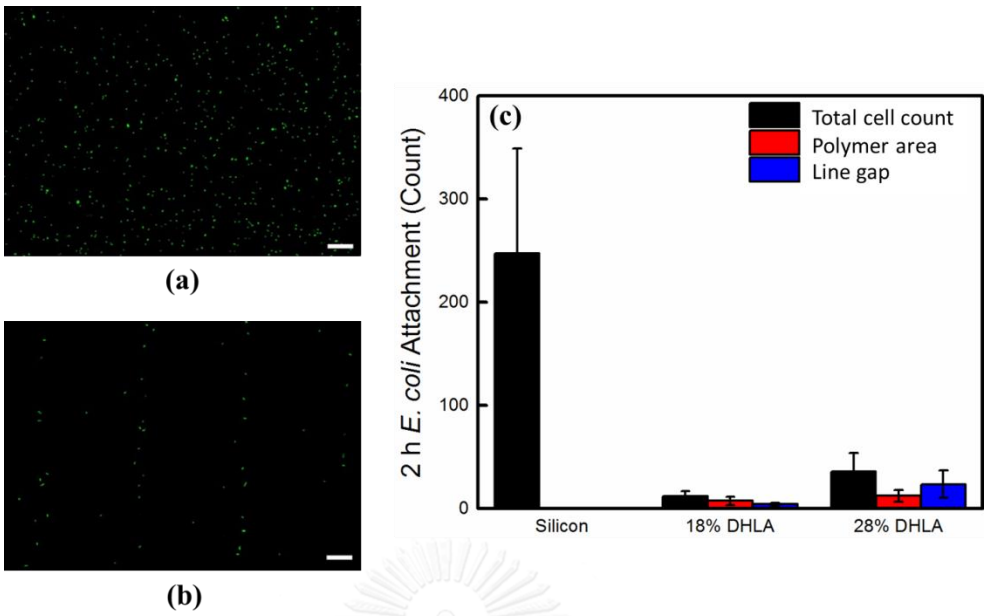

Figure 4.7 Fluorescence images of (a) bare Si wafer (b) poly(MPC-DHLA) (28% DHLA) pattern after incubating with *E.coli.* and (c) bar graph showing the number of attached bacteria on the poly(MPC-DHLA) patterned surfaces having 18% and 28% DHLA in comparison with bare Si wafer (scale bar: 10 μm).

Being in the pattern format, the coverage of the antifouling area in comparison with the fouling area can be conveniently and precisely tuned as a function of line spacing while the line width covered with the copolymer was fixed at 200 μm as demonstrated in **Figure 4.8a**. According to the fluorescence images depicted **in Figure 4.8b**, the bacteria were only trapped and adhered on the line gap. As anticipated, there were almost no bacteria adhered on the copolymer area of the pattern with the highest ratio between the line spacing and the line width (200 μm vs 10 μm) emphasizing antifouling efficacy of the copolymer. The total number of adhered bacteria on the line gap was proportionally increased as the line spacing increased. Interestingly, the number of adhered bacteria per area was independent on the line spacing (**Figure 4.8c**) and more than twice higher than that on the controlled bare Si wafer. This strongly suggested that the antifouling pattern developed from poly(MPC-DHLA) in this research may potentially be applied as a platform to accumulate other microorganisms or biomolecules besides bacteria in a

confined area as long as the line gap between the antifouling area is larger than the microorganisms.

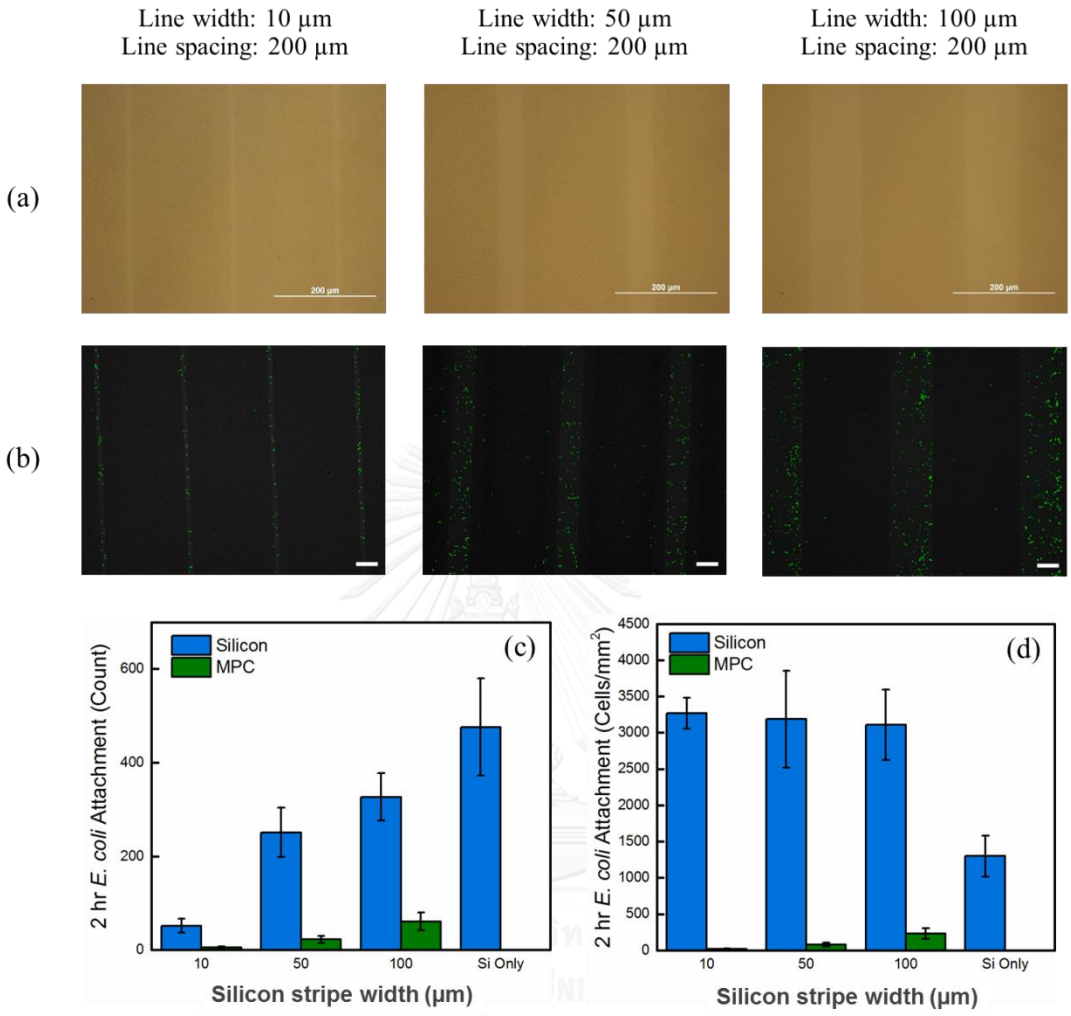

Figure 4.8 (a) Optical images of the poly(MPC-DHLA) (28% DHLA) patterns with varied silicon stripe width and (b) fluorescence images of poly(MPC-DHLA) patterns after incubating with *E.coli.* and bar graphs showing (c) the number of attached bacteria and (d) the number of attached bacteria per area on the poly(MPC-DHLA) patterned surfaces (scale bar: 50 µm).

Besides antifouling property, antibacterial activity was also introduced on poly(MPC-DHLA) patterned surface by backfilling the silicon stripe with Ag film by metal evaporation method. Antibacterial activity of the antifouling/antibacterial patterned surface was studied and compared with only poly(MPC-DHLA) pattern

without Ag lines (negative control) and a non-patterned surface entirely covered with Ag film (positive control). Fluorescence images of these surfaces after incubating with *E.coli*. for 2 h and live/dead bacteria staining illustrated in **Figure 4.9 a-c** indicated that no bacteria attached on poly(MPC-DHLA) area and dead bacteria expressed by red staining could only be seen on the surface with Ag backfilling. Killing efficiency was also quantified and shown in **Figure 4.9d**. The result is in line with those seen on fluorescence images. Patterned surface with Ag lines provided highest % *E.coli.* reduction and slightly higher than that on the surface with Ag film alone despite its lower surface coverage of bactericidal Ag film (5% Ag coverage on the surface). There are two implications that can be drawn from these set of data. (1) dual functions of both antifouling and antibacterial work supportively although not synergistically in killing bacteria. It is believed that the antifouling poly(MPC-DHLA) forced the bacteria to be confined in the area closed to line gaps covering with Ag film that can release bactericidal Ag^{+} so that the killing effect is more efficient on the patterned poly(MPC-DHLA)/Ag than the non-patterned Ag film. (2) the bacteria killing was majorly driven by Ag+ release as can be realized from %*E.coli* reduction being more than twice higher on the patterned poly(MPC-DHLA)/Ag than on the patterned poly(MPC-DHLA) without Ag backfilling.

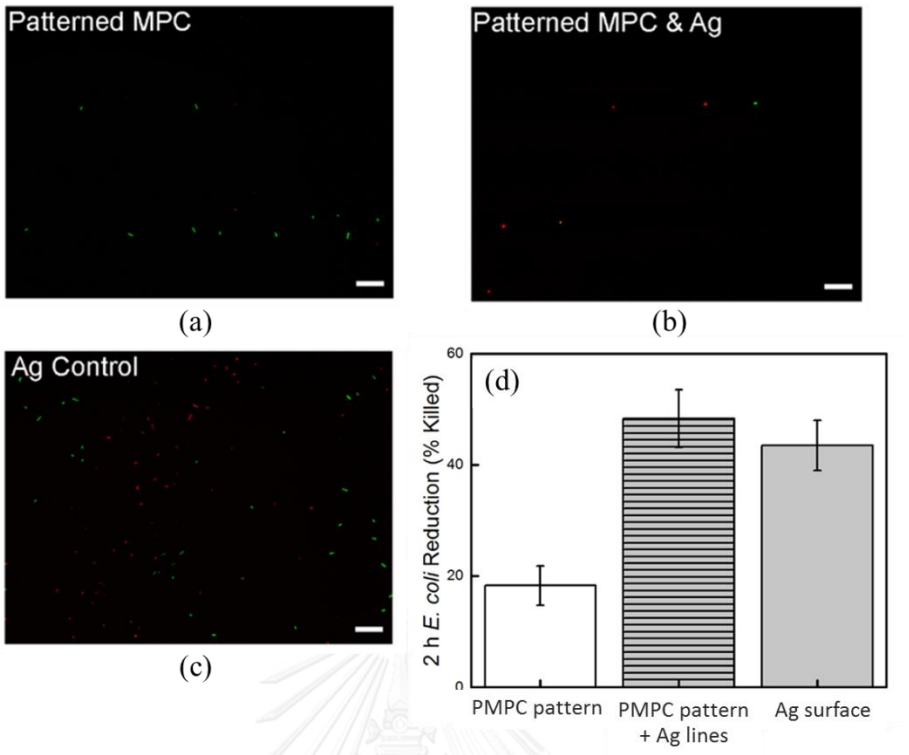

Figure 4.9 Fluorescence images (scale bar: 10 μm) of (a) poly(MPC-DHLA) pattern w/o Ag lines (b) poly(MPC-DHLA) pattern backfilled with Ag lines (line width = 10 μm and line spacing = 200 μm) (c) Non-patterned Ag film after incubating with *E.coli.* bacteria for 2 h and live/dead bacteria staining and (d) bar graph showing % bacteria reduction.

Because the killing mechanism of Ag is based on the releasing of Ag^+ which later bind and kill bacteria [128, 129], the bacterial growth in surrounding solution was also evaluated. The patterned surfaces were immersed in bacteria suspension and removed at desired times. The remaining surviving bacteria in the solution were evaluated by measuring optical density (OD) and the growth curves were plotted in **Figure 4.10**. It should be noted that GC is growth control in which bacteria should grow normally. While SC is sterile control so that there should be no bacterial growth seen under this condition. The higher OD value means more bacterial growth in solution. All patterns were found to be able to inhibit about 40% bacteria growth within 24 h of incubation time indicating a certain level of bactericidal activity of the Ag^+ release into the solution. Apparently the amount of Ag^+ deliberated from the Ag

film was not high enough to entirely suppress the bacterial growth in solution although the Ag line width was elevated from 10 to 50 (5 times) and 100 nm (10 times). Similar trend was also observed by others [126, 129, 130]. They have described this as a result of low ionization ability of Ag in the form of smooth metallic film. Besides, these Ag films were fabricated on relative flat and smooth substrate thus their exposed surface area was not high. In contrast, bacterial killing performance can be significantly improved when Ag film was deposited on much rougher substrate of nanocrystalline TiO_2 support as recently reported by *Vukoje et al.* [106] It is believed that the Ag film with enhanced surface area should be more effective in releasing Ag^+ to the solution. We do not consider this limited antibacterial activity of the patterned poly(MPC-DHLA)/Ag which is based on a combination of Ag ion releasing and contact active mechanism as a weakness, but instead recognize it as unique and useful characteristics. The fact that the antibacterial activity only function locally nearby the surface help reduce the risk of harmful toxicity to the surrounding tissues of which the medical devices coated with this dual antifouling/antibacterial pattern may come into contact.

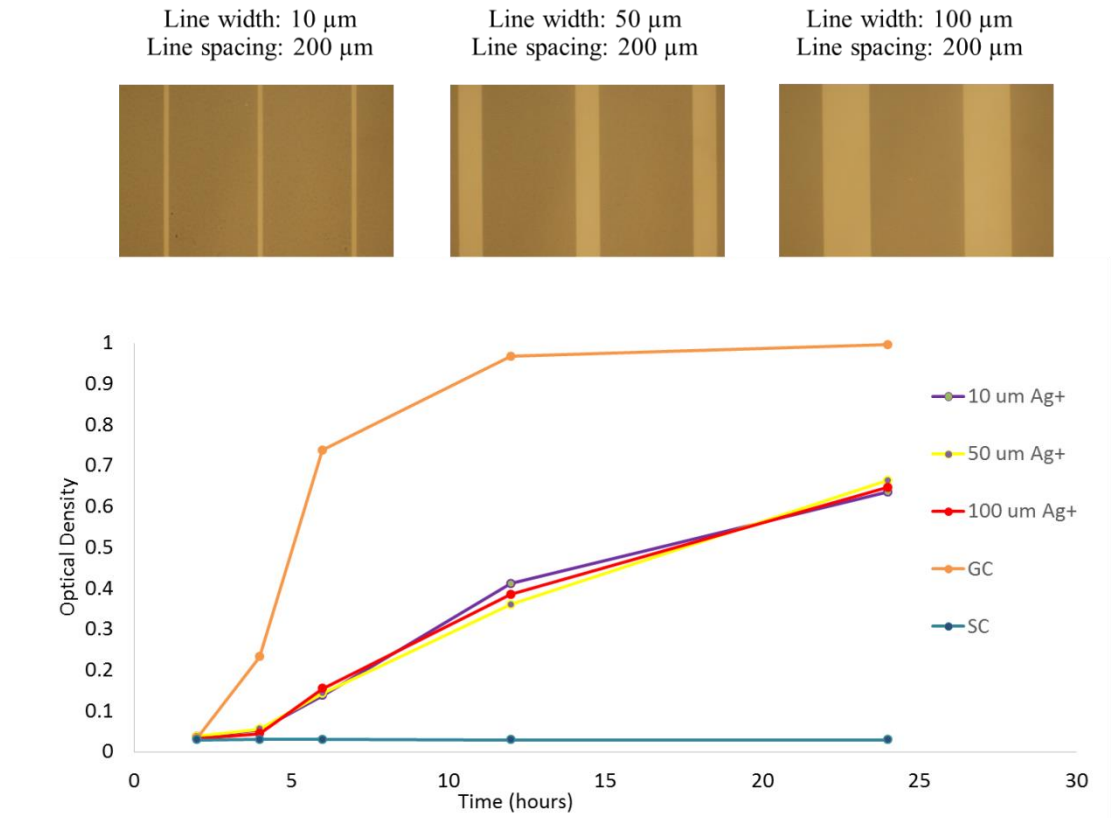

Figure 4.10 (a) Optical images of poly(MPC-DHLA) (28% DHLA) pattern backfilled with Ag lines with varied line widths and (b) growth curve of *E. coli.* in solution surrounding patterned surfaces.

4.4 Conclusions

Stable and antifouling patterned surfaces based on poly(MPC-DHLA) can be conveniently prepared by spin coating, crosslinking followed by surface patterning using photolithography. MPC is known to provide biocompatibility and biofouling resistance while crosslinking can be induced via thiol-ene click reaction of the dithiol units available in DHLA to improve stability of the coated polymer film on the surface. Photolithography using negative lift-off photoresist yielded well-defined poly(MPC-DHLA) patterns with controllable dimension as fluorescently verified after specific staining of the MPC-containing copolymer area with rhodamine 6G and morphologically confirmed by AFM analysis. Based on bacterial adhesion results, the antifouling property of the poly(MPC-DHLA) area of the pattern was so powerful that the majority of *E.coli* cells came in the close vicinity and/or to contact with the

pattern were forced to be adhered only on the area of the line gaps. The ability to accumulate the bacteria in the confined area was independent on the width of the line gap. Ag film, selected as a model of antibacterial agent, was successfully backfilled in the line gaps of the poly(MPC-DHLA) patterns by metal evaporation using titanium as adhesive layer to prepare dual functional surface with both antifouling and antimicrobial characteristics in pattern format. After Ag backfilling, the poly(MPC-DHLA)/Ag patterned surface showed both bacteria adhesion resistance on the polymer area and bacterial killing on Ag lines implying the combined antifouling and antibacterial effects which is found to be more superior than either poly((MPC-DHLA) film or Ag film alone. It is anticipated that not only can this newly developed antifouling pattern be used for preventing biofilm formation but it is also possible for protein and cell patterning applications and apply on other clinically relevant surfaces.

CHAPTER V
EXECUTIVE SUMMARY

In this thesis, three different polymer-modified surfaces have been developed for biomedical applications. In the first part, BSA-modified chitosan (BSA-CS) was used as both reducing and stabilizing agent in the synthesis of BSA-functionalized AuNPs. Because BSA was chemically attached to amino groups in chitosan structure, the bio-functionalization of the AuNPs can be concurrently done along with AuNPs synthesis in a single step. To avoid BSA denaturation, a green and non-destructive approach using sonochemical method was employed for AuNPs synthesis in the presence of BSA-CS with the need of Tween 80 as steric stabilizing agent and co-reducing agent. The BSA-CS-AuNPs underwent aggregation in the presence of anti-BSA due to the antigen-antibody specific interactions. The minimum concentration of anti-BSA that can induce aggregation of BSA-CS-AuNPs and clearly be visualized by naked eye was 20 μg/mL (125 nM). This research strongly demonstrates the potential of AuNPs stabilized by biomolecule-functionalized CS for biosensing application. It is believed that the same strategy can be implemented for other antigen-antibody pairs, and not only limited to those with reducing power.

In the second part, PMAMPC has been successfully replaced CTAB on CTAB-coated AuNRs surface to reduce toxicity, improve colloidal stability and provide reactive sites for PNA immobilization. The modification of thiol groups to prepare multidentate PMAMPC copolymer ligand was found to be necessary to attain multifunctional copolymer-stabilized AuNRs with superior stability in 10 mM PBS as well as in complex cell culture media. The PNA-immobilized AuNRs were also successfully prepared by using thiol-modified and PNA–conjugated copolymer (PNA-Cys-PMAMPC) as stabilizer. The AuNRs formed were highly stable with PNA grafting density of 1.39×10^{14} probe/cm^2. *In vitro* % PNA releasing induced by selective degradation of tetrapeptide linker by cathepsin B was found to be 22.9 %. To evaluate the possibility of employing PNA-Cys-PMAMPC-AuNRs as nanocarrier for antisense application, gene silencing in HepG2 cell will be further studied.

In the last part, the simple and universal coating method was developed to prepare antifouling patterned surface by using copolymer of poly(MPC-DHLA). MPC units could provide antifouling property whereas the stability of polymer film was obtained from DHLA unit which can act as crosslinkable groups via thiol-ene click reaction. The formation of these patterns was confirmed by AFM analysis together with rhodamine 6G staining that can specifically absorb on the MPC area. To achieve antifouling and antibacterial dual functional patterned surface for preventing biofilm formation, poly(MPC-DHLA) pattern was also backfilled with silver film as a bactericidal model by metal evaporation and using titanium as adhesive layer. The success of sliver backfilling could be verified by optical microscopy, SEM-EDX and XPS analysis. Pattern of poly(MPC-DHLA) backfilled with Ag film showed both bacteria adhesion resistance on the copolymer area and bacterial killing on the Ag lines suggesting the combined antifouling and antibacterial effects on this patterned surface. In addition, to present the advantage of pattern format in term of surface property controlling, antifouling property of only poly(MPC-DHLA) pattern with varied pattern sizes was investigated. The results suggested that the number of adhered *E. coli*. could be modulated by varying area of MPC on the surface. Interestingly, as compared with bare Si wafer, more bacteria density (number per area) was observed on poly(MPC-DHLA) antifouling pattern implying that the copolymer area could confine bacteria on the specific area indicating that the developed poly(MPC-DHLA) antifouling pattern may potentially be applied for protein or cell patterning.

REFERENCES

[1] Daniel, M.C. and Astruc, D. Gold nanoparticles: Assembly, supramolecular chemistry, quantum-size-related properties, and applications toward biology, catalysis, and nanotechnology. Chemical Reviews 104(1) (2004): 293-346.

[2] Guo, S. and Wang, E. Synthesis and electrochemical applications of gold nanoparticles. Analytica Chimica Acta 598(2) (2007): 181-192.

[3] Huang, S.H. Gold nanoparticle-based immunochromatographic test for identification of Staphylococcus aureus from clinical specimens. Clinica Chimica Acta 373(1-2) (2006): 139-143.

[4] Brust, M., Walker, M., Bethell, D., Schiffrin, D.J., and Whyman, R. Synthesis of thiol-derivatized gold nanoparticles in a 2-phase liquid-liquid system Journal of the Chemical Society-Chemical Communications (7) (1994): 801-802.

[5] Turkevich, J., Stevenson, P.C., and Hillier, J. A study of the nucleation and growth processes in the synthesis of colloidal gold. Discussions of the Faraday Society 11 (1951): 55-75.

[6] Jin, Y., et al. Gold nanoparticles prepared by sonochemical method in thiol-functionalized ionic liquid. Colloids and Surfaces a-Physicochemical and Engineering Aspects 302(1-3) (2007): 366-370.

[7] Okitsu, K., Ashokkumar, M., and Grieser, F. Sonochemical synthesis of gold nanoparticles: Effects of ultrasound frequency. Journal of Physical Chemistry B 109(44) (2005): 20673-20675.

[8] Dong, S.A. and Zhou, S.P. Photochemical synthesis of colloidal gold nanoparticles. Materials Science and Engineering B-Solid State Materials for Advanced Technology 140(3) (2007): 153-159.

[9] Housni, A., Ahmed, M., Liu, S., and Narain, R. Monodisperse protein stabilized gold nanoparticles via a simple photochemical process. Journal of Physical Chemistry C 112(32) (2008): 12282-12290.

[10] Kuthirummal, N., Dean, A., Yao, C., and Risen, W.J. Photo-formation of gold nanoparticles: Photoacoustic studies on solid monoliths of Au(III)-chitosan-

silica aerogels. Spectrochimica Acta Part a-Molecular and Biomolecular Spectroscopy 70(3) (2008): 700-703.

[11] Wei, D. and Qian, W. Chitosan-mediated synthesis of gold nanoparticles by UV photoactivation and their characterization. Journal of Nanoscience and Nanotechnology 6(8) (2006): 2508-2514.

[12] Frenkel, A.I., et al. Size-controlled synthesis and characterization of thiol-stabilized gold nanoparticles. Journal of Chemical Physics 123(18) (2005): 184701-1 to 184701-6.

[13] Warren, S.C., Jackson, A.C., Cater-Cyker, Z.D., DiSalvo, F.J., and Wiesner, U. Nanoparticle synthesis via the photochemical polythiol process. Journal of the American Chemical Society 129(33) (2007): 10072-10073.

[14] Praharaj, S., et al. Effect of bromide and chloride ions for the dissolution of colloidal gold. Journal of Photochemistry and Photobiology a-Chemistry 187(2-3) (2007): 196-201.

[15] Wangoo, N., Bhasin, K.K., Boro, R., and Suri, C.R. Facile synthesis and functionalization of water-soluble gold nanoparticles for a bioprobe. Analytica Chimica Acta 610(1) (2008): 142-148.

[16] Hussain, I., et al. Size-controlled synthesis of near-monodisperse gold nanoparticles in the 1-4 nm range using polymeric stabilizers. Journal of the American Chemical Society 127(47) (2005): 16398-16399.

[17] Jeon, H.J., et al. Synthesis of poly(ethylene oxide)-based thermoresponsive block copolymers by RAFT radical polymerization and their uses for preparation of gold nanoparticles. Colloids and Surfaces a-Physicochemical and Engineering Aspects 317(1-3) (2008): 496-503.

[18] Wang, W., Chen, Q., Jiang, C., Yang, D., Liu, X., and Xu, S. One-step synthesis of biocompatible gold nanoparticles using gallic acid in the presence of poly-(*N*-vinyl-2-pyrrolidone). Colloids and Surfaces a-Physicochemical and Engineering Aspects 301(1-3) (2007): 73-79.

[19] Bai, J., et al. One-pot synthesis of polyacrylamide-gold nanocomposite. Materials Chemistry and Physics 106(2-3) (2007): 412-415.

[20] Sun, X., Dong, S., and Wang, E. One-step preparation of highly concentrated well-stable gold colloids by direct mix of polyelectrolyte and $HAuCl_4$ aqueous solutions at room temperature. Journal of Colloid and Interface Science 288(1) (2005): 301-303.

[21] Sun, X., Dong, S., and Wang, E. One-step synthesis and characterization of polyelectrolyte-protected gold nanoparticles through a thermal process. Polymer 45(7) (2004): 2181-2184.

[22] Kumar, M.N.V.R. A review of chitin and chitosan applications. Reactive and Functional Polymers 46(1) (2000): 1-27.

[23] Huang, H. and Yang, X. Synthesis of chitosan-stabilized gold nanoparticles in the absence/presence of tripolyphosphate. Biomacromolecules 5(6) (2004): 2340-2346.

[24] Huang, H. and Yang, X. Synthesis of polysaccharide-stabilized gold and silver nanoparticles: A green method. Carbohydrate Research 339(15) (2004): 2627-2631.

[25] Potara, M., Maniu, D., and Astilean, S. The synthesis of biocompatible and SERS-active gold nanoparticles using chitosan. Nanotechnology 20(31) (2009): 315602.

[26] Shih, C.-M., Shieh, Y.-T., and Twu, Y.-K. Preparation of gold nanopowders and nanoparticles using chitosan suspensions. Carbohydrate Polymers 78(2) (2009): 309-315.

[27] Sun, C., et al. Degradation behavior of chitosan chains in the 'green' synthesis of gold nanoparticles. Carbohydrate Research 343(15) (2008): 2595-2599.

[28] Tiwari, A.D., Mishra, A.K., Mishra, S.B., Arotiba, O.A., and Mamba, B.B. Green synthesis and stabilization of gold nanoparticles in chemically modified chitosan matrices. International Journal of Biological Macromolecules 48(4) (2011): 682-687.

[29] Bhumkar, D.R., Joshi, H.M., Sastry, M., and Pokharkar, V.B. Chitosan reduced gold nanoparticles as novel carriers for transmucosal delivery of insulin. Pharmaceutical Research 24(8) (2007): 1415-1426.

[30] Guan, H., Yu, J., and Chi, D. Label-free colorimetric sensing of melamine based on chitosan-stabilized gold nanoparticles probes. Food Control 32(1) (2013): 35-41.

[31] Radhakumary, C. and Sreenivasan, K. On the observation of the need for an unusually high concentration of cysteine and homocysteine to induce aggregation of polymer-stabilized gold nano particles. Journal of Nanoparticle Research 15(2) (2013): 1439.

[32] Le, L.T., et al. Water-soluble acetylated chitosan-stabilized gold nanosphere bioprobes. Materials Chemistry and Physics 149-150 (2015): 324-332.

[33] Yakimovich, N.O., Smirnova, L.A., Gracheva, T.A., Klychkov, K.S., Bityurin, N.M., and Aleksandrov, A.P. Synthesis of chitosan-stabilized Au nanoparticles with controllable sizes. Polymer Science Series B 50(9) (2008): 238-242.

[34] Fan, C., Li, W., Zhao, S., Chen, J., and Li, X. Efficient one pot synthesis of chitosan-induced gold nanoparticles by microwave irradiation. Materials Letters 62(20) (2008): 3518-3520.

[35] Chaichi, M.J. and Alijanpour, S.O. Glucose chemiluminescence biosensor based on covalent immobilization of enzyme in glutaraldehyde-functionalized glass cell and direct coupling of chitosan-induced Au/Ag alloy nanoparticles. Journal of Analytical Chemistry 71(2) (2016): 163-171.

[36] Besner, S., Kabashin, A.V., Winnik, F.M., and Meunier, M. Synthesis of size-tunable polymer-protected gold nanoparticles by femtosecond laser-based ablation and seed growth. Journal of Physical Chemistry C 113(22) (2009): 9526-9531.

[37] Okitsu, K., Mizukoshi, Y., Yamamoto, T.A., Maeda, Y., and Nagata, Y. Sonochemical synthesis of gold nanoparticles on chitosan. Materials Letters 61(16) (2007): 3429-3431.

[38] Chen, J.-W., Lei, Y., Liu, X.-J., Jiang, J.-H., Shen, G.-L., and Yu, R.-Q. Immunoassay using surface-enhanced Raman scattering based on aggregation of reporter-labeled immunogold nanoparticles. Analytical and Bioanalytical Chemistry 392(1-2) (2008): 187-193.

[39] Du, B., Li, Z., and Cheng, Y. Homogeneous immunoassay based on aggregation of antibody-functionalized gold nanoparticles coupled with light scattering detection. Talanta 75(4) (2008): 959-964.

[40] Wang, X., et al. Detection of hepatitis B surface antigen by target-induced aggregation monitored by dynamic light scattering. Analytical Biochemistry 428(2) (2012): 119-125.

[41] Seydack, M. Nanoparticle labels in immunosensing using optical detection methods. Biosensors & Bioelectronics 20(12) (2005): 2454-2469.

[42] Gella, F.J., Serraa, J., and Generx, J. Latex agglutination procedures in immunodiagnosis. Pure and Applied Chemistry 63(8) (1991): 1131-1134.

[43] Strozyk, M.S., Chanana, M., Pastoriza-Santos, I., Perez-Juste, J., and Liz-Marzan, L.M. Protein/polymer-based dual-responsive gold nanoparticles with pH-dependent thermal sensitivity. Advanced Functional Materials 22(7) (2012): 1436-1444.

[44] Xie, J., Zheng, Y., and Ying, J.Y. Protein-directed synthesis of highly fluorescent gold nanoclusters. Journal of the American Chemical Society 131(3) (2009): 888-889.

[45] Liu, J., Chang, M.-J., Gou, X.-C., Xu, Z.-G., and Zhang, H.-L. One-step synthesis of antibody-stabilized aqueous colloids of noble metal nanoparticles. Colloids and Surfaces a-Physicochemical and Engineering Aspects 404 (2012): 112-118.

[46] Lee, Y. and Geckeler, K.E. Cytotoxicity and cellular uptake of lysozyme-stabilized gold nanoparticles. Journal of Biomedical Materials Research Part A 100A(4) (2012): 848-855.

[47] Khullar, P., et al. Bovine serum albumin bioconjugated gold nanoparticles: Synthesis, hemolysis, and cytotoxicity toward cancer cell lines. Journal of Physical Chemistry C 116(15) (2012): 8834-8843.

[48] Basu, N., Bhattacharya, R., and Mukherjee, P. Protein-mediated autoreduction of gold salts to gold nanoparticles. Biomedical Materials 3(3) (2008): 034105.

[49] Aryal, S., Bahadur, K.C.R., Bhattarai, N., Kim, C.K., and Kim, H.Y. Study of electrolyte induced aggregation of gold nanoparticles capped by amino acids. Journal of Colloid and Interface Science 299(1) (2006): 191-197.

[50] Ma, Z. and Han, H. One-step synthesis of cystine-coated gold nanoparticles in aqueous solution. Colloids and Surfaces a-Physicochemical and Engineering Aspects 317(1-3) (2008): 229-233.

[51] Liu, L., Zheng, H.-Z., Zhang, Z.-J., Huang, Y.-M., Chen, S.-M., and Hu, Y.-F. Photoluminescence from water-soluble BSA-protected gold nanoparticles. Spectrochimica Acta Part A: Molecular and Biomolecular Spectroscopy 69(3) (2008): 701-705.

[52] Don, T.-M. and Chen, H.-R. Synthesis and characterization of AB-crosslinked graft copolymers based on maleilated chitosan and *N*-isopropylacrylamide. Carbohydrate Polymers 61(3) (2005): 334-347.

[53] Grimaldo, M., et al. Hierarchical molecular dynamics of bovine serum albumin in concentrated aqueous solution below and above thermal denaturation. Physical Chemistry Chemical Physics 17(6) (2015): 4645-4655.

[54] Hormozi-Nezhad, M.R., Karami, P., and Robatjazi, H. A simple shape-controlled synthesis of gold nanoparticles using nonionic surfactants. Rsc Advances 3(21) (2013): 7726-7732.

[55] Kandori, K., Uoya, Y., and Ishikawa, T. Effects of acetonitrile on adsorption behavior of bovine serum albumin onto synthetic calcium hydroxyapatite particles. Journal of Colloid and Interface Science 252(2) (2002): 269-275.

[56] Olkhov, R.V. and Shaw, A.M. Label-free antibody-antigen binding detection by optical sensor array based on surface-synthesized gold nanoparticles. Biosensors & Bioelectronics 23(8) (2008): 1298-1302.

[57] Yan, P., Zhao, N., Hu, H., Lin, X., Liu, F., and Xu, F.-J. A facile strategy to functionalize gold nanorods with polycation brushes for biomedical applications. Acta Biomaterialia 10(8) (2014): 3786-3794.

[58] Ahmed, M., Bhuchar, N., Ishihara, K., and Narain, R. Well-controlled cationic water-soluble phospholipid polymer-DNA nanocomplexes for gene delivery. Bioconjugate Chemistry 22(6) (2011): 1228-38.

[59] Shen, J., et al. Multifunctional gold nanorods for siRNA gene silencing and photothermal therapy. Advanced Healthcare Materials 3(10) (2014): 1629-37.

[60] Braun, G.B., et al. Laser-activated gene silencing via gold nanoshell-siRNA conjugates. Acs Nano 3(7) (2009): 2007-2015.

[61] Good, L. and Nielsen, P.E. Antisense inhibition of gene expression in bacteria by PNA targeted to mRNA. Nature Biotechnology 16(4) (1998): 355-358.

[62] Ma, X., Devi, G., Qu, Q., Toh, D.-F.K., Chen, G., and Zhao, Y. Intracellular delivery of antisense peptide nucleic acid by fluorescent mesoporous silica nanoparticles. Bioconjugate Chemistry 25(8) (2014): 1412-1420.

[63] Shiraishi, T. and Nielsen, P.E. Improved cellular uptake of antisense peptide nucleic acids by conjugation to a cell-penetrating peptide and a lipid domain. Methods in Molecular Biology, 751 (2011): 209-221.

[64] Saleh, A.F., Arzumanov, A., Abes, R., Owen, D., Lebleu, B., and Gait, M.J. Synthesis and splice-redirecting activity of branched, arginine-rich peptide dendrimer conjugates of peptide nucleic acid oligonucleotides. Bioconjugate Chemistry 21(10) (2010): 1902-1911.

[65] Xiao, Z., et al. DNA self-assembly of targeted near-infrared-responsive gold nanoparticles for cancer thermo-chemotherapy. Angewandte Chemie-International Edition 51(47) (2012): 11853-11857.

[66] Ren, F., et al. Gold nanorods carrying paclitaxel for photothermal-chemotherapy of cancer. Bioconjugate Chemistry 24(3) (2013): 376-386.

[67] Li, X., Takashima, M., Yuba, E., Harada, A., and Kono, K. PEGylated PAMAM dendrimer-doxorubicin conjugate-hybridized gold nanorod for combined photothermal-chemotherapy. Biomaterials 35(24) (2014): 6576-6584.

[68] Tao, Y., Ju, E., Liu, Z., Dong, K., Ren, J., and Qu, X. Engineered, self-assembled near-infrared photothermal agents for combined tumor immunotherapy and chemo-photothermal therapy. Biomaterials 35(24) (2014): 6646-6656.

[69] Tree-Udom, T., et al. Shape effect on particle-lipid bilayer membrane association, cellular uptake, and cytotoxicity. ACS Applied Materials & Interfaces 7(43) (2015): 23993-24000.

[70] Chen, X., Lawrence, J., Parelkar, S., and Emrick, T. Novel zwitterionic copolymers with dihydrolipoic acid: Synthesis and preparation of nonfouling nanorods. Macromolecules 46(1) (2013): 119-127.

[71] Kirui, D.K., Krishnan, S., Strickland, A.D., and Batt, C.A. PAA-derived gold nanorods for cellular targeting and photothermal therapy. Macromolecular Bioscience 11(6) (2011): 779-788.

[72] Xiao, Y., et al. Gold nanorods conjugated with doxorubicin and cRGD for combined anticancer drug delivery and PET imaging. Theranostics 2(8) (2012): 757-768.

[73] Thomson, D.A., Tee, E.H., Tran, N.T., Monteiro, M.J., and Cooper, M.A. Oligonucleotide and polymer functionalized nanoparticles for amplification-free detection of DNA. Biomacromolecules 13(6) (2012): 1981-1989.

[74] Iwasaki, Y. and Ishihara, K. Cell membrane-inspired phospholipid polymers for developing medical devices with excellent biointerfaces. Science and Technology of Advanced Materials 13(6) (2016): 064101.

[75] Sangsuwan, A., Kawasaki, H., and Iwasaki, Y. Thiolated-2-methacryloyloxyethyl phosphorylcholine protected silver nanoparticles as novel photo-induced cell-killing agents. Colloids and Surface B: Biointerfaces 140 (2016): 128-134.

[76] Jin, Q., Xu, J.P., Ji, J., and Shen, J.C. Zwitterionic phosphorylcholine as a better ligand for stabilizing large biocompatible gold nanoparticles. Chemical Communication (Cambridge, England) (26) (2008): 3058-3060.

[77] Zhou, W., Shao, J., Jin, Q., Wei, Q., Tang, J., and Ji, J. Zwitterionic phosphorylcholine as a better ligand for gold nanorods cell uptake and selective photothermal ablation of cancer cells. Chemical Communication (Cambridge, England) 46(9) (2010): 1479-1481.

[78] Eliyahu, G., Kreizman, T., and Degani, H. Phosphocholine as a biomarker of breast cancer: Molecular and biochemical studies. International Journal of Cancer 120(8) (2007): 1721-1730.

[79] Egholm, M., Nielsen, P.E., Buchardt, O., and Berg, R.H. Recognition of guanine and adenine in DNA by cytosine and thymine containing peptide nucleic-acids (PNA). Journal of the American Chemical Society 114(24) (1992): 9677-9678.

[80] Nielsen, P.E., Egholm, M., Berg, R.H., and Buchardt, O. Sequence-selective recognition of DNA by strand displacement with a thymine-substituted polyamide. Science 254(5037) (1991): 1497-1500.

[81] Hyrup, B. and Nielsen, P.E. Peptide nucleic acids (PNA): Synthesis, properties and potential applications. Bioorganic & Medicinal Chemistry 4(1) (1996): 5-23.

[82] Boontha, B., Nakkuntod, J., Hirankarn, N., Chaumpluk, P., and Vilaivan, T. Multiplex mass spectrometric genotyping of single nucleotide polymorphisms employing pyrrolidinyl peptide nucleic acid in combination with ion-exchange capture. Analytical Chemistry 80(21) (2008): 8178-8186.

[83] Ananthanawat, C., Vilaivan, T., and Hoven, V.P. Synthesis and immobilization of thiolated pyrrolidinyl peptide nucleic acids on gold-coated piezoelectric quartz crystals for the detection of DNA hybridization. Sensors and Actuators B-Chemical 137(1) (2009): 215-221.

[84] Ananthanawat, C., Vilaivan, T., Hoven, V.P., and Su, X.D. Comparison of DNA, aminoethylglycyl PNA and pyrrolidinyl PNA as probes for detection of DNA hybridization using surface plasmon resonance technique. Biosensors & Bioelectronics 25(5) (2010): 1064-1069.

[85] Ananthanawat, C., Vilaivan, T., Mekboonsonglarp, W., and Hoven, V.P. Thiolated pyrrolidinyl peptide nucleic acids for the detection of DNA hybridization using surface plasmon resonance. Biosensors & Bioelectronics 24(12) (2009): 3544-3549.

[86] Ananthanawat, C., Hoven, V.P., Vilaivan, T., and Su, X.D. Surface plasmon resonance study of PNA interactions with double-stranded DNA. Biosensors & Bioelectronics 26(5) (2011): 1918-1923.

[87] Rashatasakhon, P., Vongnam, K., Siripornnoppakhun, W., Vilaivan, T., and Sukwattanasinitt, M. FRET detection of DNA sequence via electrostatic interaction of polycationic phenyleneethynylene dendrimer with DNA/PNA hybrid. Talanta 88 (2012): 593-598.

[88] Thipmanee, O., et al. Label-free capacitive DNA sensor using immobilized pyrrolidinyl PNA probe: Effect of the length and terminating head group of the blocking thiols. Biosensors & Bioelectronics 38(1) (2012): 430-435.

[89] Laopa, P.S., Vilaivan, T., and Hoven, V.P. Positively charged polymer brush-functionalized filter paper for DNA sequence determination following Dot blot hybridization employing a pyrrolidinyl peptide nucleic acid probe. Analyst 138(1) (2013): 269-277.

[90] Arayachukiat, S., et al. Bringing macromolecules into cells and evading endosomes by oxidized carbon nanoparticles. Nano Letters 15(5) (2015): 3370-3376.

[91] Akkahat, P., Kiatkamjornwong, S., Yusa, S., Hoven, V.P., and Iwasaki, Y. Development of a novel antifouling platform for biosensing probe immobilization from methacryloyloxyethyl phosphorylcholine-containing copolymer brushes. Langmuir 28(13) (2012): 5872-5881.

[92] Vilaivan, T. and Srisuwannaket, C. Hybridization of pyrrolidinyl peptide nucleic acids and DNA: Selectivity, base-pairing specificity, and direction of binding. Organic Letters 8(9) (2006): 1897-1900.

[93] Ferber, S., et al. Polymeric nanotheranostics for real-time non-invasive optical imaging of breast cancer progression and drug release. Cancer Letters 352(1) (2014): 81-89.

[94] Liu, L., Guo, X., Li, Y., and Zhong, X. Bifunctional multidentate ligand modified highly stable water-soluble quantum dots. Inorganic Chemistry 49(8) (2010): 3768-3775.

[95] Smith, A.M. and Nie, S. Minimizing the hydrodynamic size of quantum dots with multifunctional multidentate polymer ligands. Journal of the American Chemical Society 130(34) (2008): 11278.

[96] Chen, Z., et al. Controlled release of free doxorubicin from peptide-drug conjugates by drug loading. Journal of Controlled Release 191 (2014): 123-30.

[97] Zhu, X. and Jun Loh, X. Layer-by-layer assemblies for antibacterial applications. Biomaterials Science 3(12) (2015): 1505-1518.

[98] Li, H., et al. High durability and low toxicity antimicrobial coatings fabricated by quaternary ammonium silane copolymers. Biomaterial Science 4(2) (2016): 299-309.

[99] Ionov, L., Synytska, A., Kaul, E., and Diez, S. Protein-resistant polymer coatings based on surface-adsorbed poly(aminoethyl methacrylate)/poly(ethylene glycol) copolymers. Biomacromolecules 11(1) (2010): 233-237.

[100] Ginic-Markovic, M., et al. A versatile approach to grafting biofouling resistant coatings from polymeric membrane surfaces using an adhesive macroinitiator. Rsc Advances 5(77) (2015): 63017-63024.

[101] Xiong, X., Wu, Z., Yu, Q., Xue, L., Du, J., and Chen, H. Reversible bacterial adhesion on mixed poly(dimethylaminoethyl methacrylate)/ poly(acrylamidophenyl boronic acid) brush surfaces. Langmuir 31(44) (2015): 12054-12060.

[102] Broderick, A.H., Breitbach, A.S., Frei, R., Blackwell, H.E., and Lynn, D.M. Surface-mediated release of a small-molecule modulator of bacterial biofilm formation: a non-bactericidal approach to inhibiting biofilm formation in Pseudomonas aeruginosa. Advanced Healthcare Materials 2(7) (2013): 993-1000.

[103] Xu, L.Q., Li, N.N., Chen, J.C., Fu, G.D., and Kang, E.-T. Quaternized poly(2-(dimethylamino)ethyl methacrylate)-grafted agarose copolymers for multipurpose antibacterial applications. RSC Advances. 5(76) (2015): 61742-61751.

[104] Song, R., et al. Silver ions/ovalbumin films layer-by-layer self-assembled polyacrylonitrile nanofibrous mats and their antibacterial activity. Colloids Surface B: Biointerfaces 108 (2013): 322-328.

[105] Dai, J.H. and Bruening, M.L. Catalytic nanoparticles formed by reduction of metal ions in multilayered polyelectrolyte films. Nano Letters 2(5) (2002): 497-501.

[106] Vukoje, I.D., et al. Silver film on nanocrystalline TiO2 support: Photocatalytic and antimicrobial ability. Materials Research Bulletin 60 (2014): 824-829.

[107] Voo, Z.X., et al. Antimicrobial coatings against biofilm formation: The unexpected balance between antifouling and bactericidal behavior. Polymer Chemistry 7(3) (2016): 656-668.

[108] Sileika, T.S., Kim, H.D., Maniak, P., and Messersmith, P.B. Antibacterial performance of polydopamine-modified polymer surfaces containing passive and active components. Acs Applied Materials & Interfaces 3(12) (2011): 4602-4610.

[109] Xia, Y., Cheng, C., Wang, R., Nie, C.X., Deng, J., and Zhao, C.S. Ag-nanogel blended polymeric membranes with antifouling, hemocompatible and bactericidal capabilities. Journal of Materials Chemistry B 3(48) (2015): 9295-9304.

[110] Gullapalli, R.P. and Mazzitelli, C.L. Polyethylene glycols in oral and parenteral formulations--A critical review. International Journal of Pharmaceutical 496(2) (2015): 219-239.

[111] Ishihara, K., Nomura, H., Mihara, T., Kurita, K., Iwasaki, Y., and Nakabayashi, N. Why do phospholipid polymers reduce protein adsorption? Journal of Biomedical Materials Research 39(2) (1998): 323-330.

[112] Wang, B.L., et al. Bio-inspired terpolymers containing dopamine, cations and MPC: A versatile platform to construct a recycle antibacterial and antifouling surface. Journal of Materials Chemistry B 3(27) (2015): 5501-5510.

[113] Fuchs, A.V., Ritz, S., Putz, S., Mailander, V., Landfester, K., and Ziener, U. Bioinspired phosphorylcholine containing polymer films with silver nanoparticles combining antifouling and antibacterial properties. Biomaterials Science 1(5) (2013): 470-477.

[114] Jang, K., et al. An efficient surface modification using 2-methacryloyloxyethyl phosphorylcholine to control cell attachment via photochemical reaction in a microchannel. Lab Chip 10(15) (2010): 1937-1945.

[115] Iwata, R., Suk-In, P., Hoven, V.P., Takahara, A., Akiyoshi, K., and Iwasaki, Y. Control of nanobiointerfaces generated from well-defined biomimetic polymer brushes for protein and cell manipulations. Biomacromolecules 5(6) (2004): 2308-2314.

[116] Nakai, K., Morigaki, K., and Iwasaki, Y. Molecular recognition on fluidic lipid bilayer microarray corralled by well-defined polymer brushes. Soft Matter 6(23) (2010): 5937-5943.

[117] Jang, K., Sato, K., Mawatari, K., Konno, T., Ishihara, K., and Kitamori, T. Surface modification by 2-methacryloyloxyethyl phosphorylcholine coupled to a photolabile linker for cell micropatterning. Biomaterials 30(7) (2009): 1413-1420.

[118] Enomoto, R., et al. Surface patterned graft copolymerization of hydrophilic monomers onto hydrophobic polymer film upon UV irradiation. Journal of Polymer Science Part A: Polymer Chemistry 52(19) (2014): 2822-2829.

[119] Kuroda, K., et al. Poly(dimethylsiloxane) (PDMS) surface patterning by biocompatible photo-crosslinking block copolymers. RSC Advances. 5(58) (2015): 46686-46693.

[120] McRae Page, S., Martorella, M., Parelkar, S., Kosif, I., and Emrick, T. Disulfide cross-linked phosphorylcholine micelles for triggered release of camptothecin. Molecular Pharmaceutics 10(7) (2013): 2684-2692.

[121] Sangsuwan, A., Narupai, B., Sae-ung, P., Rodtamai, S., Rodthongkum, N., and Hoven, V.P. Patterned Poly(acrylic acid) Brushes Containing Gold Nanoparticles for Peptide Detection by Surface-Assisted Laser Desorption/Ionization Mass Spectrometry. Analytical Chemistry 87(21) (2015): 10738-46.

[122] Kolewe, K.W., Peyton, S.R., and Schiffman, J.D. Fewer bacteria adhere to softer hydrogels. ACS Applied Materials & Interfaces 7(35) (2015): 19562-9.

[123] Chang, C.-C., et al. Underwater superoleophobic surfaces prepared from polymer zwitterion/dopamine composite coatings. Advanced Materials Interfaces 3(6) (2016): 1500521.

[124] Wang, J.H., et al. The use of rhodamine 6G and fluorescence microscopy in the evaluation of phospholipid-based polymeric biomaterials. Journal of Microscopy-Oxford 217 (2005): 216-224.

[125] Wang, Z., Cai, X., Chen, Q., and Chu, P.K. Effects of Ti transition layer on stability of silver/titanium dioxide multilayered structure. Thin Solid Films 515(5) (2007): 3146-3150.

[126] Godoy-Gallardo, M., Rodriguez-Hernandez, A.G., Delgado, L.M., Manero, J.M., Javier Gil, F., and Rodriguez, D. Silver deposition on titanium surface by electrochemical anodizing process reduces bacterial adhesion of

Streptococcus sanguinis and Lactobacillus salivarius. Clinical Oral Implants Research 26(10) (2015): 1170-1179.

[127] Papierska, J., et al. Modification of emission properties of ZnO layers due to plasmonic near-field coupling to Ag nanoislands. Plasmonics 8(2) (2013): 913-919.

[128] Xiu, Z.M., Zhang, Q.B., Puppala, H.L., Colvin, V.L., and Alvarez, P.J. Negligible particle-specific antibacterial activity of silver nanoparticles. Nano Letters 12(8) (2012): 4271-4275.

[129] Calderon V, S., Ferreri, I., Escobar Galindo, R., Henriques, M., Cavaleiro, A., and Carvalho, S. Electrochemical vs antibacterial characterization of ZrCN–Ag coatings. Surface and Coatings Technology 275 (2015): 357-362.

[130] Carvalho, I., Henriques, M., Oliveira, J.C., Almeida Alves, C.F., Piedade, A.P., and Carvalho, S. Influence of surface features on the adhesion of Staphylococcus epidermidisto Ag–TiCN thin films. Science and Technology of Advanced Materials 14(3) (2016): 035009.

APPENDIX

APPENDIX A

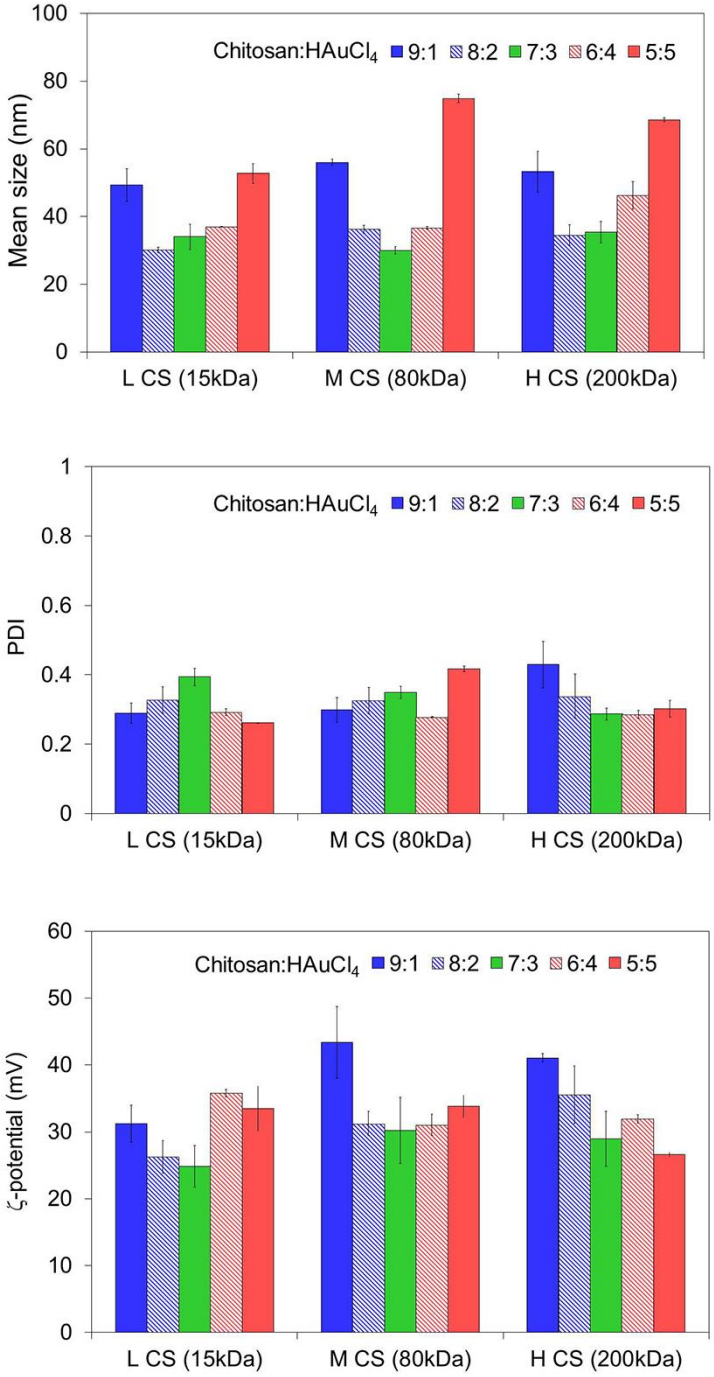

Figure A-1 Mean (±SD) size, PDI and ζ-potential of the CS-AuNPs synthesized from five different CS:$HAuCl_4$ (v/v) ratios and three different molecular weight of chitosan, as analyzed by PCS (independent experiment = 3).

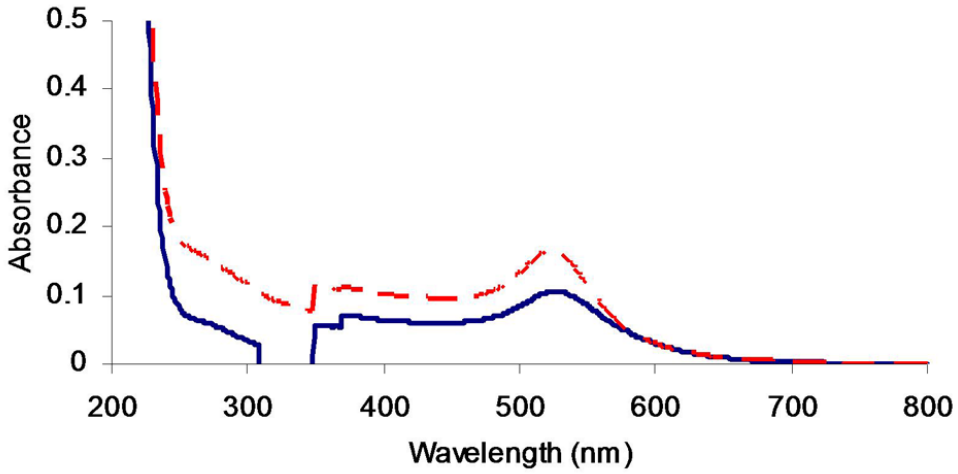

Figure A-2 UV-vis absorption spectra of (a) as-synthesized CS-AuNPs (blue solid line) and (b) CS-AuNPs after storing for more than 4 months (red dashed line).

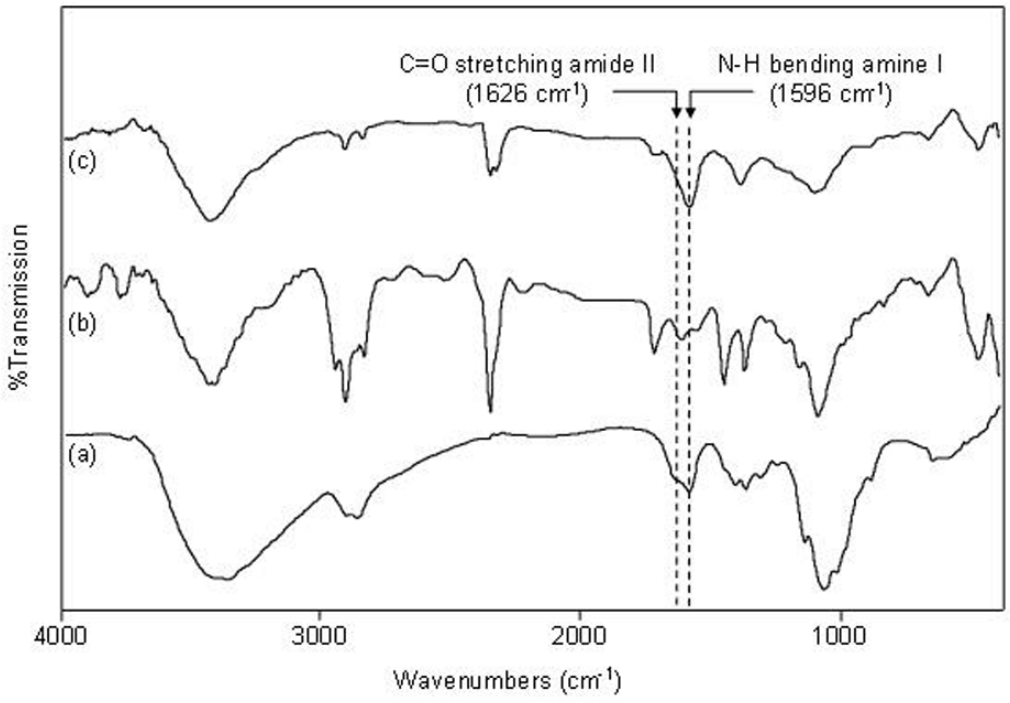

Figure A-3 FTIR spectra of (a) CS, (b) CS-AuNPs and (c) AuNPs stabilized by trisodium citrate.

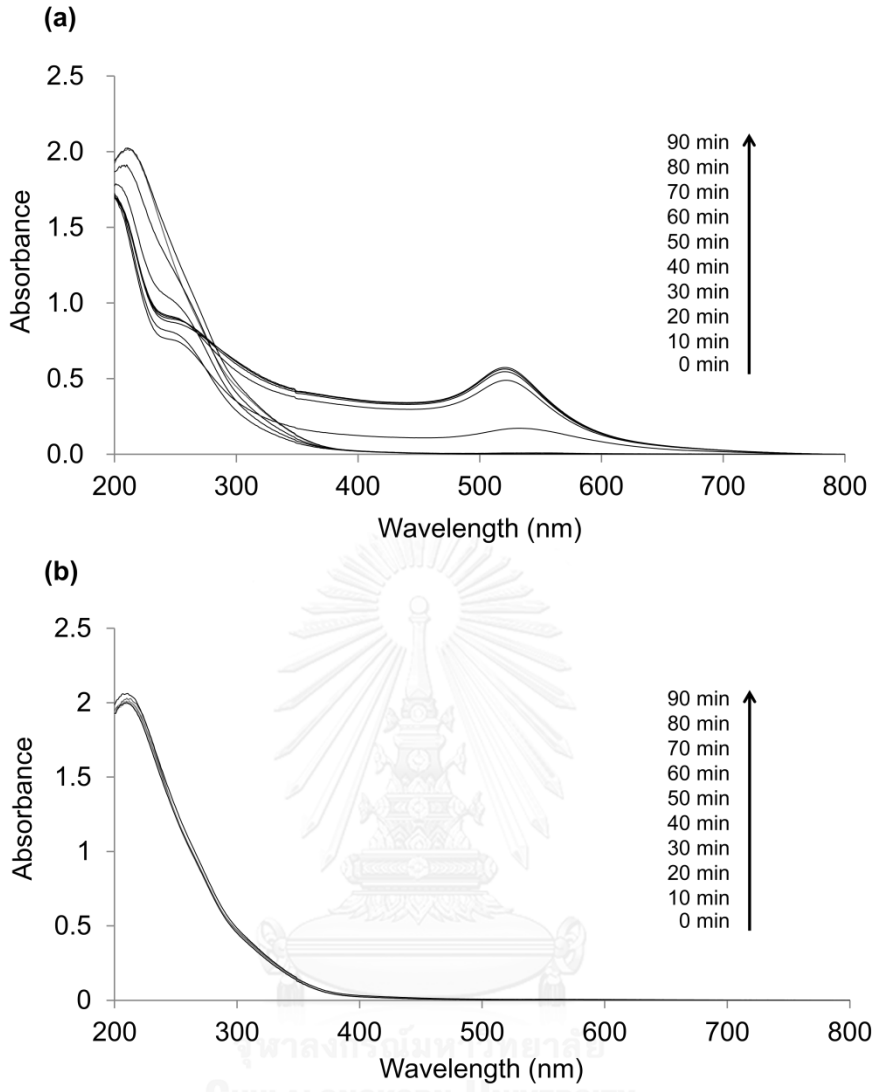

Figure A-4 UV-vis absorption spectra recorded at different time of CS-AuNPs synthesized by (a) heating method and (b) sonochemical method.

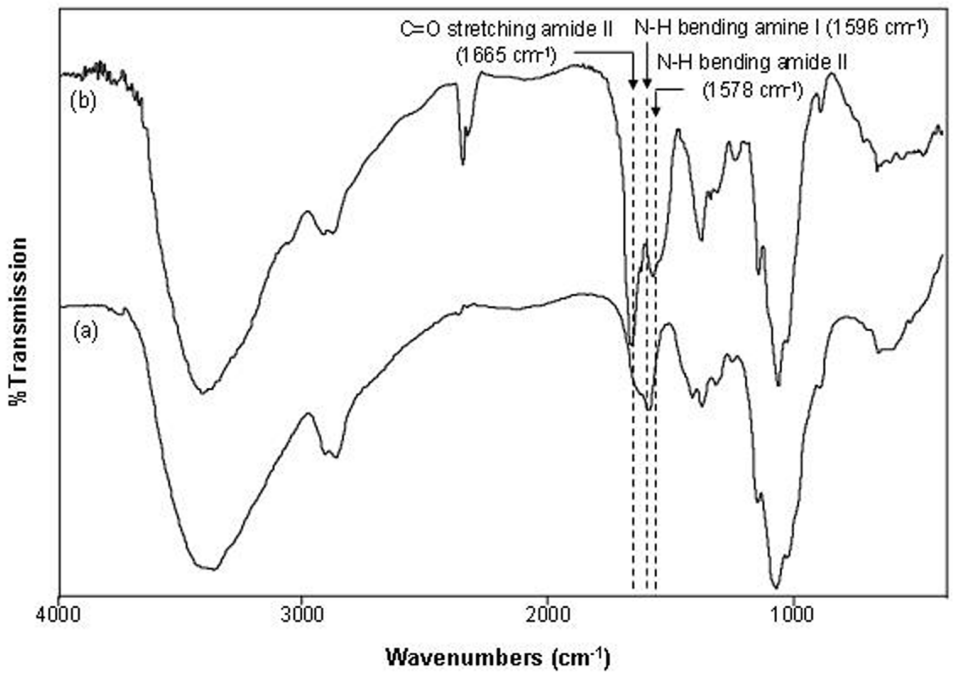

Figure A-5 FTIR spectra of (a) CS and (b) SA-CS.

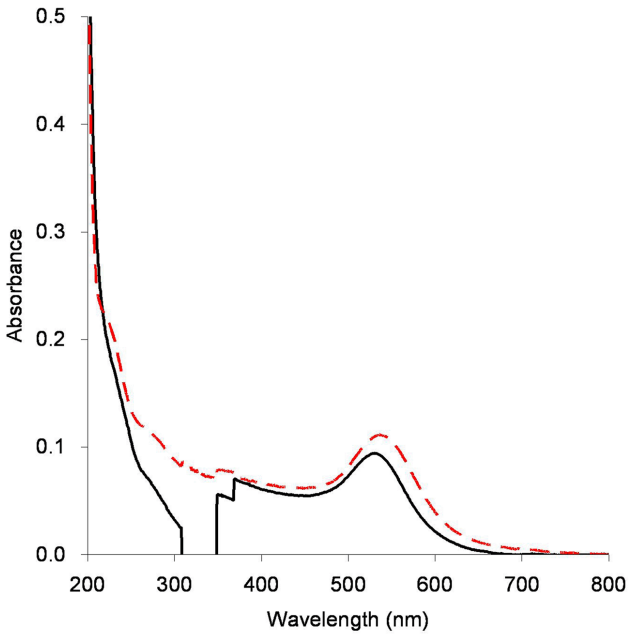

Figure A-6 UV-vis absorption spectra of BSA-CS-AuNPs: (a) as-synthesized (black solid line) and (b) after one month storage (red dashed line). Spectra shown are representative of those seen from three independent repeats.

APPENDIX B

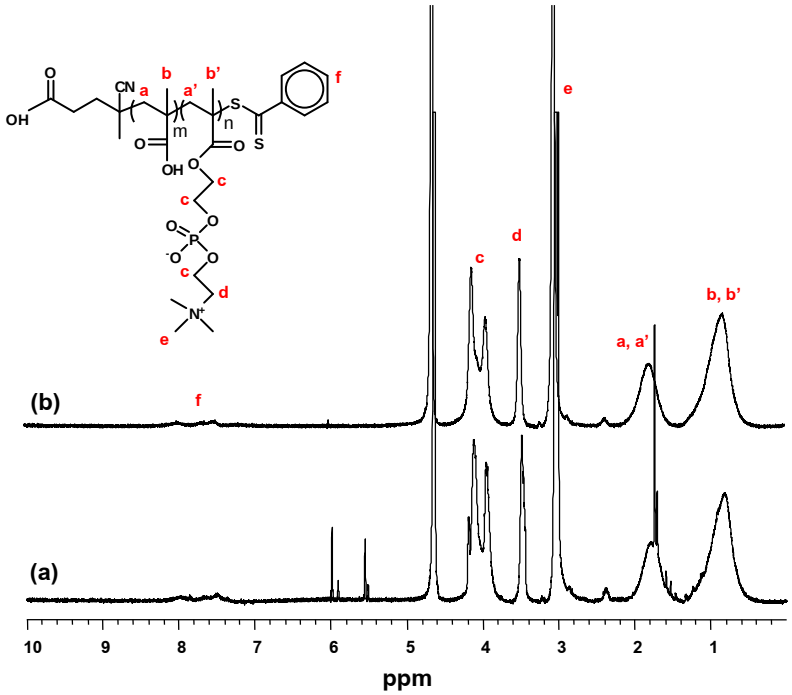

Figure B-1 ^{1}H NMR spectra of (a) crude and (b) purified PMAMPC in D_2O.

The % conversion was calculated from ^{1}H-NMR spectrum before purification by using the relative ratio between the peak integration of methylene protons in polymer backbone at 1.6-2.2 ppm and sum of integral intensities of methylene protons in polymer backbone and vinyl protons in the remaining monomer which appear at 5.5 ppm and 6.0 ppm as shown in equation B1. The degree of polymerization (DP) and copolymer composition (MA:MPC) could also be determined from purified ^{1}H-NMR spectrum by comparing peak $H_{b,b'}$ at 0.9 ppm (from polymer backbone) and peak H_d at 3.5 ppm (from MPC) with peak H_f at around 7.4-8.2 ppm (from aromatic end group) as shown in equation B2-6.

$$\% \text{ Conversion} = \left[\frac{\int \text{a,a}'(\text{polymer; 1.6–2.2 ppm})}{\int \text{a,a}'(\text{polymer; 1.6–2.2 ppm}) + \int \text{a,a}'(\text{monomer; 5.5–6.0 ppm})}\right] \times 100 \quad \text{(B1)}$$

$$\text{Total unit} = \left[\frac{\int \text{b,b}\prime}{6} \Big/ \frac{\int \text{f}}{5}\right] \times 2 \quad \text{(B2)}$$

$$\text{MPC unit} = \frac{\int d}{2} \Big/ \frac{\int f}{5} \quad \text{(B3)}$$

$$\text{MA unit} = \text{Total unit} - \text{MPC unit} \quad \text{(B4)}$$

$$\%\ \text{MPC} = \frac{\text{MPC unit}}{\text{Total unit}} \times 100 \quad \text{(B5)}$$

$$\%\ \text{MA} = \frac{\text{MA unit}}{\text{Total unit}} \times 100 \quad \text{(B6)}$$

APPENDIX C

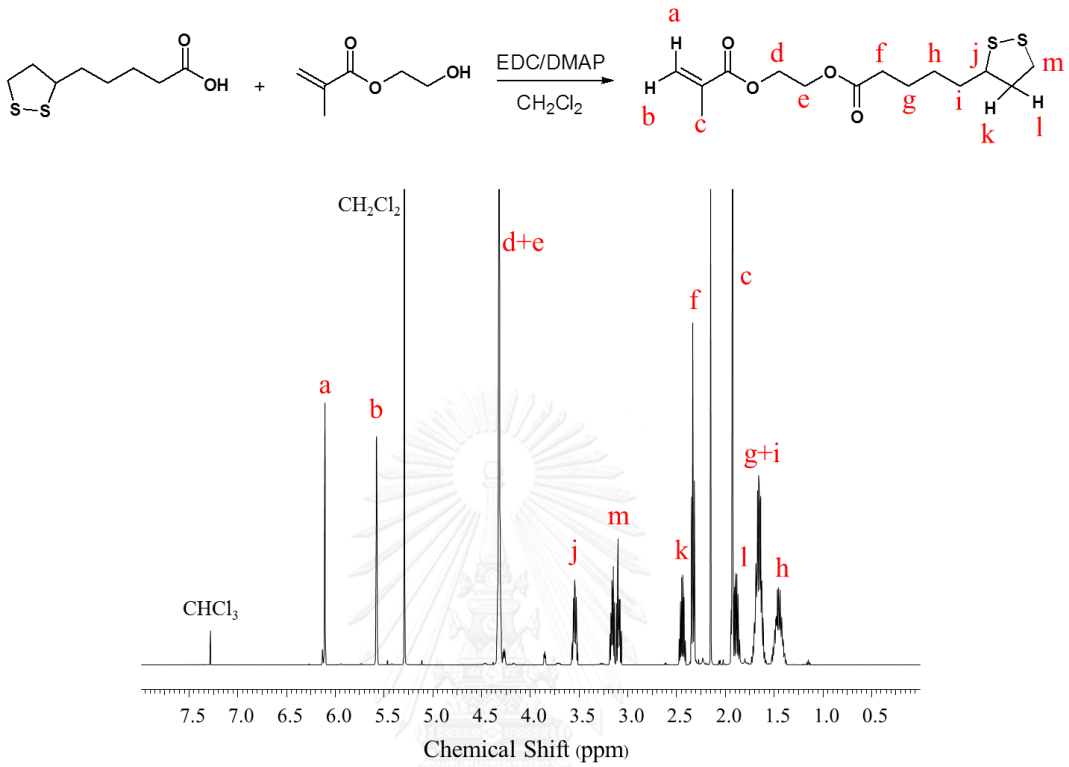

Figure C-1 ^{1}H NMR spectrum of HEMA-LA in $CDCl_3$.

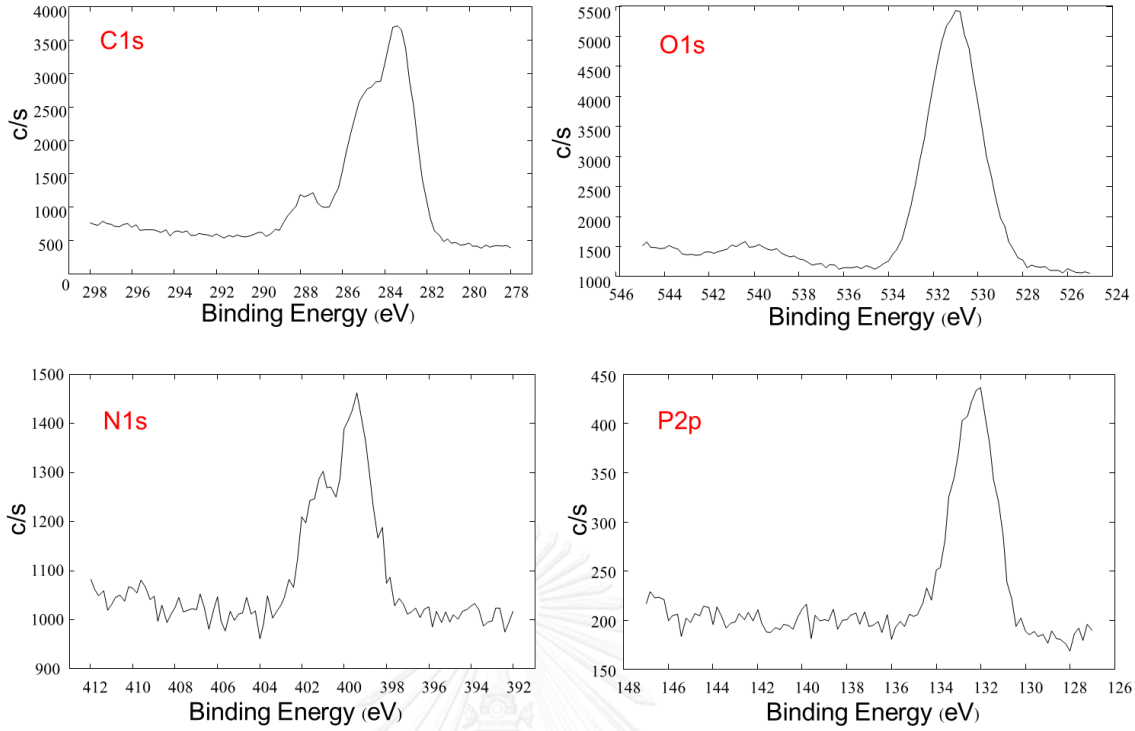

Figure C-2 XPS spectra of patterned surface on poly(MPC-DHLA) area.

VITA

Miss Pornpen Sae-ung was born in Bangkok, Thailand, on May 13th, 1984. She received a Bachelor Degree (Department of Chemistry) and Master Degree (Program of Petrochemistry and Polymer Science) from the Faculty of Science, Chulalongkorn University, Bangkok in 2006 and 2009, respectively. In 2010, she started as a PhD Degree student with a major in Program of Macromolecular Science, Faculty of Science, Chulalongkorn University.

Publications:

1. Kusolkamabot, K.; Sae-ung, P.; Niamnont, N.; Wongravee, K.; Sukwattanasinitt, M.; Hoven, V.P. "Poly(N‑isopropylacrylamide)-stabilized Gold Nanoparticles in Combination with Tricationic Branched Phenylene-Ethynylene Fluorophore for Protein Identification" Langmuir, 2013, 29, 12317–12327.

2. Sangsuwan, A.; Narupai, B.; Sae-ung, P.; Rodtamai, S.; Rodthongkum, N.; Hoven, V.P. "Patterned Poly(acrylic acid) Brushes Containing Gold Nanoparticles for Peptide Detection by Surface-Assisted Laser Desorption/Ionization Mass Spectrometry" Anal. Chem., 2015, 87, 10738–10746.

3. Sae-ung, P.; Tumcharern, G.; Hoven, V.P. "Green Synthesis and Potential Biosensing Application of Gold Nanoparticles Stabilized by Biomolecule-Modified Chitosan" J. Nanopart. Res., submitted manuscript.

4. Sae-ung, P.; Kolewe, K.W.; Bai, Y.; Schiffman, J.D.; Hoven, V.P.; Emrick, T. "Antifouling and Antibacterial Patterned Surfaces Prepared from Silver-Backfilled Zwitterionic Copolymer Films" (manuscript in preparation).